COMPUTATION OF SURROUND MODULATION ACROSS LAYERS OF THE PRIMATE PRIMARY VISUAL CORTEX

by

Maryam Bijanzadeh

A dissertation submitted to the faculty of
The University of Utah
in partial fulfillment of the requirements for the degree of

Doctor of Philosophy

Interdepartmental Program in Neuroscience

The University of Utah

May 2017

The University of Utah Graduate School

STATEMENT OF DISSERTATION APPROVAL

The dissertation of **Maryam Bijanzadeh**

has been approved by the following supervisory committee members:

Alessandra Angelucci	, Chair	**11/29/2016** Date Approved
Jeffrey Anderson	, Member	**11/29/2016** Date Approved
Paul Bressloff	, Member	**11/29/2016** Date Approved
Sarah Creem-Regehr	, Member	**11/29/2016** Date Approved
Matthew Wachowiak	, Member	**11/29/2016** Date Approved

and by **Richard Dorsky** , Chair/Dean of

the Department/College/School of **Interdepartmental Program in Neuroscience**

and by David B. Kieda, Dean of The Graduate School.

ABSTRACT

Primate primary visual cortex (V1) consists of six anatomical layers. There are both heterogeneous and homogeneous functional properties found across layers. Surround modulation (SM) occurs when neuronal responses to stimulation of a neuron's receptive field (RF) is modulated by simultaneous simulation outside of the RF. There are three potential candidates for SM: feedforward (FF) and intra-V1 horizontal (HZ) connections underpin the region nearby RF (near surround), while the modulatory signal arising from distant regions (far surround) are conveyed by feedback (FB) connections from higher visual areas. Also, V1 layers show distinct patterns of FF, HZ, and FB terminations. The goal of my dissertation research was to study 1) the properties of SM across V1 layers, 2) how simple visual stimuli in the RF and surround of a V1 column activate V1 layers, and (3) what specific afferent circuits to and within the V1 column of these stimuli recruit.

Using single electrode recordings sampling from all the layers of V1, I found that near SM is more sharply orientation-tuned in the superficial layers (L3B, 4B and 4Cα), where there are prominent horizontal connections. However, far SM is more orientation-tuned in L4B, possibly reflecting the orientation organization of feedback connections to this layer. Using laminar recordings, I investigated the temporal dynamics of inputs (local field potentials, LFPs) to each layer when stimulating surround elements. Near surround stimulation simultaneously localized the first inputs in superficial and deep layers with a significant delay in L4C, suggesting both HZ and FB contribute to near SM. Feedback

recipient layers (L1/2A and L5/6) received the earliest inputs with far surround stimulation. Measuring the latency of spiking activity while co-stimulating RF and surround, the untuned near SM first emerged in L4C, but, tuned near SM and far SM, emerged outside thalamic recipient layers, suggesting a cortical origin.

Finally, I found that brain oscillations in response to stimuli in the surround, mirror the structure of the underlying horizontal and feedback connections. Grating patches positioned on the collinear axis to a cell's preferred orientation, evoke a greater power in different frequency bands of LFP, including alpha, beta, and gamma, compared to orthogonal position in both near and far surround. We propose that horizontal and feedback connections, substrates of near and far surround, are aligned collinearly in the visual field and help generate brain oscillations.

TABLE OF CONTENTS

ACKNOWLEDGEMENTS

I would like to express my special appreciation and gratitude to my advisor Alessandra Angelucci, for her priceless support and motivation. She inspired me with her thorough knowledge and intellect. She taught me how to build a scientific state of mind and overcome the difficulties through my research path. I am grateful and thankful to have had such an outstanding advisor, both personally and scientifically. I would also like to thank my committee members, Drs. Jeffrey Anderson, Paul Bressloff, Sarah Creem-Regehr, and Matt Wachowiak, for their invaluable comments and guidance throughout my research training.

I also appreciate members of the Angelucci Lab who provided a warm and supportive environment to perform research and do science. I thank Jennifer Ichida, Lauri Nurminen, Sam Merlin, Fredrick Federer, Jeff Yarch, and Kesi Sainsbury, who helped me with their critical scientific discussions and guided me to improve my skillsets. Many thanks to the Interdepartmental Program in Neuroscience especially Tracy Marble, Dr. Kristen Keefe, and Dr. Richard Dorsky, who provided dynamic training environment.

Finally, I would like to thank my family for their encouragement and infinite love. I especially thank my spouse who helped me to overcome difficulties throughout my research.

My research was funded by the National Science Foundation grant to Alessandra Angelucci and Research to Prevent Blindness, Inc. grant to the Department of

Ophthalmology, University of Utah and Neuroscience Achievement fellowships that were granted to me by the Neuroscience Program, University of Utah.

CHAPTER 1

INTRODUCTION

Despite years of research on the visual system, we still do not fully understand how simple visual stimuli are processed. Complex neuronal networks in different cortical areas transform the retinal image into contours, object boundaries, depth, motion, color, shapes, and eventually, faces. Numerous studies have investigated the basic functional properties as well as the anatomical circuits of each visual area, providing a substantial body of literature.

Visually responsive neurons at various levels of the visual system monitor discrete regions of visual space, known as the receptive field (RF). Encoding the stimulus features that are presented in the RF is performed by multilevel processing. The degree of complexity that can be extracted from the stimulus varies along the visual system hierarchy, with higher visual areas being able to extract increasingly more complex features. For instance, retinal RFs are selective to contrast and small spots of light, while visual cortex 1 (V1) and visual cortex 4 (V4) RFs are selective to edges and simple shapes, respectively. In addition, hierarchical processing occurs within two main parallel pathways, called the “dorsal” and “ventral” streams. Electrophysiological and clinical studies have revealed that these two hierarchical streams are responsible for processing the

spatial aspects of the visual world and object recognition, respectively.

After almost a century of research, a primary question in visual neuroscience still remains: how do structurally segregated streams with distinct functional features lead to a unified percept of the natural world? Besides information flowing from lower to higher visual centers via feedforward (bottom-up) projections, there are also inter-areal feedback (top-down) projections from higher to lower visual centers. It has been shown that these feedback connections, which are sending back the processed information at each level of the hierarchy, can modulate the neuronal responses in lower centers. These bidirectional (feedforward and feedback) interactions between different brain areas at every stage of processing, can likely expand the dynamic range of information processing in the visual system, as well as generating a unified percept of the visual world.

The primary visual cortex (V1) is the main hub between lower (retina, LGN) and higher visual centers, such as areas V2, V4, and MT that are dependent upon V1 inputs for their visual responses. V1 RFs are selective to basic visual features of natural scenes including the orientation of edges and stimulus contrast. Some features, such as orientations, are processed in modules that span across a column of cortex, from layers 1 to 6. V1 RFs provide information to extrastriate cortex for further analysis along the visual hierarchy. However, the information available at the level of V1 RFs is influenced by contextual effects. Specifically, neuronal responses to stimuli inside their RF can be modulated by stimuli outside their RF, i.e., in the RF surround, a phenomenon called “surround modulation”. Surround modulation at the level of V1 is thought to contribute to perceptual tasks such as contour integration and figure-ground segregation.

Since surround modulation is one of the main properties of neurons throughout the

visual system, there has been much interest in trying to understand its underlying circuitry and mechanisms. Years of anatomical and electrophysiological studies have uncovered three potential candidate circuits for surround modulation: feedforward thalamocortical connections, intra-V1 horizontal connections, and feedback connections from the extrastriate cortex. These connections also have distinct patterns of termination across layers of V1. The aim of this dissertation is to reexamine the underlying circuits of surround modulation and identify how V1 layers with distinct connection patterns contribute to the processing of surround modulation, reflecting its underlying mechanisms.

The main question driving my research is: Do temporal and functional properties of neuronal inputs/outputs across layers reflect the hypothesized circuitry underlying surround modulation? I have also examined the frequency content of population activity across layers in response to surround stimuli and asked whether rhythmic oscillations mirror the underling circuits. In the remainder of this chapter, an overview of the visual system is provided, in addition to a review of the RF and surround properties of V1 neurons.

1.1 The Central Visual Pathway

The pattern of light detected by the photoreceptors in the back of the retina transverses across many stages of visual processing before resulting in visual perception. Figure 1.1-A shows a schematic of visual information flow from the retina to the lateral geniculate nucleus of the thalamus (LGN) and then to the first cortical area: primary visual cortex (V1). After processing by V1 neurons, the signal will be sent to higher visual centers that integrate more complex features.

1.1.1 Basic Properties of Neurons Along the Visual Pathway

Retinotopy is One of the main properties of visual neurons, is the mapping of the visual world along the visual pathway (Connolly and Van Essen, 1984). For example, adjacent neurons in each visual area encode adjacent locations in the visual field. An example of receptive fields and the visual space monitored by RGCs is shown in Figure 1.1-B.

A higher proportion of photoreceptors map the center of the gaze, called **fovea**, while a lower fraction maps more distant visual field from the center of gaze, called **periphery**. This pattern of localization results in higher visual acuity in the fovea than in the periphery. This asymmetrical property is also maintained in the visual cortical areas (Figure 1.1-C represents the visual map of fovea and periphery in V1). Specifically, in V1, the cortical magnification factor, which is the millimeters of cortex devoted to a degree of visual space, decreases inversely with eccentricity outside of the fovea (Connolly and Van Essen, 1984).

1.1.2 Retina and LGN

From the photoreceptors, visual information is passed through a number of processing stages before reaching the retinal ganglion cells. Retinal ganglion cells send this information to the LGN via the optic nerve. The optic nerve is a bottleneck (Callaway, 2005) of information transfer due to the large amount of information captured by the retina that must be transferred through pact bundle of axons. This information from 1.6 million RGCs (Rodieck and Rodieck, 1998) has to be compressed and efficient (Sterling, 2004) in order to get to the brain, and the brain has to extract and elaborate upon that information.

In both the retina and LGN, segregation of information is maintained by different cell types. In the retina, there are three main classes of RGCs: midget, parasol, and bistratified

ganglion cells. The midget cells have small somas, slower axonal conduction, and are spectrally sensitive, while parasol cells have larger cell bodies, fast conducting axons, and are less sensitive to spectral information (Callaway, 2005). Bistratified cells are sensitive to short wavelengths of light (blue cones) (Dacey and Packer, 2003). Information from these neurons will be sent to distinct targets in the LGN. Interestingly, the input from these cells remains segregated in the early stages of parallel processing, but the information becomes reorganized within the cortex.

The LGN is an important structure in visual processing because it relays information to the primary visual cortex (V1), from the retina. Like the retina, there are different classes of cells in the LGN. Magnocellular (M) neurons in the LGN receive information from high contrast parasol RGCs, and are located in the ventral layers of LGN. These neurons have large and achromatic receptive fields. Parvocellular (P) neurons have smaller RFs and are located in the four dorsal layers of the LGN. These neurons obtain information from midget cells that are spectrally sensitive. There are also Koniocellular (K) neurons that are intercalated across LGN. In summary, the architecture of LGN allows retinal information to remain segregated through M, P, and K pathways before it is passed onto the primary visual cortex.

1.1.3 The Extrastriate Cortex

Visual areas beyond the primary visual cortex are called extrastriate cortex in the primate brain. The extrastriate cortex consists of many different visual areas, including V2, V3, V4, MT/V5, and infero temrporal (IT) cortex. The RF properties across these areas are selective to more complex features than V1 RFs. In particular, V2 neurons respond to both

orientation and illusory contours (Kandel et al., 2000), V4 neurons are selective to the orientation of non-luminance contours similar to V2, color and form, MT neurons are selective to pattern direction, speed gradient, and motion (Kandel et al., 2000; Orban, 2008) and IT cortex is selective to a wide range of complex objects such as faces.

Previous anatomical studies have demonstrated the existence of two major parallel visual processing streams beyond V1 called dorsal (or where) and ventral (or what) pathways (Figure 1.2). The dorsal stream projects from V1 and V2, to V3 and MT, and terminates in the parietal cortex; it processes information about location and object motion and sends them to motor cortex to guide eye and body movements. The ventral stream projects from V1 and V2 to V4 and the temporal lobe, and processes information about form, object, and faces. This stream plays a role in object identification and face recognition by interaction with memory related regions (Kandel et al., 2000). As mentioned above, along these feedforward dorsal and ventral pathways, there are reciprocal feedback connections projecting from higher to lower areas, and back to V1, which modulate neuronal responses.

1.1.4 The Primary Visual Cortex (V1)

Area V1 is the first cortical area to receive LGN input. After processing through complex circuitry in V1 (which is discussed in this chapter), information is reorganized by different functional modules and is distributed to a number of different cortical areas in the extrastriate cortex. V1 is about 2mm thick and only a few square inches in surface area, contains about 200 million neurons, and is the largest cortical area in nonhuman primates (Palmer, 1999). Higher visual areas depend on V1 to function normally. In addition, many

higher visual area attributes, such as figure-ground segregation, detection of object boundaries, and contour completion, all rely on the mechanisms and underlying circuitry of V1. The specific organization and function of V1 is described in fine detail below, and is of primary importance for this doctoral thesis.

1.1.4.1 V1 cortical modules and maps

There are multiple functional structures in V1 processing visual information. If V1 is stained for cytochrome oxidase (CO), which is a metabolic enzyme, two major regions in the superficial layers (specifically L2/3) will emerge: dark CO patches called "blobs" and CO-pale intervening "interblob" regions. Blobs are selective to color and low spatial frequency while interblobs are sensitive to orientations and mid- to high-spatial frequency, although, this segregation is not rigid (Sincich and Horton, 2005). The outputs from these structures remain segregated, terminating in V2 CO domains called "stripes." Blobs primarily project to thin stripes that are more selective to color, while interblobs project to orientation selective thick stripes and pale stripes. Thus, in V1 and V2 there are different functional structures that encode specific visual attributes in parallel.

In addition, individual neurons in V1 are selective to specific stimulus features including: orientation, contrast, spatial and temporal frequency, and so forth. To investigate each of these properties independently, sinusoidal gratings have typically been used in the literature. Using different imaging techniques, it has been found that there are clusters of neurons showing selectivity to these features, and that many of these features are organized into systematic maps. In particular, orientation (Blasdel and Salama, 1986) and spatial frequency (Shoham et al., 1997) maps were discovered in V1. "**Functional maps**" are

found in most visual cortical areas.

In addition to functional maps that can be imaged from the superficial layers of V1 in the tangential domain, vertical functional modules were also discovered, mainly using single electrode recordings from pia to white matter. Initially these modules were termed **cortical columns**. Orientation and ocular dominance columns (receiving input from one eye) were the first such modules that were discovered in the primary visual cortex of cat and monkey by Nobel prize winners, Hubel and Wiesel (Hubel and Wiesel, 1959, 1962, 1974) in the 1960s. They recorded all layers of the cortex along a trajectory vertical to the cortical surface, and observed that all sampled neurons map to similar locations of the visual field (similar RF location), and have similar preferred orientation. However, the cortical spread of RF and orientation modules are different (orientation column=50μm (Berens et al., 2008), RF column~=1-2 mm). We will discuss the structural and physiological properties of this laminar cortical module in the next section.

1.1.4.2 The laminar structure of V1

V1, similar to most of the neocortex, is comprised of six layers. In V1, multiple specialized inputs from the LGN are segregated into distinct layers. Magnocellular afferents, arising from cells with high luminance contrast sensitivity and high temporal resolution (involved in luminance and motion processing) terminate primarily in L4Cα and lower L6. Parvocellular afferents, arising from cells with sensitivity to color contrast and low temporal resolution (involved in processing of color and fine patterns) terminate primarily in L4Cβ and upper L6 (Callaway, 2005; Sincich and Horton, 2005). Also, koniocellular afferents terminate in L2/3, specifically in the blobs, and there are some direct

inputs to L4A (Callaway, 2005).

Distinct types of excitatory and inhibitory neurons such as, pyramids and stellates, somatostatin and basket cells, as well as distinct recurrent networks across layers add significant degree of processing stages to integrate the received information. For instance, there are many classes of inhibitory cells in the neocortex performing specific functions. Basket cells in L4C of V1 that receive similar thalamic information as L4C excitatory cells control the gain, and balance the total level of excitation by making postsynaptic contacts on the cell bodies (Hirsch et al., 2003). In contrast, somatostatin inhibitory cells contact preferentially the more distal dendrite, and are more selective for features coded by V1 (e.g., orientation)(Somogyi et al., 1998). Cortical dynamic range is increased by usage of different cell types, cortical modules as wells as parallel and intermingled information pathways.

1.1.4.2.1 Feedback and horizontal terminations across V1 layers

Along the canonical rout, L4C neurons make synapses on supragranular neurons (SG, above L4C) and then SG cells synapse on to infragranular ones (IG). After the signal is being processed across V1 layers, the output will be sent from SG layers to the extrastriate cortex for further visual processing. Moreover, most of L6 cells do not make direct cortico-cortical connections, but there are groups of pyramidal cells, called Meynert cells that project directly to area MT (Fries et al., 1985). Infragranular layers (L5 and L6) send the processed information back to subcortical regions such as superior colliculus (Lund et al., 1975).

Furthermore, the extrastriate cortex feeds the signal back to both upper and lower layers

of V1 avoiding L4C (Rockland and Pandya, 1979; Felleman and Van Essen, 1991; Casagrande and Kaas, 1994). The feedback axonal terminations are prominent in L1, where there are almost no cell bodies (Rockland and Pandya, 1979; Ungerleider and Desimone, 1986), L2A, L5B, and L6 of V1, and only form sparse terminations in L3 and L4B (Webb et al., 2002; Federer et al., 2015). There is also an alternative cortico-thalamo-cortical path that passes through pulvinar nucleus. Specifically, some L5 neurons in V1 target pulvinar nucleus of thalamus that would send outputs to other cortical areas (Guillery and Sherman, 2002). Supposedly, this L5 neurons also send sensory signals to subcortical motor structures (i.e., superior colliculus) via their collaterals (Lund et al., 1975).

In addition to feedforward, feedback and interlaminar projections, there are intrinsic horizontal axons connecting pyramidal cells in tangential plane to the cortical surface. Horizontal connections are patchy and dense in L2, L3, L4B, and L5 link neurons of different cortical columns (Figure 1.3, red arrows)(Gilbert, 1983; Lund and Wu, 1997). These projections are thought to play an important role in V1 physiological properties such as, orientation selectivity and surround modulation.

In the next section, we provide a thorough review of the physiological properties of V1 neurons such as, RF and RF-Surround that are basic principles to understanding the presented results in this thesis.

1.2 Receptive Field and Surround

1.2.1 Receptive Field and Surround in LGN

A specific part of the visual field that evokes the maximum neuronal responses is called RF. The RF is a fundamental property of all sensory neurons across sensory cortices. The

size of RF and visual features that are coded by RF in each area varies as the visual information travels from lower to higher visual centers. V1 RFs varying 0.5-2° (close to fovea) in size, are selective to simple attributes such as, orientation of edges while IT cells having ~30° RF encode complex features like faces and objects. However, in each area, the size of receptive field does not have a uniform distribution, neurons at the fovea have much smaller RFs compared with neurons in the periphery.

The receptive field properties also vary between retina and V1 cells. The LGN receptive fields are generally circular with concentric subfields. Depending on the luminance response the subfields are either "on" type, the higher the luminance the higher the neuronal responses, or "off" type, the lower the luminance the higher the response. Based on the polarity of the RF center, the neuron is called "on" or "off" cell. For example, the off cell has off central subfield with on surroundings. This effect is called "classical center-surround" at the level of LGN that has been modeled via linear filters mapping visual images to the neuronal responses (Carandini et al., 2005).

In addition to the classical center-surround property of LGN cells, another suppressive effect is found that cannot be explained by on and off subfields. By activation of the extra-classical surround the responses saturate when stimulus contrast increases, and decrease by superimposition of another stimulus or enlarging the stimulus size. The surround suppression by increasing stimulus size is also observed in V1. In contrast to classical surround that could be excitatory or inhibitory, the LGN extra-classical surround is strongly suppressive (Solomon et al., 2002; Bonin et al., 2005; Sceniak et al., 2006). Bonin et al.(2005), proposed that the response plateau due to high contrast stimulation of extra-classical surround, is well matched with a change in contrast gain. Specifically, this

nonlinear contrast gain control in LGN is mainly generated by retina (Shapley and Victor, 1978) and is strengthened in LGN (Kaplan et al., 1987); also, it is generated too fast to involve corticogeniculate feedback from V1 (Alitto and Usrey, 2008). The size of LGN extra-classical surround in primates on average is <2.5° at parafoveal eccentricities (0.8°-~5°) (Sceniak et al., 2006).

1.2.2 The Receptive Field of V1 Cells and Its Properties

V1 receptive fields also have on and off regions (Hubel and Wiesel, 1965, 1968; Carandini et al., 2005). V1 neurons were initially categorized as simple, complex, and hypercomplex cells by Hubel and Wiesel (1968). But, later on, the hypercomplex cells were termed "end-stopping" and "side-inhibition" or surround suppression, which we will explain it in depth in the following sections. Simple cells that are more common in L4C and L6 (Ringach et al., 2002; Martinez et al., 2005) have spatially distinct on and off rectangular subfields, while complex cells that are more populated in other layers have overlapping excitatory and inhibitory regions (Hubel and Wiesel, 1968).

V1 RFs are also selective to other stimulus attributes, such as orientation, spatial frequency, spatial phase, and temporal frequency. As mentioned earlier, these parameters can be independently studied by drifting sinusoidal gratings. In the former experiments that were performed by Hubel and Wiesel, the **orientation selectivity** of V1 cells was also explored. V1 cells elicit significant spiking when a bar of light was shown in a specific orientation and their responses were decreased below baseline when the orientation was gradually changed to orthogonal relative to the preferred orientation (Hubel and Wiesel, 1959, 1968). The alignment of the circular center-surround RF of presynaptic cells in LGN

on a target V1 cell is thought to produce orientation tuning in V1 (Figure 1.4-A) (Hubel and Wiesel, 1962). Figure 1.4-B represents an example orientation tuning curve.

In addition to orientation, **contrast** is a dominant visual feature that drives V1 neurons. It is defined as the difference between the lowest and highest luminance of the visual stimuli (Palmer, 1999). The contrast controls the balance of excitation and inhibition causing changes in the RF size (see section 1.2.5). Another property of V1 neurons, **spatial frequency** is defined as light/dark cycles per degree of visual angles (Palmer, 1999). The spatial frequency of V1 cells varies in the range of 0.5-8° (Foster et al., 1985) at eccentricities of 2-5°, and is broadly tuned. **Spatial phase**, which is the position of the sinusoid relative to a reference point, is a dominant property of simple cells. Simple cells respond to specific phase of sinusoidal gratings, in which the opposite phase inhibits the response to the baseline. Instead, complex cells do not show selectivity to on and off subfield, so they are not selective to spatial phase. Also, V1 neurons respond to the speed and movement direction of drifting gratings. **Temporal frequency** is the speed of movement of the bars in each second measured in cycles/seconds. In V1 temporal frequency varies in the range of 0.5-16 (cycles/seconds). Some V1 cells are also **direction selective,** responding to one direction of movement.

In the next section we will investigate some characteristics of RFs across layers.

1.2.3 The Receptive Field Properties Across V1 Layers

The receptive field properties across layers have been studied since the former reports (Hubel and Wiesel, 1962, 1968) introducing orientation and ocular dominance columns. Later, other studies observed distinct orientation selectivity across layers being broader in layers 4C, L3B, and L5 (Ringach et al., 2002). Investigating the dynamics of orientation

tuning, Ringach et al.(1997) reported that the orientation tuning develops in time, being sharper in 30-40ms and persisting for 40-85ms, specifically in output layers (2, 3, 4B, 5, and 6). But orientation tuning in input layers 4Cα and 4Cβ does not change and remains broad. This result suggests that sharpness of orientation tuning, which is due to suppression of other orientations, is emerged by intracortical V1 connections or feedback projections.

Similar to cats, it is observed that simple cells are denser in L4C and L6 of primates' V1 (Ringach et al., 2002; Martinez et al., 2005). In addition, there is broad spatial frequency tuning in V1 (De Valois et al., 1982), which is preserved across the cortical column, so different layers are acting as different spatial filters. There is also heterogeneity in the tuning of temporal frequency across layers. However, if recorded vertically all layers have similar RF (Hubel and Wiesel, 1968), while there are slight changes in the size of RF across layers being larger in L6. Thus, because of variations in physiological characteristics between V1 layers, the idea of V1 being structured by homogenous building blocks such as columns is reevaluated.

1.2.4 Surround (Extra-Classical Surround) of V1 cells

Stimulation of RF by a prolonged bar of light changed the spiking pattern (mostly decreased) of V1 cells. Hubel and Wiesel named the cells that showed this effect as "hypercomplex" cells (Hubel and Wiesel, 1968). However, the region around the classical RF was named extra-classical surround and was observed in most of V1 cells (Blakemore and Tobin, 1972; Maffei and Fiorentini, 1976; Nelson and Frost, 1978; Allman et al., 1985; Gilbert and Wiesel, 1990; Li et al., 2001). The effects of surround regions are modulatory meaning that there would be no activation of spikes (i.e., similar to baseline) when the

surrounding region is stimulated in isolation but costimulation of RF and surround would modulate the response. This modulation is either suppressive or facilitatory. In this dissertation, we focused on the mechanisms that generate surround modulation (SM), specifically suppression in Chapters 2 and 4.

1.2.5 Spatial Extent of the RF and the Surround

It is crucial to define the border between the RF and surround to study its underlying mechanisms that are different from the RF (Fitzpatrick, 2000). One way to map the RF is to use a small stimulus (flashing light or dark bar or a grating) that has the proper orientation for the cell to evoke spikes. This method is called minimum response field (mRF) because it covers the low threshold excitatory field of the cell (Hubel and Wiesel, 1962; Barlow et al., 1967). Later, the high threshold excitatory field was introduced, which does not evoke responses in the absence of mRF stimulation (Bringuier et al., 1999). To map this region of the visual field covering both mRF and high threshold region, size tuning curves (Figure 1.5-A) of V1 cells are obtained. To probe the size tuning curve a circular high contrast grating at varying radii will be centered on the mRF. A typical V1 cell increases its spiking rate up to a peak and then decreases its response to larger radii (surround suppression effect). We refer to this peak as high contrast summation RF (h-sRF, black curve in Figure 1.5-A), which at parafoveal eccentricities is two to three times larger than mRF (Angelucci et al., 2002). At a specific radius, the size tuning curve asymptotes referred to the extent of surround region.

Stimulating the summation RF with low contrast gratings lead to a larger peak size of the size-tuning curve with a reduction in spike rate at all radii. The peak at low contrast

referred to l-sRF is twofold larger than the h-sRF (gray curve in Figure 1.5-B) (Sengpiel et al., 1997; Sceniak et al., 1999; Angelucci and Shushruth, 2014).

1.2.6 Near Surround and Far Surround Definitions

As a result of the contrast dependent sRF size, there would be a region between h-sRF and l-sRF that could be either facilitatory (low contrast) or suppressive (high contrast; the orange region in Figure 1.5-A). We refer to this region as "near" surround. The region beyond the l-sRF is referred to as far surround. The near surround extends to 2-3° while far surround extends to 12° in radius in V1.

1.2.7 Modulatory Effects of the Surround

The strength of surround modulation (SM) that is reported to be suppressive or facilitatory depends on many factors such as contrast of the surround grating, its distance from RF (i.e., near vs. far) and the relative orientation between RF and surround gratings (Nurminen and Angelucci, 2014).

There is disagreement about the factors that affect the sign of surround modulation, for example, what leads to **facilitation** or **suppression?** Stimulating the mRF and near surround region with oriented bars (at the cell preferred orientation) that are aligned collinearly in visual space with each other, facilitates neuronal firing rates compared with sRF stimulation (known as "collinear facilitation"). This effect is stronger when the mRF is stimulated by low contrast gratings, but changes to suppression with high contrast mRF (Kapadia et al., 2000; Mizobe et al., 2001). This can be explained by the definition of near surround, in which at low contrast any stimulus in this region would activate the cell's RF,

and at high contrast it would be suppressive due to engaging inhibitory circuits (Fitzpatrick, 2000; Cavanaugh et al., 2002a; Angelucci and Bullier, 2003). However, there is another facilitatory effect by stimulation of the far surround at 12°, which is distinct from the low contrast near surround (Ichida et al., 2007; Shushruth et al., 2012).

The sign or strength of surround modulation also depends on the **contrast** of the stimulus inside the RF and surround. For instance, if the RF is strongly stimulated by a high contrast grating at the preferred orientation, regardless of the surround contrast the effect would be suppressive (DeAngelis et al., 1994; Sengpiel et al., 1998; Sceniak et al., 2001; Cavanaugh et al., 2002a; Ichida et al., 2007; Shushruth et al., 2009). Though, simulating both center and surround with low contrast leads to facilitation in most cases. In particular, Ichida et al.(2007) showed that if an optimally orientated RF is at low contrast near the cell's contrast threshold and the surround is stimulated by low contrast annular grating facilitation happens; decreasing the surround contrast causes stronger facilitation while increasing the width of surround annuli alters the effect to suppression.

Two main sets of stimuli have been used to measure the **strength and spatial extent** of the surround. (1) The expanding grating patch, which is broadly used because the peak of the curve would be indicative of RF size and the asymptotic point would be an indicative of surround size, and (2) the expanding annular grating in which the outer diameter of the grating is fixed but the inner diameter is decreased systematically. The annulus diameter at which the response falls to 2SD below center-only response is defined to be the full extent of surround. The disadvantage of the former stimuli is that activating both near and far surround would not let us investigate each surround region properties independently. However, the annular grating, by masking the near surround reveals the weak suppression

as a result of far surround stimulation. The average surround size used with the expanding patch at parafoveal eccentricities of macaque V1 is ~1.6° that reaches 3° (Cavanaugh et al., 2002a; Levitt and Lund, 2002; Shushruth et al., 2009), but the average surround size using annular gratings is larger at 5.5° and maximizes at 12.5°.

Generally, it has been shown that near surround suppression (Sceniak et al., 2001; Shushruth et al., 2009) is much stronger than far surround suppression in monkeys (mean of 58% vs. 25%) (Shushruth et al., 2009). Additionally, annular grating in the surround at similar **orientation** as the center, draws the maximum suppression from the cell, while the suppression decreases or turns to facilitation if the orientation difference between RF and surround increases (Sillito et al., 1995). In most of the studies, the orientation tuning of SM was addressed with the stimuli that was covering both near and far surround. However, using annular gratings, we recently showed that near surround is more sharply orientation tuned than far surround in a population of suppressive cells (Shushruth et al., 2013) (Chapter 2). We will discuss this effect in more detail in Chapter 2.

A few number of studies investigated the SM orientation sensitivity by changing the orientation of both RF and surround. Sillito et al.(1995) reported that strongest suppression occurs when stimuli in both RF and surround are of the same orientation, regardless of being optimal for the cell. Shushruth et al.(2012), reinvestigated this effect and found that orientation of SM is more selective to relative orientation rather than absolute RF orientation, but RF orientation affects the strength. In particular, iso-oriented RF and surround suppressed the cell even if it was not the preferred orientation. Contrast also affects orientation tuning of SM, the low contrast RF stimulation makes the SM tuning broader (Cavanaugh et al., 2002b; Hashemi-Nezhad and Lyon, 2012).

Overall, measuring the spatial extent of the surround needs a precise mapping of RF assuming the contrast level. For example, one would study near surround when RF is stimulated at high contrast so that there would be no activation of RF. Also, the behavior of the surround depends on other attributes such as relative orientation. The main question in this thesis is to understand how V1 is encoding these attributes as an interaction of global information (i.e. surround stimuli) with the local one (i.e. RF) across its layers. In the next section, we will review the anatomical and physiological mechanisms underlying SM.

1.3 Underlying Mechanisms of Surround Modulation

1.3.1 The Role of Feedforward Connections from LGN

Spatially restricted thalamocortical terminations of magno- and parvocellular axons in L4Cα and L4Cβ connect the regions of LGN and V1 that have similar RF (Perkel et al., 1986). It is proposed that LGN feedforward connections are contributing to the spatial and tuning properties of V1 neuronal RFs (Hubel and Wiesel, 1962; Bauer et al., 1999; Reid and Usrey, 2004). As mentioned in section 1.2.1, in addition to center-surround LGN property, LGN cells have an extra-classical surround that is strongly suppressive and non-linear, which is thought to play as a contrast gain control for V1 RFs (Solomon et al., 2002; Bonin et al., 2005; Sceniak et al., 2006). This LGN surround is probably relayed from the retina, and intrinsic lateral LGN connections (Alitto and Usrey, 2008) and not from the cortex (Ozeki et al., 2004). Comparing the size of LGN surround with that of V1 suggests that LGN surround (0.8° at parafoveal eccentricities) is at most contributing to the near surround (averaging 1.6° using expanding patch, refer to section 2.5.3). Combining electrophysiological and anatomical methods, Angelucci and colleagues (2002)

investigated the circuits underlying the RF and surround. They measured, using single unit recordings, the extent of the RF and surround of cells in V1, and then injected viral tracers at the recorded locations. Using published values of magnification factor and RF scatter in V1 and extrastriate cortex, they were able to convert the cortical extent of horizontal and feedback connections to the injected site into visual field extent. They compared the visuotopic extent of the connections with the extent of the RF and surround at the injected locations. In a subsequent study, (Angelucci and Sainsbury, 2006), also compared the extent of V1 RF and surrounds with the spatial extent of feedforward axons from the LGN. These studies demonstrated that the extent of thalamocortical afferents is commensurate with the size of V1 RF and the near surround (Figure 1.5-B green arrows), suggesting that feedforward connections contribute to, but cannot account for the full surround size. Moreover, it was shown that blockade of intra-V1 inhibition did not eliminate the surround suppression in the near region (Ozeki et al., 2004). This suggests that LGN is contributing to near surround suppression.

Webb et al.(2005) showed that there are two components to the surround suppression in V1, the untuned and orientation tuned. The more spatially restricted surround that is untuned can be mediated by LGN but due to the fact that LGN surrounds are less orientation specific than cortical surround (Ozeki et al., 2009), the tuned component arise strongly by cortical circuits. This result was confirmed by another group (Xing et al., 2005), who measured the latency of tuned and untuned surround suppression and found that untuned surround suppression is as fast as excitatory RF signal but the tuned element is 17ms later. This result was also replicated by Henry et al. (2013) demonstrating that the tuning emerges in the second 25ms bin after excitation of RF, while the untuned component

emerges in the first 25ms .

Moreover, activation of visual field optimal to V1 cells, suppresses LGN cells that have smaller RF. So at the peak of size tuning curve, the thalamic inputs are already suppressed but do not result in suppression at V1. It is proposed that the untuned early component of surround with strict spatial extent, observed specifically in input layers, is partly originated by geniculocortical inputs (Webb et al., 2005; Xing et al., 2005). While spatially broader and orientation-specific surround might have cortical origins (Angelucci and Shushruth, 2014).

1.3.2 The Role of Intra-V1 Horizontal Connections

Horizontal connections that arise from excitatory pyramidal neurons in L2/3, L4B, upper 4Cα and 5, link regions over several millimeters (Rockland and Lund, 1983). The properties of the horizontal connections are well studied in L2/3 but there are much less known in other layers. These long-range connections in L2/3 are patchy (Rockland and Lund, 1983) and link neurons with similar orientation preference (Malach et al., 1993). The RFs of the linked neurons are aligned along an axis collinear with the optimal orientation (Bosking et al., 1997), which would suit to result in collinear facilitation. Furthermore, horizontal connections of L2/3 contact both excitatory and inhibitory neurons (McGuire et al., 1991) that would be useful for both suppression and facilitation effects of surround. However, in the same study that was mentioned in section 1.3.1, Angelucci et al.(2002) showed that the extent of monosynaptic horizontal connections are commensurate with the near surround but it cannot monosynaptically take account for far surround.

A number of studies reported the physiological properties of these connections and compared them with the latency of SM. The chain of polysynaptic horizontal connections is also not a good candidate for far surround because their conduction velocity, 0.1-0.3 m/s (Grinvald et al., 1994; Bringuier et al., 1999; Slovin et al., 2002) is smaller than observed temporal dynamics of far SM. In particular, 12° far surround in parafoveal V1 which equals to 29mm in the cortex (magnification factor of $2.3\frac{mm}{^\circ}$ at 5° eccentricity) (Connolly and Van Essen, 1984) would take 290 ms to reach RF via horizontal connections with 0.1 m/s (97 ms at 0.3 m/s); while the onset of fast far surround suppression is reported to be 9-60ms (Bair et al., 2003). But the timing of horizontal connections encompassing 3mm of the cortex (Angelucci et al., 2002), would match the latency of near surround suppression which is about 10-30ms. In sum, the spatial extent, dynamics and other connection properties of horizontal connections are well suited to generate near surround suppression.

1.3.3 The Role of Feedback Connections

Initially, it has been assumed that feedback contributes predominantly in higher order perceptual tasks, such as figure-ground segregation (Self et al., 2013) and cognitive functions, such as visual attention (Roelfsema et al., 1998; McAdams and Reid, 2005; Roelfsema et al., 2007). Remarkably, attention enhances the neuronal responses to salient features (McAdams and Maunsell, 1999; Maunsell and Treue, 2006) which are thought to be conveyed by feedback.

Recently, it has been purported that the top-down stream is playing a dominant role in visual processing, specifically serves as one of the main mechanisms of far SM in V1 (Bullier et al., 2001; Angelucci et al., 2002; Bair et al., 2003; Angelucci and Bressloff,

2006). First, feedback contacting both excitatory and inhibitory neurons does not drive V1 cells but modulate their responses to RF stimulation (Sandell and Schiller, 1982; Hupé et al., 2001; Gonchar and Burkhalter, 2003). Second, the spatial extent of feedback to V1 is well matched to the size of far surround (Angelucci et al., 2002; Angelucci and Sainsbury, 2006); specifically, V2, V3, and MT have larger RFs than V1 and activation of SM would activate their RFs sending back information from a visual field of 5,10, and 25 times larger than h-sRF of V1 cells. Third, inactivation of area MT (Hupé et al., 1998), area V2 and V3 by reversible cooling of the cortex (Nassi et al., 2013) reduces surround suppression in monkeys. Fourth, using electrical stimulation of V1 and V2, feedback conduction velocities were measured at 2-6m/s that are 10-20 times faster than horizontal connections (Girard et al., 2001), making them better estimator of temporal dynamics of far surround.

However, there are still many controversies about the properties of feedback connections to V1, for example, some showed that V2-V1 are patchy and orientation specific (Angelucci et al., 2002; Shmuel et al., 2005; Angelucci and Bressloff, 2006) while others showed that they are anatomically divergent (Rockland and Pandya, 1979; Maunsell and Van Essen, 1983) and orientation-unspecific (Stettler et al., 2002). One hypothesis is that there might be layer-specific feedback channels having distinct characteristics.

In sum, based on the model (Figure 1.5-B) proposed by Angelucci et al.(2006) and years of evidence, all feedforward, horizontal, and feedback connections are integrated to produce RF and surround specific properties. These connections are contributing based on their spatiotemporal scales. The thalamocortical feedforward connections arise by LGN cells are mainly contributing to the h-sRF of V1 neurons (light green arrows in Figure 1.5-B). Near surround is generated by all connections including LGN afferents, monosynaptic

horizontal connections and feedback connections. However, the temporal profile of near surround is compatible with being mainly generated by LGN and horizontal connections (red arrows in Figure 1.5-B). Far surround modulation is mainly generated by feedback connections from the extrastriate cortex (blue arrows in Figure 1.5-B). In addition, the feedback and horizontal connections are also contributing to RF properties but at later stages than feedforward afferents. In sum, feedforward, horizontal, and feedback connections are contributing to computation of SM based on different spatiotemporal scales.

1.4 Synaptic Mechanisms of Surround Modulation

In addition to identifying the underlying circuits of SM, understanding its synaptic mechanisms is of essential importance for disentangling the processing of sensory stimuli. To date, there has been a good deal of debate about the synaptic mechanisms of these circuits resulting to different SM properties such as contrast dependent facilitation and its orientation selectivity. Intracellular recordings, as well as computational models enabled the field to examine the underlying synaptic mechanisms of SM.

There are two main hypothesis stating increase in inhibition or withdrawal of recurrent excitation. For example, activating the V1 RF and surround would suppress LGN cells causing withdrawal of feedforward excitation (0.8˚ LGN surround vs. 1.6˚ V1 near surround size). As it is also mentioned earlier, LGN is contributing in the fast and untuned surround suppression of near surround.

Ozeki et al. (2009) proposed a model explaining the steady state decrease in both excitation and inhibition that was initially affected by transient increase in inhibition, which

was observed experimentally(Anderson et al., 2001). The model is based on the balance of recurrent excitation by recurrent inhibition in V1 (Ozeki et al., 2009). Recently, optogenetic stimulation of horizontal connections of L2/3 pyramids in mouse V1, enhanced activation of somatostatin inhibitory cells which led to suppression of contacting pyramidal cells, and thus caused surround suppression (Adesnik et al., 2012).

Former mechanistic models also proposed that, the suppression at high contrast and facilitation at low contrast are mainly generated by imbalance of the excitatory and inhibitory responses (Stemmler et al., 1995; Somers et al., 1998). In both models, excitatory and inhibitory cells are contacted by the horizontal connections of other hypercolumns. In response to weak visual inputs the inhibitory cells are not activated while the excitation from the surround causes facilitation; this is in line with low contrast facilitation observed in extracellular recordings (Levitt and Lund, 2002; Ichida et al., 2007; Shushruth et al., 2009). While the strong inputs such as high contrast stimuli, would evoke both inhibitory and excitatory cells causing suppression. The effect is explained by inhibitory cells reaching their higher threshold (relative to excitatory cells) and subsequently fire action potentials to inhibit excitatory post synaptic targets. Later on, Schwabe and colleagues (2006) elaborated on Somers's model and added the contribution of feedback connections to the larger spatial extent of the surround. The model could take account for most of different effects that were obtained by experimentalists such as, fast suppression of the far surround (Bair et al., 2003), suppression and facilitation from the far surround (Ichida et al., 2007; Shushruth et al., 2009) and contrast dependent suppression (Levitt and Lund, 1997; Cavanaugh et al., 2002a; Schwabe et al., 2010). In addition, Nassi et al. (2014) showed that the corticocortical feedback increases the spatial extent of surround

suppression.

In sum, the feedforward LGN cells contribute in untuned surround suppression via withdrawal of excitation mostly, while horizontal and feedback connections contacting on both inhibitory and excitatory cells are contributing to SM via recurrent excitation, inhibition loops.

1.4.1 LFP, Gamma Oscillations, and Surround Suppression

Lately, there are various reports about the frequency contents of local field potentials (LFP) as a reflective of synaptic mechanisms. In particular, it is proposed that the fast-spiking inhibitory neurons like GABA-A basket cells are contributing to the generation of gamma (30-100 Hz) rhythmic activity (Galarreta and Hestrin, 1999; Gieselmann and Thiele, 2008). These basket cells are thought to be the main source of lateral inhibition in the neocortex (Markram et al., 2004). But also excitatory pyramidal cells with their distal dendrites are the main contributor to current sink and sources generating LFP (Berens et al., 2008). The new proposal is that inhibitory interneurons contacting on the pyramidal membranes are generating and maintaining the rhythmic inhibition, which by itself were driven by strong excitation (Bartos et al., 2007; Fries et al., 2007).

Moreover, Gieselmann and Theile (2008) , has shown that gamma band is reflective of surround modulation in primates. While the spiking activity decreased, due to stimulation of surround by expanding grating disk, the gamma power increased. The increase in the gamma power during surround suppression observed in spiking activity, suggested an inhibitory source for gamma activity.

Feedforward, horizontal, and feedback connections that are thought to serve into

surround modulation might generate the rhythmic recurrent activity reflected in the population LFP. Specially, long-range patchy horizontal projections contacting on both excitatory and inhibitory neurons might be the contributor to gamma increase in the population activity while generating suppression in spiking activities (Gieselmann and Thiele, 2008). Optogenetic stimulation of different cell types in vivo as well as simultaneous patch clamping of inhibitory and excitatory neurons, would shed light on the synaptic mechanisms that generate rhythmic oscillations.

In the next two sections, we will describe roles of SM in perception and what is known about computation of RF and surround across V1 layers.

1.5 Role of Surround Modulation in Perception

In the visual cortex, global attributes can help to disambiguate local information that is coded at the level of the neuronal receptive field. Dissimilar stimuli in the RF and surround, like stimulation of RF by preferred orientation and surround by orthogonal, would enhance neuronal responses. A number of reports suggested that surround modulation is playing an important role in visual saliency and pop-out perceptual tasks (Knierim and Van Essen, 1992; Nothdurft et al., 1999). Specifically, orientation-tuned surround modulation is one of the best examples of contextual modulation (Albright and Stoner, 2002; Bair et al., 2003) which results in the initial processing of figure-ground segregation (Lamme, 1995) at the object boundaries (Nothdurft et al., 2000). Using texture defined stimuli, Lamme et al. (1995) and Zipser et al. (1996) claimed that when RF was on the figure, neuronal responses were higher compared when it was on the ground, although they were identical stimuli. Thus, they proposed that V1 responses encode early processing of figure-ground

segregation.

Another perceptual phenomena, “contour integration” is thought to have basis on the collinear facilitation observed in V1. Collinear facilitation is reported when near surround was activated by iso-oriented stimuli as RF. Kapadia et al.(1995) performed psychophysical studies in humans as well as electrophysiological recordings in monkey V1. They placed collinear flankers around a target line which was addressing Gestalt principles of good continuation, that is, “continuous contours make object salient from the background” (Hess and Field, 1999). The flankers decreased the detection threshold (enhancing detectability) in human subjects and increased V1 neuronal responses to an iso-oriented line segment inside the RF. These behaviors of neuronal and perceptual measures implies that surround modulation in a specific stimulus set up would contribute to detection of boundaries.

1.6 Role of V1 Layers in Computation of Surround Modulation

Although there are some homogenous physiological properties across the cortical column such as similar RF location or same preferred orientation, still many other functional characteristics such as temporal frequency, spatial frequency, density of simple versus complex cells, and orientation selectivity vary across layers (Rodman et al., 2001; Ringach et al., 2002) (see section 1.2.3). In addition, the structural diversity of each laminae including different cell types (pyramids vs. stellates and various inhibitory neurons), cell densities, and connection patterns including inputs, projection targets and feedback connections makes scientist to reevaluate their view of the cortical column as a stack of interconnected layers with lots of heterogeneity (Xing et al., 2012). In spite of huge body

of literature about V1 since 1950, still, there is an open question how different layers are contributing in the processing of visual signals.

Despite the fact that surround modulation is observed in all V1 layers (Sceniak et al., 2001; Levitt and Lund, 2002) , there are some differences across layers of V1 (Ichida et al., 2007). Using annular gratings, it is observed that the far surround size, averaging at 5.5+-2.64° in V1, was significantly smaller in input layer 4C than other layers (Shushruth et al., 2009). Moreover, suppression index of iso-oriented gratings was larger in layers above L4B than deeper layers in both near and far surround (SI_{patch} >0.6 and $SI_{annulus}$ >0.35, Figure 1.6). Thus, physiological properties of different surround regions vary across layers of V1 reflecting that they might have different anatomical circuits.

Furthermore, as discussed previously, there are distinct projection patterns of bottom-up, top-down and intrinsic connections across layers. Extrastriate cortex (V2, V3, MT, and V4) sends back information to V1, which is a bidirectional path to the feedforward information from V1 (Felleman and Van Essen, 1991). Superficial and deep layers of extrastriate cortex send the feedback projections to V1 layer 1, L2A, L5B, and L6 with sparser ones in L4B and L3 (Ungerleider and Desimone, 1986; Federer et al., 2015). While the thalamic inputs terminate in L4C. Hence, studying the functional and mechanistic properties of V1 layers will help to undermine the sub-serving circuit of SM. In general, understanding the processing of visual information by different layers of V1 would shed light on how the sensory system takes advantage of its laminar network capacity.

In this thesis, we study the role of different V1 layers in computation of near and far surround stimulation. In Chapter 2, we specifically measure the orientation selectivity of the two surround elements across layers and then in Chapter 3, we examine whether the

temporal dynamics of inputs to cortical layers reflect the underlying feedback, feedforward and intrinsic V1 connections. In Chapter 4, we ask in which layer does the orientation selectivity of surround regions first emerge? and whether it is similar to the emergence of the untuned suppression. Studying the time course of surround modulation, and its spatial extent (near versus far regions) across the layers of V1 will provide robust basis on both functional and structural properties of the proposed circuits. In Chapter 5, we investigate whether the frequency content of inputs reflects different circuits underlying collinear and non-colliner surround that is thought to be important in contour integration tasks. And finally, in Chapter 6, we provide a summary of the findings of this thesis and propose future directions.

1.7 References

Adesnik H, Bruns W, Taniguchi H, Huang ZJ, Scanziani M (2012) A neural circuit for spatial summation in visual cortex. Nature 490:226-231.

Albright TD, Stoner GR (2002) Contextual influences on visual processing. Ann Rev Neurosci 25:339-379.

Alitto HJ, Usrey WM (2008) Origin and dynamics of extraclassical suppression in the lateral geniculate nucleus of the macaque monkey. Neuron 57:135-146.

Allman J, Miezin F, Mc Guinness E (1985) Stimulus specific responses from beyond the classical receptive field: Neurophysiological mechanisms for local-global comparisons in visual neurons. Ann Rev Neurosci 8:407-430.

Anderson JS, Lampl I, Gillespie DC, Ferster D (2001) Membrane potential and conductance changes underlying length tuning of cells in cat primary visual cortex. J Neurosci 21:2104-2112.

Angelucci A, Bullier J (2003) Reaching beyond the classical receptive field of V1 neurons: horizontal or feedback axons? J Physiol (Paris) 97:141-154.

Angelucci A, Bressloff PC (2006) The contribution of feedforward, lateral and feedback connections to the classical receptive field center and extra-classical receptive field

surround of primate V1 neurons. Prog Brain Res 154:93-121.

Angelucci A, Sainsbury K (2006) Contribution of feedforward thalamic afferents and corticogeniculate feedback to the spatial summation area of macaque V1 and LGN. J Comp Neurol 498:330-351.

Angelucci A, Shushruth S (2014) Beyond the classical receptive field: surround modulation in primary visual cortex. In: The New Visual Neurosciences (Chalupa LM, Werner JS, eds), pp 425-444. Cambridge: MIT press.

Angelucci A, Levitt JB, Walton E, Hupé JM, Bullier J, Lund JS (2002) Circuits for local and global signal integration in primary visual cortex. J Neurosci 22:8633-8646.

Bair W, Cavanaugh JR, Movshon JA (2003) Time course and time–distance relationships for surround suppression in macaque V1 neurons. J Neurosci 23:7690-7701.

Barlow HB, Blakemore C, Pettigrew JD (1967) The neural mechanisms of binocular depth discrimination. J Physiol 193:327-342.

Bartos M, Vida I, Jonas P (2007) Synaptic mechanisms of synchronized gamma oscillations in inhibitory interneuron networks. Nat Rev Neurosci 8:45-56.

Bauer U, Scholz M, Levitt JB, Lund JS, Obermayer K (1999) A model for the depth dependence of receptive field size and contrast sensitivity of cells in layer 4C of macaque striate cortex. Vision Res 39:613-629.

Berens P, Keliris GA, Ecker AS, Logothetis NK, Tolias AS (2008) Comparing the feature selectivity of the gamma-band of the local field potential and the underlying spiking activity in primate visual cortex. Front Syst Neurosci 2:2.

Blakemore C, Tobin EA (1972) Lateral inhibition between orientation detectors in the cat's visual cortex. Exp Brain Res 15:439-440.

Blasdel GG, Salama G (1986) Voltage-sensitive dyes reveal a modular organization in monkey striate cortex. Nature 321:579-585.

Bonin V, Mante V, Carandini M (2005) The suppressive field of neurons in lateral geniculate nucleus. J Neurosci 25:10844-10856.

Bosking WH, Zhang Y, Schofield B, Fitzpatrick D (1997) Orientation selectivity and the arrangement of horizontal connections in tree shrew striate cortex. J Neurosci 17:2112-2127.

Bringuier V, Chavane F, Glaeser L, Frégnac Y (1999) Horizontal propagation of visual activity in the synaptic integration field of area 17 neurons. Science 283:695-699.

Bullier J, Hupé J-M, James AC, Girard P (2001) The role of feedback connections in shaping the responses of visual cortical neurons. Prog Brain Res 134:193-204.

Callaway EM (2005) Structure and function of parallel pathways in the primate early visual system. J Physiol (Lond) 566:13-19.

Carandini M, Demb JB, Mante V, Tolhurst DJ, Dan Y, Olshausen BA, Gallant JL, Rust NC (2005) Do we know what the early visual system does? J Neurosci 25:10577-10597.

Casagrande VA, Kaas JH (1994) The afferent, intrinsic, and efferent connections of primary visual cortex. In: Primary Visual Cortex of Primates (Peters A, Rockland KS, eds), pp 201-259. New York, NY: Plenum Press.

Cavanaugh JR, Bair W, Movshon JA (2002a) Nature and interaction of signals from the receptive field center and surround in macaque V1 neurons. J Neurophysiol 88:2530-2546.

Cavanaugh JR, Bair W, Movshon JA (2002b) Selectivity and spatial distribution of signals from the receptive field surround in macaque V1 neurons. J Neurophysiol 88:2547-2556.

Connolly M, Van Essen D (1984) The representation of the visual field in parvicellular and magnocellular layers of the lateral geniculate nucleus in the macaque monkey. J Comp Neurol 226:544-564.

Dacey DM, Packer OS (2003) Colour coding in the primate retina: diverse cell types and cone-specific circuitry. Curr Opin Neurobiol 13:421-427.

De Valois RL, Albrecht DG, Thorell LG (1982) Spatial frequency selectivity of cells in macaque visual cortex. Vision Res 22:545-559.

DeAngelis GC, Freeman RD, Ohzawa I (1994) Length and width tuning of neurons in the cat's primary visual cortex. J Neurophysiol 71:347-374.

Federer F, Merlin S, Angelucci A (2015) Anatomical and functional specificity of V2-toV1 feedback circuits in the primate visual cortex. Soc Neurosci Abstr Online.

Felleman DJ, Van Essen DC (1991) Distributed hierarchical processing in the primate cerebral cortex. Cereb Cortex 1:1-47.

Fitzpatrick D (2000) Seeing beyond the receptive field in primary visual cortex. Curr Opin Neurobiol 10:438-443.

Foster K, Gaska JP, Nagler M, Pollen D (1985) Spatial and temporal frequency selectivity of neurones in visual cortical areas V1 and V2 of the macaque monkey. J Physiol

365:331-363.

Fries P, Nikolić D, Singer W (2007) The gamma cycle. Trends Neurosci 30:309-316.

Fries W, Keizer K, Kuypers H (1985) Large layer VI cells in macaque striate cortex (Meynert cells) project to both superior colliculus and prestriate visual area V5. Exp Brain Res 58:613-616.

Galarreta M, Hestrin S (1999) A network of fast-spiking cells in the neocortex connected by electrical synapses. Nature 402:72-75.

Gieselmann MA, Thiele A (2008) Comparison of spatial integration and surround suppression characteristics in spiking activity and the local field potential in macaque V1. Eur J Neurosci 28:447-459.

Gilbert CD (1983) Microcircuitry of the visual cortex. Ann Rev Neurosci 6:217-247.

Gilbert CD, Wiesel TN (1990) The influence of contextual stimuli on the orientation selectivity of cells in primary visual cortex of the cat. Vision Res 30:1689-1701.

Girard P, Hupé JM, Bullier J (2001) Feedforward and feedback connections between areas V1 and V2 of the monkey have similar rapid conduction velocities. J Neurophysiol 85:1328-1331.

Gonchar Y, Burkhalter A (2003) Distinct GABAergic targets of feedforward and feedback connections between lower and higher areas of rat visual cortex. J Neurosci 23:10904-10912.

Grinvald A, Lieke EE, Frostig RD, Hildesheim R (1994) Cortical point-spread function and long-range lateral interactions revealed by real-time optical imaging of macaque monkey primary visual cortex. J Neurosci 14:2545-2568.

Guillery R, Sherman SM (2002) Thalamic relay functions and their role in corticocortical communication: generalizations from the visual system. Neuron 33:163-175.

Hashemi-Nezhad M, Lyon DC (2012) Orientation tuning of the suppressive extraclassical surround depends on intrinsic organization of V1. Cereb Cortex 22:308-326.

Henry CA, Joshi S, Xing D, Shapley RM, Hawken MJ (2013) Functional characterization of the extraclassical receptive field in macaque V1: contrast, orientation, and temporal dynamics. J Neurosci 33:6230-6242.

Hess R, Field D (1999) Integration of contours: new insights. Trends Cogn Sci 3:480-486.

Hirsch JA, Martinez LM, Pillai C, Alonso J-M, Wang Q, Sommer FT (2003) Functionally distinct inhibitory neurons at the first stage of visual cortical processing. Nat

Neurosci 6:1300-1308.

Hubel DH, Wiesel TN (1959) Receptive fields of single neurones in the cat's striate cortex. J Physiol 148:574-591.

Hubel DH, Wiesel TN (1962) Receptive fields, binocular interaction and functional architecture in the cat's visual cortex. J Physiol (Lond) 160:106-154.

Hubel DH, Wiesel TN (1965) Receptive fields and functional architecture in two nonstriate visual areas (18 and 19) of the cat. J Neurophysiol 28:229-289.

Hubel DH, Wiesel TN (1968) Receptive fields and functional architecture of monkey striate cortex. J Physiol (Lond) 195:215-243.

Hubel DH, Wiesel TN (1974) Sequence regularity and geometry of orientation columns in the monkey striate cortex. J Comp Neurol 158:267-293.

Hupé JM, James AC, Girard P, Bullier J (2001) Response modulations by static texture surround in area V1 of the macaque monkey do not depend on feedback connections from V2. J Neurophysiol 85:146-163.

Hupé JM, James AC, Payne BR, Lomber SG, Girard P, Bullier J (1998) Cortical feedback improves discrimination between figure and background by V1, V2 and V3 neurons. Nature 394:784-787.

Ichida JM, Schwabe L, Bressloff PC, Angelucci A (2007) Response facilitation from the "suppressive" receptive field surround of macaque V1 neurons. J Neurophysiol 98:2168-2181.

Kandel ER, Schwartz JH, Jessell TM, Siegelbaum SA, Hudspeth A (2000) Principles of neural science: McGraw-hill New York.

Kapadia MK, Westheimer G, Gilbert CD (2000) Spatial distribution of contextual interactions in primary visual cortex and in visual perception. J Neurophysiol 84:2048-2062.

Kapadia MK, Ito M, Gilbert CD, Westheimer G (1995) Improvement in visual sensitivity by changes in local context: parallel studies in human observers and in V1 of alert monkeys. Neuron 15:843-856.

Kaplan E, Purpura K, Shapley RM (1987) Contrast affects the transmission of visual information through the mammalian lateral geniculate nucleus. J Physiol 391:267.

Knierim JJ, Van Essen D (1992) Neuronal responses to static texture patterns in area V1 of the alert macaque monkey. J Neurophysiol 67:961-980.

Lamme VAF (1995) The neurophysiology of figure-ground segregation in primary visual

cortex. J Neurosci 15:1605-1615.

Levitt JB, Lund JS (1997) Contrast dependence of contextual effects in primate visual cortex. Nature 387:73-76.

Levitt JB, Lund JS (2002) The spatial extent over which neurons in macaque striate cortex pool visual signals. Vis Neurosci 19:439-452.

Li W, Thier P, Wehrhahn C (2001) Neuronal responses from beyond the classic receptive field in V1 of alert monkeys. Exp Brain Res 139:359-371.

Lund JS, Wu CQ (1997) Local circuit neurons of macaque monkey striate cortex: IV. Neurons of laminae 1-3A. J Comp Neurol 384:109-126.

Lund JS, Lund RD, Hendrickson AE, Bunt AH, Fuchs AF (1975) The origin of efferent pathways from the primary visual cortex, area 17, of the macaque monkey as shown by retrograde transport of horseradish peroxidase. J Comp Neurol 164:287-303.

Maffei L, Fiorentini L (1976) The unresponsive regions of visual cortical receptive fields. Vis Res 16:1131-1139.

Malach R, Amir Y, Harel M, Grinvald A (1993) Relationship between intrinsic connections and functional architecture revealed by optical imaging and in vivo targeted biocytin injections in primate striate cortex. Proc Natl Acad Sci USA 90:10469-10473.

Markram H, Toledo-Rodriguez M, Wang Y, Gupta A, Silberberg G, Wu C (2004) Interneurons of the neocortical inhibitory system. Nat Rev Neurosci 5:793-807.

Martinez LM, Wang Q, Reid RC, Pillai C, Alonso JM, Sommer FT, Hirsch JA (2005) Receptive field structure varies with layer in the primary visual cortex. Nat Neurosci 8:372-379.

Maunsell JH, Treue S (2006) Feature-based attention in visual cortex. Trends Neurosci 29:317-322.

Maunsell JHR, Van Essen DC (1983) The connections of the middle temporal visual area (MT) and their relationship to a cortical hierarchy in the macaque monkey. J Neurosci 3:2563-2586.

McAdams CJ, Maunsell JH (1999) Effects of attention on orientation-tuning functions of single neurons in macaque cortical area V4. J Neurosci 19:431-441.

McAdams CJ, Reid CR (2005) Attention modulates the responses of simple cells in monkey primary visual cortex. J Neurosci 25:11023-11033.

McGuire BA, Gilbert CD, Rivlin PK, Wiesel TN (1991) Targets of horizontal connections in macaque primary visual cortex. J Comp Neurol 305:370-392.

Mizobe K, Polat U, Pettet MW, Kasamatsu T (2001) Facilitation and suppression of single striate-cell activity by spatially discrete pattern stimuli presented beyond the receptive field. Vis Neurosci 18:377-391.

Nassi JJ, Callaway EM (2009) Parallel processing strategies of the primate visual system. Nat Rev Neurosci 10:360-372.

Nassi JJ, Lomber SG, Born RT (2013) Corticocortical feedback contributes to surround suppression in V1 of the alert primate. J Neurosci 33:8504-8517.

Nassi JJ, Gomez-Laberge C, Kreiman G, Born RT (2014) Corticocortical feedback increases the spatial extent of normalization. Front Syst Neurosci 8:105.

Nelson JI, Frost B (1978) Orientation selective inhibition from beyond the classical visual receptive field. Brain Res 139:359-365.

Nothdurft HC, Gallant JL, Van Essen DC (1999) Response modulation by texture surround in primate area V1: Correlates of "popout" under anesthesia. Vis Neurosci 16:15-34.

Nothdurft HC, Gallant JL, Van Essen DC (2000) Response profiles to texture border patterns in area V1. Vis Neurosci 17:421-436.

Nurminen L, Angelucci A (2014) Multiple components of surround modulation in primary visual cortex: multiple neural circuits with multiple functions? Vision Res 104:47-56.

Orban GA (2008) Higher order visual processing in macaque extrastriate cortex. Physiol Rev 88:59-89.

Ozeki H, Finn IM, Schaffer ES, Miller KD, Ferster D (2009) Inhibitory stabilization of the cortical network underlies visual surround suppression. Neuron 62:578-592.

Ozeki H, Sadakane O, Akasaki T, Naito T, Shimegi S, Sato H (2004) Relationship between excitation and inhibition underlying size tuning and contextual response modulation in the cat primary visual cortex. J Neurosci 24:1428-1438.

Palmer SE (1999) Vision science: Photons to phenomenology: MIT press.

Perkel DJ, Bullier J, Kennedy H (1986) Topography of the afferent connectivity of area 17 in the macaque monkey: a double-labelling study. J Comp Neurol 253:374-402.

Reid RC, Usrey WM (2004) Functional connectivity in the pathway from retina to striate

cortex. In: The Visual Neurosciences (Chalupa LM, Werner JS, eds), pp 673-679. Cambridge, MA: MIT Press.

Ringach DL, Hawken MJ, Shapley R (1997) Dynamics of orientation tuning in macaque primary visual. Nature 387:5.

Ringach DL, Shapley RM, Hawken MJ (2002) Orientation selectivity in macaque V1: diversity and laminar dependence. J Neurosci 22:5639-5651.

Rockland KS, Pandya DN (1979) Laminar origins and terminations of cortical connections of the occipital lobe in the rhesus monkey. Brain Res 179:3-20.

Rockland KS, Lund JS (1983) Intrinsic laminar lattice connections in primate visual cortex. J Comp Neurol 216:303-318.

Rodieck RW, Rodieck RW (1998) The first steps in seeing: Sinauer Associates Sunderland, MA.

Rodman HR, Sorenson KM, Shim AJ, Hexter DP (2001) Calbindin immunoreactivity in the geniculo-extrastriate system of the macaque: implications for heterogeneity in the koniocellular pathway and recovery from cortical damage. J Comp Neurol 431:168-181.

Roelfsema PR, Lamme VA, Spekreijse H (1998) Object-based attention in the primary visual cortex of the macaque monkey. Nature 395:376-381.

Roelfsema PR, Tolboom M, Khayat PS (2007) Different processing phases for features, figures, and selective attention in the primary visual cortex. Neuron 56:785-792.

Sandell JH, Schiller PH (1982) Effect of cooling area 18 on striate cortex cells in the squirrel monkey. J Neurophysiol 48:38-48.

Sceniak MP, Hawken MJ, Shapley RM (2001) Visual spatial characterization of macaque V1 neurons. J Neurophysiol 85:1873-1887.

Sceniak MP, Chatterjee S, Callaway EM (2006) Visual spatial summation in macaque geniculocortical afferents. J Neurophysiol 96:3474-3484.

Sceniak MP, Ringach DL, Hawken MJ, Shapley R (1999) Contrast's effect on spatial summation by macaque V1 neurons. Nat Neurosci 2:733--739.

Schwabe L, Obermayer K, Angelucci A, Bressloff PC (2006) The role of feedback in shaping the extra-classical receptive field of cortical neurons: a recurrent network model. J Neurosci 26:9117-9129.

Schwabe L, Ichida JM, Shushruth S, Mangapathy P, Angelucci A (2010) Contrast-

dependence of surround suppression in macaque V1: Experimental testing of a recurrent network model. Neuroimage 52:777-792.

Self MW, van Kerkoerle T, Super H, Roelfsema PR (2013) Distinct roles of the cortical layers of area V1 in figure-ground segregation. Curr Biol 23:2121-2129.

Sengpiel F, Sen A, Blakemore C (1997) Characteristics of surround inhibition in cat area 17. Exp Brain Res 116:216-228.

Sengpiel F, Baddley RJ, Freeman TCB, Harrad R, Blakemore C (1998) Different mechanisms underlie three inhibitory phenomena in cat area 17. Vision Res 38:2067-2080.

Shapley R, Victor J (1978) The effect of contrast on the transfer properties of cat retinal ganglion cells. J Physiol 285:275.

Shmuel A, Korman M, Sterkin A, Harel M, Ullman S, Malach R, Grinvald A (2005) Retinotopic axis specificity and selective clustering of feedback projections from V2 to V1 in the owl monkey. J Neurosci 25:2117-2131.

Shoham D, Hübener M, Schulze S, Grinvald A, Bonhoeffer T (1997) Spatio–temporal frequency domains and their relation to cytochrome oxidase staining in cat visual cortex. Nature 385:529-533.

Shushruth S, Ichida JM, Levitt JB, Angelucci A (2009) Comparison of spatial summation properties of neurons in macaque V1 and V2. J Neurophysiol 102:2069-2083.

Shushruth S, Mangapathy P, Ichida JM, Bressloff PC, Schwabe L, Angelucci A (2012) Strong recurrent networks compute the orientation-tuning of surround modulation in primate primary visual cortex. J Neurosci 4:308-321.

Shushruth S, Nurminen L, Bijanzadeh M, Ichida JM, Vanni S, Angelucci A (2013) Different orientation-tuning of near and far surround suppression in macaque primary visual cortex mirrors their tuning in human perception. J Neurosci 33:106-119.

Sillito AM, Grieve KL, Jones HE, Cudeiro J, Davis J (1995) Visual cortical mechanisms detecting focal orientation discontinuities. Nature 378:492-496.

Sincich LC, Horton JC (2005) The circuitry of V1 and V2: integration of color, form and motion. Ann Rev Neurosci 28:303-326.

Slovin H, Arieli A, Hildesheim R, Grinvald A (2002) Long-term voltage-sensitive dye imaging reveals cortical dynamics in behaving monkeys. J Neurophysiol 88:3421-3438.

Solomon SG, White AJR, Martin PR (2002) Extra-classical receptive field properties of parvocellular, magnocellular, and koniocellular cells in the primate lateral geniculate nucleus. J Neurosci 22:338-349.

Somers DC, Todorov EV, Siapas AG, Toth LJ, Kim DS, Sur M (1998) A local circuit approach to understanding integration of long-range inputs in primary visual cortex. Cereb Cortex 8:204-217.

Somogyi P, Tamas G, Lujan R, Buhl EH (1998) Salient features of synaptic organisation in the cerebral cortex. Brain Res Brain 26:113-135.

Stemmler M, Usher M, Niebur E (1995) Lateral interactions in primary visual cortex: a model bridging physiology and psychophysics. Science 269:1877.

Sterling P (2004) How retinal circuits optimize the transfer of visual information. Vis Neurosci 2:234.

Stettler DD, Das A, Bennett J, Gilbert CD (2002) Lateral connectivity and contextual interactions in macaque primary visual cortex. Neuron 36:739-750.

Ungerleider LG, Desimone R (1986) Cortical connections of visual area MT in the macaque. J Comp Neurol 248:190-222.

Van Essen DC, Newsome WT, Maunsell JH (1984) The visual field representation in striate cortex of the macaque monkey: asymmetries, anisotropies, and individual variability. Vision Res 24:429-448.

Webb BS, Dhruv NT, Solomon SG, Taliby C, Lennie P (2005) Early and late mechanisms of surround suppression in striate cortex of macaque. J Neurosci 25:11666-11675.

Webb BS, Tinsley CJ, Barraclough NE, Easton A, Parker A, Derrington AM (2002) Feedback from V1 and inhibition from beyond the classical receptive field modulates the responses of neurons in the primate lateral geniculate nucleus. Vis Neurosci 19:583-592.

Xing D, Shapley RM, Hawken MJ, Ringach DL (2005) Effect of stimulus size on the dynamics of orientation selectivity in Macaque V1. J Neurophysiol 94:799-812.

Xing D, Shen Y, Burns S, Yeh CI, Shapley R, Li W (2012) Stochastic generation of gamma-band activity in primary visual cortex of awake and anesthetized monkeys. J Neurosci 32:13873-13880a.

Zipser K, Lamme VA, Schiller PH (1996) Contextual modulation in primary visual cortex. J Neurosci 16:7376-7389.

A

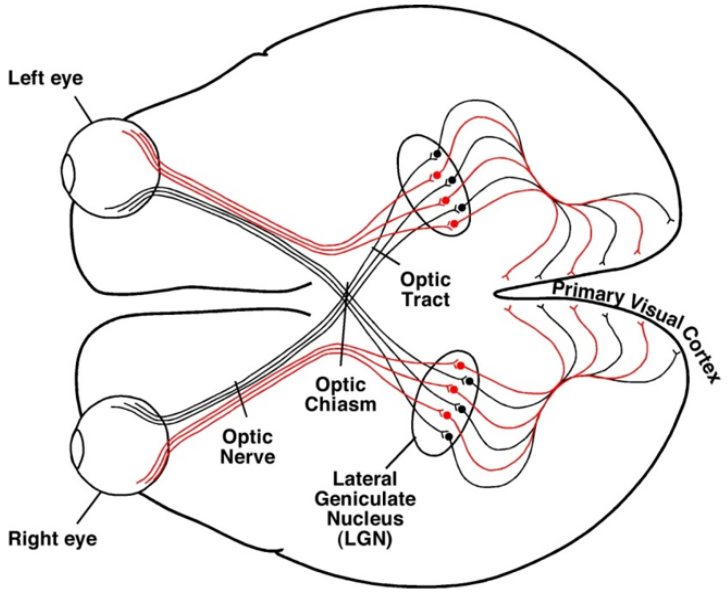

B C

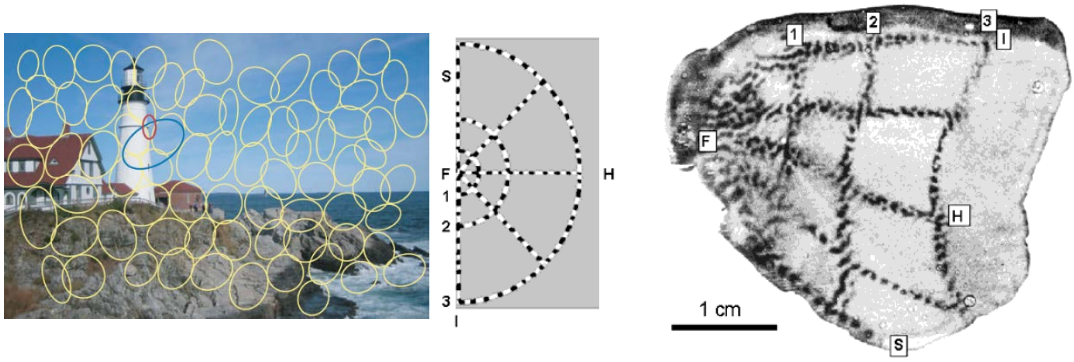

Figure 1.1: The flow of visual information along with visual field mapping and topography. A) Represents the flow of visual information from retina to the primary visual cortex passing through optic chiasm and LGN. B) Depicts the mosaic of RGC receptive fields (Nassi and Callaway, 2009), C) Topographical presentation of fovea and periphery in V1(Palmer, 1999).

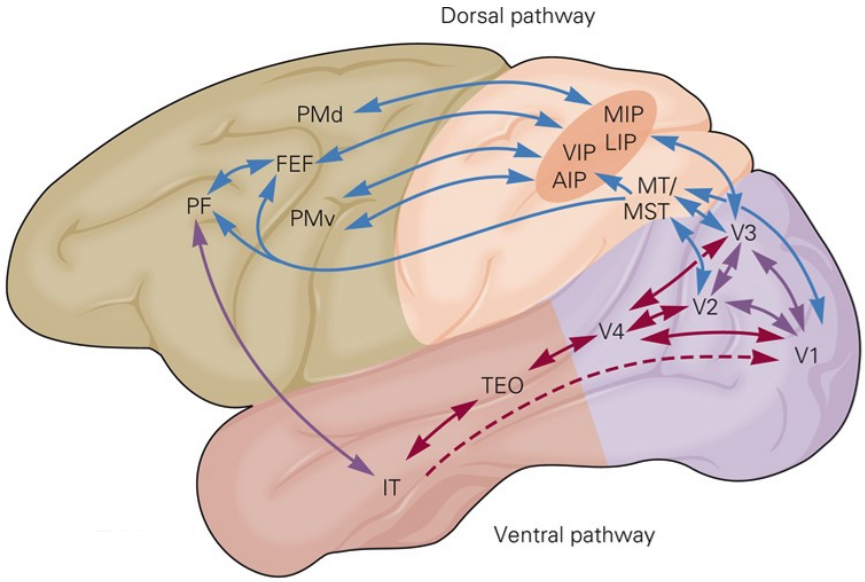

Figure 1.2: Shows dorsal and ventral streams with modifications from principal of neural sciences (Kandel et al., 2000).

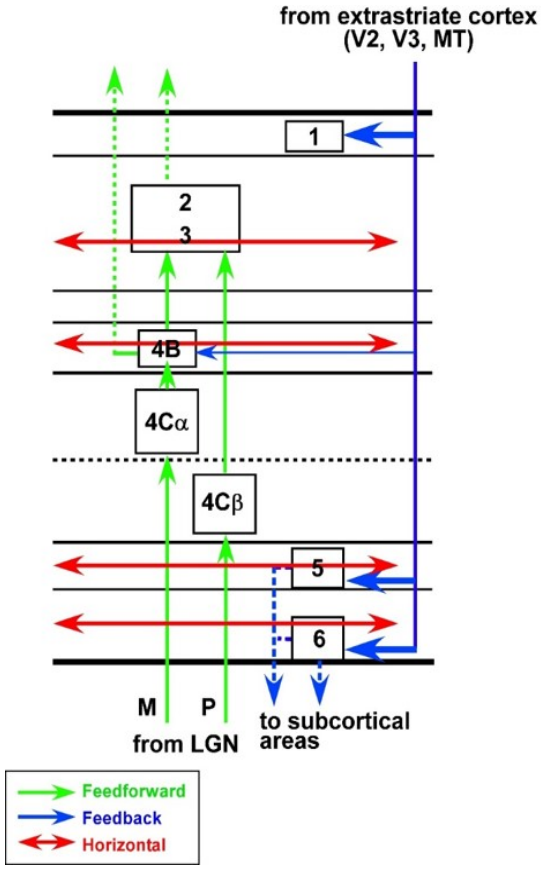

Figure 1.3 Simplified schematic of feedback, feedforward, and horizontal terminations across V1 layers.

A

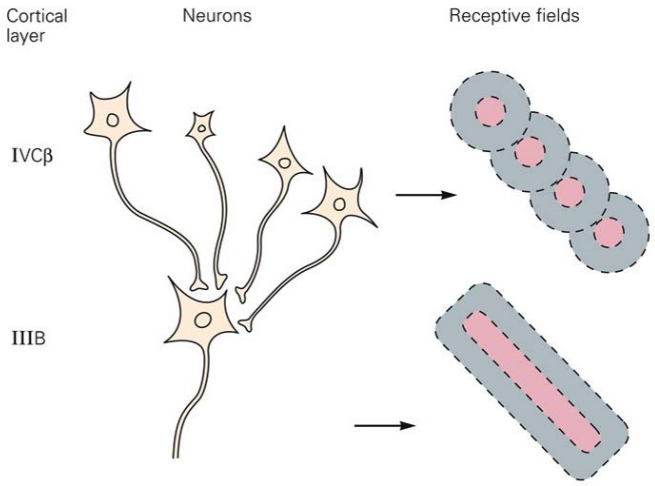

B

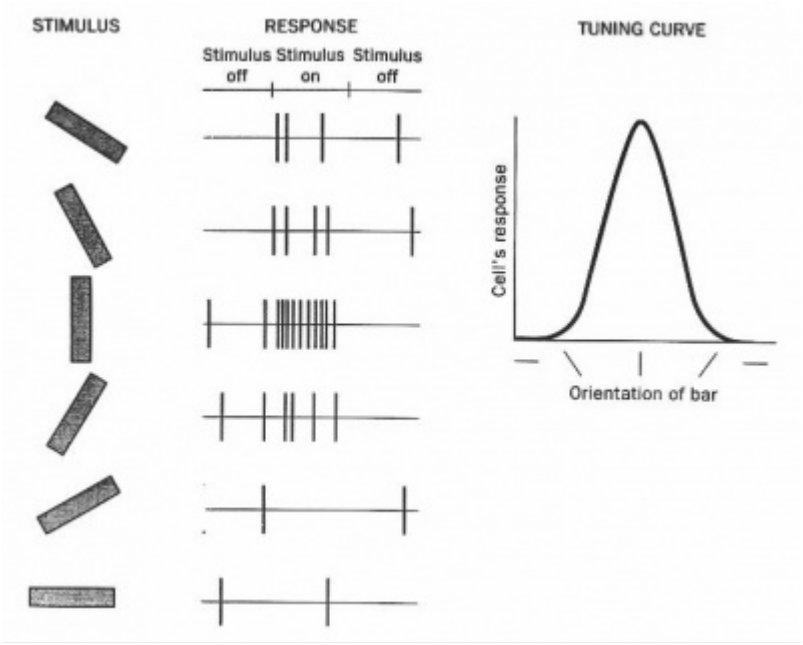

Figure 1.4: Orientation tuning of a V1 cell. A) Represents how alignment of the LGN on cells receptive field is generating orientation tuning at a V1 target cell (Kandel et al., 2000). B) Shows spike rates of a V1 cells preferentially responding to specific orientation of a bar. The right panel is an example orientation tuning curve (Hubel and Wiesel, 1959).

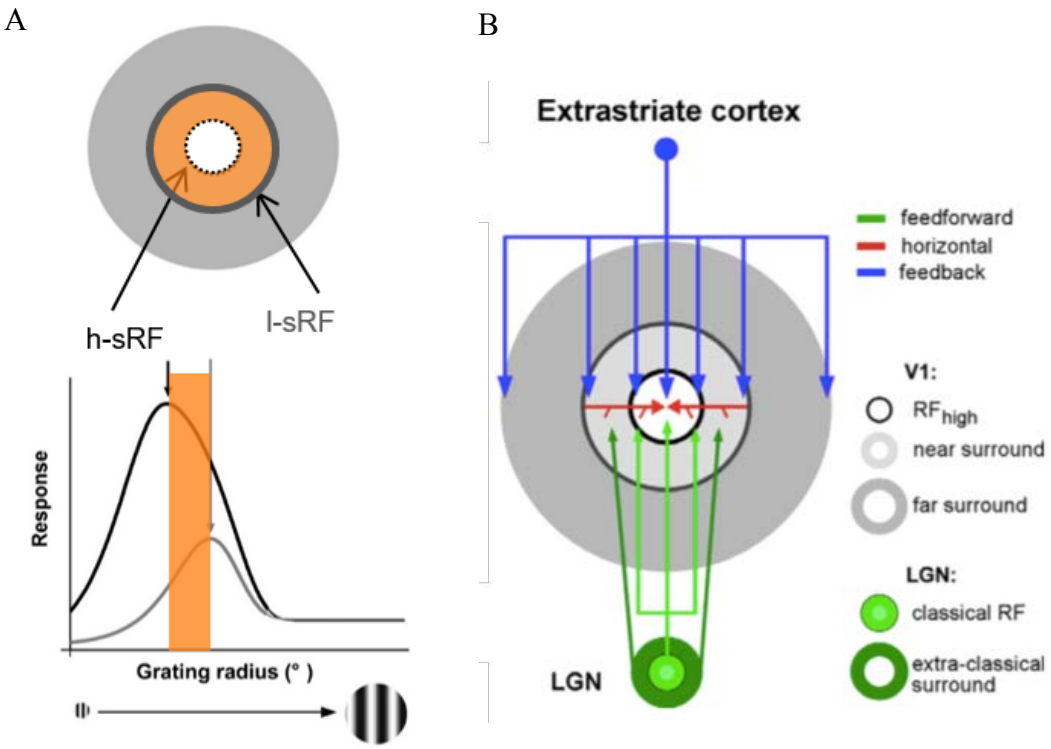

Figure 1.5: Different surround components A) The schematic of near surround (orange region) far surround (grey region) and h-sRF black dashed line, bottom panel shows an example size tuning curve. B) Proposed model of underlying circuit of surround modulation by Angelucci & Bresslof (2006)

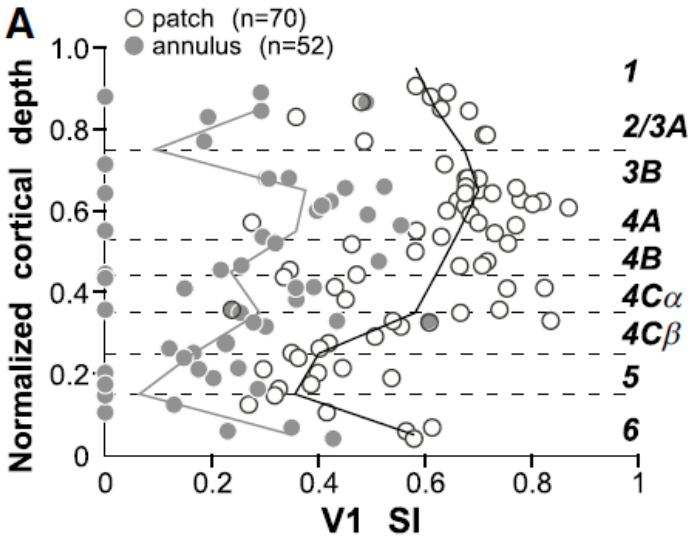

Figure 1.6 The strength of surround suppression probed by iso oriented grating patch (near surround) and iso-oriented annulus (far surround) (Shushruth et al., 2009).

CHAPTER 2

DIFFERENT ORIENTATION TUNING OF NEAR- AND FAR-SURROUND SUPPRESSION IN MACAQUE PRIMARY VISUAL CORTEX MIRRORS THEIR TUNING IN HUMAN PERCEPTION

Reprinted with permission from the Society for Neuroscience,

S. Shushruth, Lauri Nurminin, Jeniffer M.Ichida,

Simo Vanni, and Alessandra Angelucci

Journal of Neuroscience, 33(1): 106-119, 2013

106 • The Journal of Neuroscience, January 2, 2013 • 33(1):106–119

Systems/Circuits

Different Orientation Tuning of Near- and Far-Surround Suppression in Macaque Primary Visual Cortex Mirrors Their Tuning in Human Perception

S. Shushruth,[1]* Lauri Nurminen,[3]* Maryam Bijanzadeh,[1] Jennifer M. Ichida,[2] Simo Vanni,[3] and Alessandra Angelucci[2]

[1]Neuroscience Program and [2]Department of Ophthalmology and Visual Science, Moran Eye Center, University of Utah, Salt Lake City, Utah 84132, and [3]Brain Research Unit, O.V. Lounasmaa Laboratory, Aalto University, FI-00076 Helsinki, Finland

In primary visual cortex (V1), neuronal responses to stimuli inside the receptive field (RF) are usually suppressed by stimuli in the RF surround. This suppression is orientation specific. Similarly, in human vision surround stimuli can suppress perceived contrast of a central stimulus in an orientation-dependent manner. The surround consists of two regions likely generated by different circuits: a near-surround generated predominantly by geniculocortical and intra-V1 horizontal connections, and a far-surround generated exclusively by interareal feedback. Using stimuli confined to the near- or far-surround of V1 neurons, and similar stimuli in human psychophysics, we find that near-surround suppression is more sharply orientation tuned than far-surround suppression in both macaque V1 and human perception. These results point to a similarity between surround suppression in macaque V1 and human vision, and suggest that feedback circuits are less orientation biased than horizontal circuits. We find the sharpest tuning of near-surround suppression in V1 layers (3, 4B, 4Cα) with patterned and orientation-specific horizontal connections. Sharpest tuning of far-surround suppression occurs in layer 4B, suggesting greater orientation specificity of feedback to this layer. Different orientation tuning of near- and far-surround suppression may reflect a statistical bias in natural images, whereby nearby edges have higher probability than distant edges of being co-oriented and belonging to the same contour. Surround suppression would, thus, increase the coding efficiency of frequently co-occurring contours and the saliency of less frequent ones. Such saliency increase can help detect small orientation differences in nearby edges (for contour completion), but large orientation differences in distant edges (for directing saccades/attention).

Introduction

In primary visual cortex (V1), neuronal responses to stimulation of the receptive field (RF) are modulated by simultaneous stimulation of the RF surround (Blakemore and Tobin, 1972; Maffei and Fiorentini, 1976; Nelson and Frost, 1978; Allman et al., 1985). In human vision, spatial context alters the perceived contrast of a central target stimulus (Ejima and Takahashi, 1985; Chubb et al., 1989; Cannon and Fullenkamp, 1991) and contrast sensitivity (Snowden and Hammett, 1998; Petrov et al., 2005). Surround stimulation usually suppresses the cell's spiking response to a high-contrast grating in its RF (DeAngelis et al., 1994; Levitt and Lund, 1997; Sengpiel et al., 1997; Walker et al., 2000). This suppression is orientation specific, typically being strongest when the stimuli in the RF and surround are of similar orientation, and weakest when they are of orthogonal orientation (DeAngelis et al., 1994; Sillito et al., 1995; Sengpiel et al., 1997; Walker et al., 1999; Cavanaugh et al., 2002), even when the stimulus in the RF is at a suboptimal orientation for the recorded cell (Shushruth et al., 2012). In human vision, the strength of surround effects is similarly orientation-dependent (Cannon and Fullenkamp, 1991; Solomon et al., 1993; Petrov et al., 2005).

We previously suggested that the surround consists of two regions, termed "near' and "far" (based on their proximity to the RF), subserved by different anatomical circuits (Angelucci and Bressloff, 2006) (Fig. 1). Specifically, the large spatial extent (Levitt and Lund, 2002; Shushruth et al., 2009) and fast onset (Bair et al., 2003) of far-surround suppression in V1 suggest that this is generated by highly divergent (Angelucci et al., 2002) and fast-conducting (Girard et al., 2001) feedback connections from extrastriate cortex. The small spatial extent (Angelucci et al., 2002) and slow conduction velocity (Grinvald et al., 1994; Bringuier et al., 1999; Girard et al., 2001) of intra-V1 horizontal axons, instead, suggest they contribute only to near-surround modulation. Surround suppression in the LGN (Sceniak et al., 2006; Alitto and Usrey, 2008) also contributes to near-surround suppression in V1 (Ozeki et al., 2004). In human vision, surround suppression shows similar spatial extent as in macaque V1 (Nurminen et al., 2009).

Received May 22, 2012; revised Oct. 22, 2012; accepted Oct. 26, 2012.

Author contributions: S.S., L.N., S.V., and A.A. designed research; S.S., L.N., M.B., J.M.I., and A.A. performed research; S.S., L.N., and M.B. analyzed data; S.S., L.N., S.V., and A.A. wrote the paper.

We are grateful for support from the National Science Foundation (Grant IOS-0848106 to A.A.), the National Institute of Health (Grant EY015262 to A.A.), the Academy of Finland (Grants 124698, 218054, and 140726 to S.V.), the Finnish Graduate School of Neuroscience (to L.N.), the Academy of Finland National Programme for Centres of Excellence 2006-2011 (to L.N. and S.V.), and by a grant from Research to Prevent Blindness, Inc., to the Department of Ophthalmology, University of Utah. We thank Kesi Sainsbury for excellent histological assistance. We thank Dr. Sam Merlin for help with one experiment.

*S.S. and L.N. contributed equally to this work.

Correspondence should be addressed to Alessandra Angelucci, 65 Mario Capecchi Drive, Salt Lake City, UT 84132. E-mail: alessandra.angelucci@hsc.utah.edu.

S. Shushruth's present address: HHMI, University of Washington, Seattle, WA 98195.

DOI:10.1523/JNEUROSCI.2518-12.2013

 0270-6474/13/330106-14$15.00/0

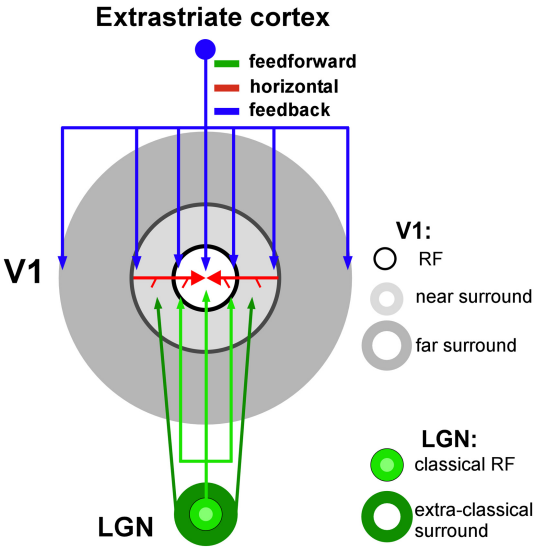

Figure 1. Presumptive anatomical circuits for surround modulation. Different components of the RF (white area) and surround (gray areas) of a V1 neuron, and their presumptive underlying circuits (arrows). Monosynaptic horizontal connections in V1 (red) extend into the near surround; their spread is commensurate with the size of a V1 neuron's spatial summation area measured at low contrast (Angelucci et al., 2002), which is on average about twice the diameter of the cell's RF, or spatial summation area measured at high contrast (Sceniak et al., 1999). The spread of feedforward connections to V1 from the LGN (Angelucci and Sainsbury, 2006) added to the size of suppressive surrounds of LGN cells (Sceniak et al., 2006; Alitto and Usrey, 2008) (dark green) is commensurate with a V1 cell's near surround. Interareal feedback connections (blue) are commensurate with the far surround (Angelucci et al., 2002) and contribute to all components of the RF and surround, but are the only connections contributing to the far surround.

Previous psychophysical and physiological studies of the orientation dependence of surround suppression have not distinguished between near- and far-surround stimulation. Thus, potential differences in the orientation tuning of these two regions are unknown. Here, using annular gratings confined to the near or far surround of macaque V1 neurons, and similar stimuli in human psychophysical experiments, we find that near-surround suppression is more sharply orientation tuned than far-surround suppression in both macaque V1 and human perception. These results suggest different orientation specificities of the circuits underlying near- and far-surround suppression, and point to an important relationship between surround suppression in V1 and human perception. V1 laminar differences in surround orientation tuning further suggest laminar-specific connectivity. The different tuning of near- and far-surround suppression may reflect a statistical dependency in the joint distribution of oriented elements in natural images and may serve different perceptual roles.

Materials and Methods

Electrophysiological recordings

Extracellular recordings were made from parafoveal (range: 3–9° eccentricity; mean: 5.7°) V1 of three (two males, one female) anesthetized (sufentanil citrate, 4–12 μg/kg/h) and paralyzed (vecuronium bromide, 0.1–0.3 μg/kg/h) macaque monkeys (*Macaca fascicularis*). All procedures conformed to the guidelines of the University of Utah Institutional Animal Care and Use Committee. The procedure of single-unit recording from V1 has been previously detailed (Shushruth et al., 2009). Briefly, animals were artificially respirated with a 30:70 mixture of O_2 and N_2O, and vital signs were monitored continuously. The pupils were dilated with topical atropine, the corneas were protected with rigid gas-permeable contact lenses, and the eyes were refracted. The locations of the foveas were plotted at the beginning of the experiment and periodically thereafter, using a reversible ophthalmoscope.

Single-unit recordings were made with Epoxylite-coated tungsten microelectrodes (4–6 MΩ; FHC). Spikes were conventionally amplified, bandpass filtered between 400 Hz and 5 kHz, and sampled at 22 kHz by a dual-processor G5 Power Macintosh computer running custom software (EXPO, https://sites.google.com/a/nyu.edu/expo) courtesy of Dr. Peter Lennie. Spikes were displayed on a monitor, and templates for discriminating spikes were constructed by averaging multiple traces. The timing of waveforms that matched the templates was recorded with an accuracy of 0.1 ms.

Visual stimuli. Sinusoidal gratings of the same mean luminance as the background were generated using the same software that recorded spikes and were displayed on a calibrated monitor (GDM-C520K, Sony) of mean luminance of ~45.7 cd/m^2, resolution of 1024 × 768 pixels, refreshed at 100 Hz, and placed at a viewing distance of 57 cm. For each cell, recordings were made through the dominant eye, with the nondominant eye covered. We first determined the preferred orientation, drift direction, and spatial and temporal frequencies. Then the area and center of the minimum response field (mRF) were carefully located quantitatively using a grating patch of 0.2° diameter. The area of the mRF was defined as the visual field region in which the small grating patch elicited a response at least 2 SDs above the spontaneous rate, and the geometric center of this area was defined as the mRF center. We performed spatial summation measurements at 75% contrast using a circular drifting grating patch of increasing radius centered over the cell's mRF (e.g., Fig. 2*A*, black solid curve). The patch radius ranged from 0.1 to 13° and consisted of 16 radii (in five steps of 0.1° from 0.1 to 0.6°, and then 0.75, 0.9, 1, 1.2, 1.8, 2.5, 5, 7.5, 10, and 13°). From these area summation functions for each cell, we extracted as a measure of RF size the patch radius at peak response (Fig. 2*A*, black arrow, corresponding to Fig. 2 *B*, *C*, radius of the center grating patch). We then measured the cell response to an annular grating stimulus of 2° thickness presented at varying distances from the RF, thus defined, in the absence of a central grating (Fig. 2*A*, purple curve). This procedure allowed us to determine the exact boundary of the RF excitatory zone (Fig. 2*A*, purple arrow, corresponding to Fig. 2*B*, purple circle, inner radius of the near-surround annulus), and to ascertain that surround stimuli presented alone outside this boundary did not evoke a spiking response from the cell.

The stimulus used to characterize the orientation tuning of near- and far-surround suppression consisted of a center circular grating patch matched to the RF diameter of the cell, surrounded by an annular grating presented in one of two possible configurations. In the near configuration (Fig. 2*B*), used to probe the near surround, the surround annular grating had an inner diameter of fixed size (purple circle), located 0.25° outside the border of the neuron's RF or just outside the boundary of the excitatory zone, whichever was larger, and an outer diameter (blue circles) of two sizes, i.e., 4° and 6°. In macaque, these diameters encompass the extent of most V1 neurons' horizontal connections (Angelucci et al., 2002) and the diameters of the suppressive surround fields for most LGN neurons (Sceniak et al., 2006; Alitto and Usrey, 2008). Therefore, this stimulus configuration maximized stimulation of the horizontal and feedforward connection-dominated near surround. In the far configuration (Fig. 2*C*), used to probe the far surround, the outer diameter of the surround annular grating was fixed in size and extended to the edge of the display (26°), while its inner diameter was of two sizes, i.e., 6° and 4° (Fig. 2*C*, blue circles); therefore, the surround stimulus activated spatially complementary regions to that of the near-surround stimulus. This stimulus configuration maximized stimulation of the far surround, presumably mediated by interareal feedback connections.

In both near- and far-surround configurations, the center and surround gratings were presented at the optimal spatial and temporal frequency for the neuron and at 75% contrast. The center grating (overlaying the RF) was always presented at the neuron's optimal orientation. The surround grating, instead, was presented at orientations

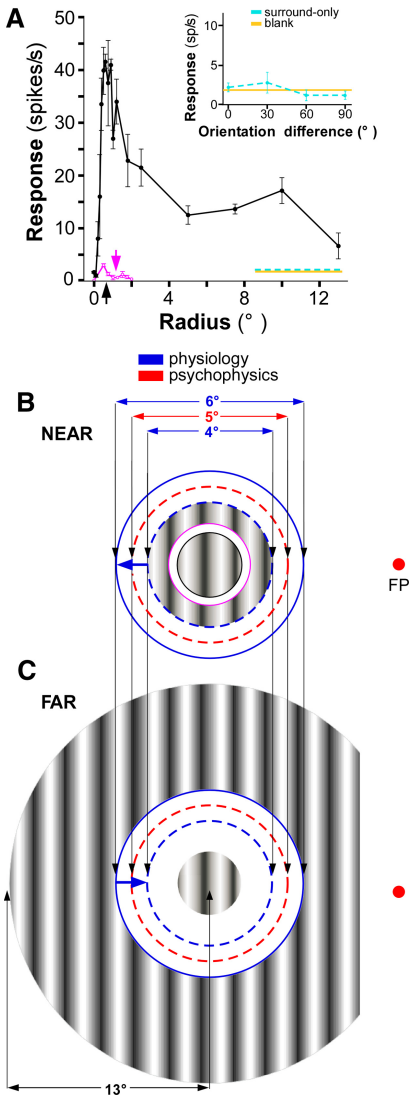

Figure 2. Visual stimuli used to characterize the orientation tuning of near- and far-surround suppression. ***A***, Area summation function for an example cell (same cell as in Fig. 5*C*). The black curve represents the cell response as a function of the radius of a grating patch centered on the mRF. The peak of this curve (marked by a black arrow) was taken to be the cell's RF radius and the center grating patch in ***B*** and ***C*** (marked by a solid black circle in ***B***) was set to be at this radius. The purple curve is the cell's response to an annular grating of 2° thickness presented alone as a function of its inner radius. The purple arrow marks the outer boundary of the RF excitatory zone, and it was the smallest radius of this annulus at which there was no response from the cell. The inner radius of the near-surround grating in ***B*** (purple circle) was set to be at this value or 0.25° outside the center grating, whichever was larger. Yellow line here and in the inset: spontaneous activity (i.e., response to the blank). Cyan line here and in the inset: response to a near4° surround grating alone (i.e., the grating marked by the dashed blue and purple circles in ***B***) at 0° center-surround orientation difference (in the main panel) or as a function of orientation difference (in the inset). Note the lack of response to the near-surround-only stimulus. ***B***, Near-surround configuration. For each recorded cell, the center grating was matched to the cell's RF diameter (black arrow in ***A***), and the annular grating in the surround was presented with an outer diameter of 4° and 6° (blue circles). For psychophysics experiments, the center grating diameter was fixed at 2°, and the inner (purple circle) and outer (red circle) diameters of the surround grating were 3° and 5°, respectively. Here and in the far ranging from optimal to orthogonal in 15° steps (seven conditions). Each stimulus was presented for 700 ms, with the first 200 ms consisting only of the center grating, and the surround grating appearing for the remaining 500 ms. The relative phase of the center and surround gratings was randomized, but phase should not affect responses, because there was a gap between the center and surround gratings. This gap prevents brightness induction at the border between the center and surround gratings, thus rendering the surround suppression phase insensitive (Ejima and Takahashi, 1985; Petrov and McKee, 2006). The interstimulus interval was 1 s. The delayed presentation enabled us to study the modulation of the steady-state response of the neuron, and to avoid ambiguities caused by the nonspecific response onset. The short presentation time also enabled us to examine these effects in a physiologically relevant time window, as the mean duration of fixations between saccades is ~350 ms (Gallant et al., 1998). Each stimulus was presented for 10 trials, and the response to each condition was calculated as the average of the response to each trial during the last 500 ms of the stimulus. Because of the short stimulus duration, neurons with preferred temporal frequencies of <2 cycles/s whose responses were strongly modulated by the temporal frequency of the stimulus (F1/F0 ratio >1) were not characterized with surround stimuli. Control conditions included a blank screen of the same luminance as the background for a measure of spontaneous activity (e.g., Fig. 2*A*, yellow line), a center-alone condition for a baseline response and surround annulus-alone conditions at all orientations and sizes, to ensure that the surround stimulus alone did not evoke a spiking response from the cell (e.g., Fig. 2*A*, dashed cyan line). A mask with the same luminance as the background was placed over the hemifield ipsilateral to the recorded hemisphere and extending 1.5° beyond the vertical meridian into the contralateral hemifield, to prevent recruitment of callosal connections by the far-surround grating (Fig. 2*C*).

Data analysis. Spike trains were imported into Matlab and analyzed using custom scripts. The strength of surround suppression for each stimulus orientation was expressed as a suppression index (SI), which was calculated as

$$SI(\theta) = 1 - \frac{R_{CS}}{R_C}$$

where θ is the surround orientation for the condition, R_C is the response to the center-only stimulus, and R_{CS} is the response to the center plus surround stimulus. Thus, SI = 0 indicates complete lack of suppression, whereas SI = 1 indicates that the cell's response was completely suppressed by the surround stimulus.

To characterize the orientation tuning of surround suppression, we used three complementary measures of orientation tuning: the circular variance (Cavanaugh et al., 2002; Ringach et al., 2002), the difference in suppression index (ΔSI), and the iso-orientation suppression fraction.

We calculated the circular variance (CV) as a measure of the orientation selectivity of surround suppression for each cell as

$$CV = \frac{\left|\sum_n (R_{max} - R_n)\exp(i\theta_n)\right|}{\sum_n (R_{max} - R_n)}$$

where R_{max} is the maximal response of the cell (typically the response to the center-only stimulus at the optimal orientation for the cell), and R_n is the response to the nth surround stimulus orientation. As we only presented seven surround orientations, θ_n was one of seven orientations

←

configuration the red dot indicates the location of the fixation point (FP) in the psychophysics experiment (6° from the center of the stimulus). ***C***, Far-surround configuration. The center grating was as in the near stimulus configuration. The surround grating had a 26° (electrophysiology) or 24° (psychophysics) outer diameter, and an inner diameter of two different sizes (6° and 4°, blue circles) for the electrophysiology experiments, but of 5° for the psychophysics experiments (red circle). The portion of the far-surround grating located between 1.5° from the vertical meridian in the hemisphere ipsilateral to the location of the stimulus to the contralateral hemisphere was masked, to avoid activation of callosal connections.

chosen to be equally spaced between 0 and 2π. This transformation projects the surround responses as vectors with equal angular separation along a circle, and hence, their normalized vector sum (CV) takes a value between 0 and 1. A CV of 1 indicates that suppression is seen at only one surround orientation, whereas a CV of 0 indicates either equal suppression at all surround orientations or no suppression at any orientation. Thus, CV is a global measure of the shape of the tuning curve.

ΔSI was calculated as the difference between the mean SI for surround orientations close to optimal (θ to $\theta + 15$) and the mean SI for surround orientations close to orthogonal ($\theta + 75$ to $\theta + 90$). This index is positive if the surround orientations close to optimal are more suppressive than the surround orientations close to orthogonal.

We defined iso-orientation suppression fraction for each cell as the area under the cell's suppression tuning curve between surround orientations of 0° and 30° as a fraction of the total area under the tuning curve (i.e., between surround orientations of 0° and 90°). This was calculated from fitting the suppression index tuning curves with Gaussians of the form

$$SI(\theta) = SI_{min} + ke^{-(\theta/\alpha)^2}$$

where SI_{min}, k, and α are the fitted parameters, and deriving the area under the fitted curves by numerical integration between the aforementioned surround orientation bounds. Thus, iso-orientation suppression fraction is a local measure of the sharpness of the tuning curve around its peak.

Statistical tests used to determine significance are reported in the Results, and, unless specified otherwise, the metrics reported are in terms of mean ± SEM.

Histology and electrode track reconstruction. Electrolytic lesions (1 μA for 30–40 s, tip negative) were made along the length of the each penetration to assign laminar location to recorded cells. Our electrode penetrations were angled approximately orthogonal to the pial surface. At the end of the experiment, the animal was killed with sodium pentobarbital and perfused transcardially with saline, followed by 4% paraformaldehyde for 15–20 min. The brain was exposed by removing the top of the skull, the animal's head was repositioned in the stereotaxic apparatus, and the brain was blocked in a plane parallel to that of the electrode tracks. The blocked brain was removed from the rest of the skull, postfixed in the same fixative overnight and sectioned at 40 μm parallel to the plane of blocking (i.e., a near-to-coronal plane). Alternate sections were stained for Nissl or cytochrome oxidase to reveal the V1 laminae. Electrode tracks were reconstructed by drawing lesions on each section using a camera lucida connected to a light microscope, and individual sections were aligned using vascular landmarks.

Psychophysics

Subjects. We report data from five subjects who participated in the current study. Subjects S1, S3, and S5 were naive to the purpose of the study. Subjects S2 and S4 were non-naive, and S2 was one of the authors of this study. Data from two additional inexperienced subjects was discarded because near-surround stimuli did not reliably suppress perceived contrast of the central stimulus. All subjects had normal or corrected-to-normal visual acuity.

Apparatus. The stimuli were displayed on a calibrated 22 inch Diamond Pro 2070 CRT monitor (NEC-Mitsubishi Electronics Display-Europe) via a Visage system (Cambridge Research Systems) that provides 14-bit grayscale resolution. The resolution of the monitor was 800 × 600 pixels (39.0 × 29.2 cm) at a 100 Hz refresh rate. The binocular viewing distance was stabilized to 68 cm with a chin rest.

Procedure. We used a contrast matching task, because this relates to the mean of the underlying response distribution better than contrast detection or discrimination paradigms (as discussed in Chen and Tyler, 2002). Such comparison assumes that neuronal firing rate is monotonically related to perceived contrast. However, differences between the psychophysical and electrophysiological approach, as well as possible interspecies differences, only allow for qualitative comparison between psychophysical and electrophysiological results.

Each trial began with a 300 ms presentation of the fixation point. After the initial fixation period, the fixation point disappeared for 100 ms. Then the fixation point appeared again simultaneously with either the test or the comparison stimulus. The test stimulus consisted of a center and a surround grating, while the comparison stimulus consisted of only the center grating. The temporal order of the test and the comparison stimulus were randomized. The stimulus duration was 300 ms, and the interstimulus interval was 1000 ms. At the end of a trial, the subjects indicated with a keyboard button press the interval in which the contrast of the center grating appeared higher. The subject's answer initiated the next trial. We measured the perceived contrast of the center grating using a two-interval staircase procedure. Specifically, if the subject indicated that the contrast of the comparison stimulus appeared higher than the contrast of the test stimulus, the contrast of the comparison stimulus was decreased. Likewise, if the comparison stimulus appeared to have lower contrast, its contrast was increased. There were two independently progressing staircases. A reversal point was defined as the contrast at which the direction of the staircase changed. The perceived contrast of the test center grating was defined as the mean of the last four reversal points of both staircases. The first two reversals were disregarded as practice.

Visual stimuli. Stimuli were similar to those used for the electrophysiological experiments. The test stimulus consisted of a center sinusoidal grating patch surrounded by an annular grating (Fig. 2*B*,*C*). The test center grating was always displayed at horizontal orientation. The orientation of the surround grating was varied from collinear to orthogonal (relative to the center) in 15° intervals. The Michelson contrast of the center grating was 20%, and that of the surround was 40%. These contrasts were selected to avoid saturation of V1 population contrast responses. The 20% contrast used here is above semi-saturation for approximately half of V1 cells (Albrecht and Hamilton, 1982). This contrast value is lower than that used for the physiology experiments. However, we expect this to have minor effects on the orientation tuning of surround suppression in contrast matching, because, at least in V1, the effect of contrast on the orientation tuning of suppression is small (Cavanaugh et al., 2002): it affects ~50% of cells and is not necessarily consistent across the cell population (Levitt and Lund, 1997). The spatial frequency of the center and surround gratings was 1 cycle per degree, relative spatial phase was fixed, and in phase the diameter of the center grating was 2°, and the stimuli were centered at 6° eccentricity. This eccentricity corresponds approximately to the mean of the distribution of eccentricities for the V1 cell population. In the near-surround configuration, the inner diameter of the surround annulus was 3° (Fig. 2*B*, purple circle) and its outer diameter was 5° (Fig. 2*B*, red circle). In the far-surround configuration, the inner diameter of the surround annulus was 5° (Fig. 2*C*, red circle) and its outer diameter was 24°. The far-surround stimulus was partially masked so that the display from 1.5° from the vertical meridian to the hemifield opposite to the stimuli had no luminance modulation (Fig. 2*C*). The comparison stimulus was identical to the center grating of the test stimulus except that its contrast was varied.

Data analysis. The orientation tuning of surround suppression was quantified as for V1 cells, but here spike rates were replaced with the corresponding perceived contrasts. In all figures, we report the mean of the four reversals for the four staircases (see above) and the SEs of these means. Bootstrapping was used for statistical testing because the number of subjects was relatively low. For statistical analysis of a given metric of orientation tuning (e.g., CV), data for near- and far-surround conditions were first pooled together. Corresponding to the number of subjects, two samples containing five values were randomly drawn with replacement, and the difference between the samples' means was computed. This procedure was repeated 10,000 times. The reported p values refer to the probability that the difference in the resampled means exceeded the actual measured difference.

Results

We characterized the orientation tuning of the suppression arising from the near- and far-surround in macaque V1 and compared it with near- and far-surround suppression of perceived contrast in humans using similar visual stimuli at similar retinal eccentricities.

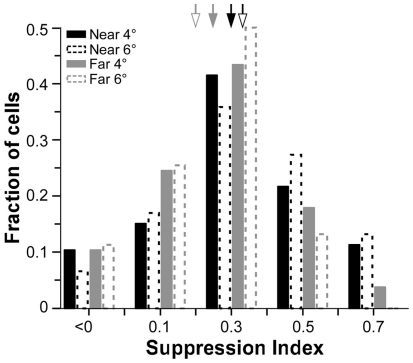

Figure 3. Distribution of suppression index across the cell population. SI was computed at 0° center-surround orientation difference for near- and far-surround stimuli of 4 and 6°, as color coded in the legend. Arrows: population means ($n = 106$ cells) as follows. Near4° (solid black arrow) = 0.3 ± 0.02; near6° (hollow black) = 0.33 ± 0.02; far4° (solid gray) = 0.25 ± 0.02; far6° (hollow gray) = 0.2 ± 0.03.

Orientation tuning of surround suppression in macaque V1 neurons and human perception

Electrophysiology

Extracellular single-unit recordings were made from 106 neurons in parafoveal V1 of three macaque monkeys. Center-surround stimuli were presented in two configurations (near and far), each at two surround stimulus sizes (Fig. 2). The near-surround grating activated a region larger than the V1 cells' peak spatial summation area measured at low contrast (the latter corresponding to the average extent of V1 horizontal connections), but commensurate with the extent of the suppressive extraclassical surround of LGN afferents (Fig. 1). The far-surround grating activated the surround region beyond that activated by the near-surround stimuli, i.e., beyond the range of horizontal and geniculocortical connections, but within the range of interareal feedback connections. We chose two different near- and far-surround grating sizes for this study (4° and 6°), because we wished to match for each cell the strength of suppression evoked by iso-oriented stimuli in the near and far surround, and previous studies have shown that far-surround suppression is weaker than near-surround suppression (Shushruth et al., 2009). Matching the strength of iso-orientation suppression for near- and far-surround stimulation allowed us to eliminate the possible confound that differences in orientation tuning of near- and far-surround suppression could simply arise as a result of differences in their suppression strength. Figure 3 indeed shows similar distributions for near- and far-surround suppression strengths (expressed as SI) across our population, at the surround sizes used in this study.

Figure 4*A* shows for one example V1 cell in layer 3B, the orientation tuning curves of near- and far-surround suppression. The response to the center grating presented alone is indicated by the purple horizontal line, while black and gray curves indicate the neuron response as a function of the difference in orientation between the center grating and the near- or far-surround grating, respectively. For this example cell, the near-surround grating suppressed the response to the center grating more strongly when the center and surround gratings were of similar orientation (orientation difference at or near 0°, or iso-orientation suppression) than when they were of orthogonal orientation (orientation difference at or near 90°, or ortho-orientation suppression). This

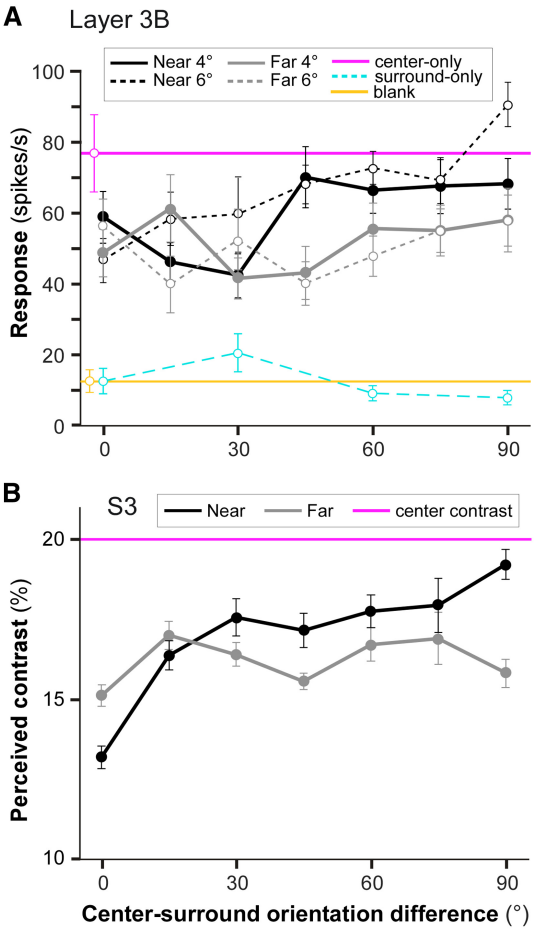

Figure 4. Orientation tuning of near- and far-surround suppression for an example V1 cell and an example human subject. ***A***, Response of an example V1 cell in layer 3B as a function of the orientation difference between the center and surround gratings. The black curves indicate the near-surround responses, the gray curves the far-surround responses, the purple line the center-only response, the cyan curve the response to a near4° surround grating alone, and the yellow line the spontaneous activity. ***B***, Perceived contrast for subject S3 as a function of the center-surround orientation difference. The purple line represents the actual contrast of the center stimulus.

was the case for both the near4° (solid black curve) and near6° (dashed black curve) surround stimuli. The near6° stimulus in addition caused a slight facilitation at orthogonal center-surround stimulus orientations. For the same cell, far4° (solid gray curve) and far6° (dashed gray curve) surround gratings presented at iso-orientation exerted similar response suppression as iso-oriented near-surround stimuli; however, far-surround gratings of ortho-orientation were more suppressive than ortho-oriented near-surround gratings. As a result, the orientation tuning curves for far-surround suppression were flatter than the tuning curves for near-surround suppression, i.e., far-surround suppression was more broadly orientation-tuned than near-surround suppression.

In Figure 5*A*, we show for the same cell as in Figure 4*A* the orientation-tuning curve for near- and far-surround suppression, but here tuning is expressed as SI as a function of the differ-

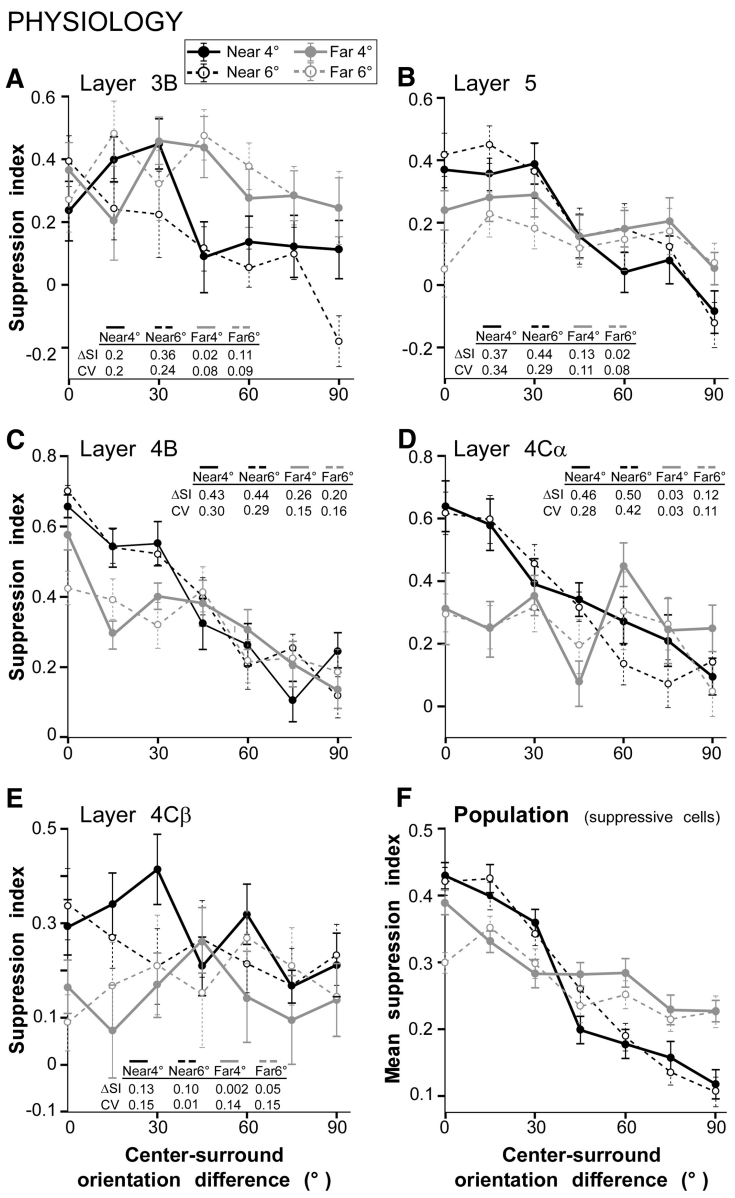

Figure 5. Orientation tuning of near- and far-surround suppression in V1. ***A–E***, Orientation tuning curves of near-surround (black curves) and far-surround (gray curves) suppression for five example V1 cells located in different V1 layers (as indicated). Solid and dashed curves indicate measurements performed for different surround stimulus sizes as indicated in the legend. The tuning functions are expressed as suppression index as a function of the difference in orientation between the stimuli in the RF and surround. The tables in each panel indicate for the specific cell the values of ΔSI and CV for near- and far-surround suppression. ***F***, Average tuning curves at each surround condition, for the population of V1 cells that showed surround suppression. Error bars are SEM. Mean ΔSI and CV for each surround conditions are as follows: 0.28 ± 0.03 and 0.24 ± 0.02 (near4°; $n = 68$ cells), 0.3 ± 0.03 and 0.25 ± 0.01 (near6°; $n = 68$ cells), 0.13 ± 0.02 and 0.12 ± 0.01 (far4°; $n = 65$ cells), 0.11 ± 0.01 and 0.14 ± 0.01 (far6°; $n = 54$ cells).

ence in orientation between the center and surround gratings. Note that in this format, a lower response of the cell corresponds to a larger value of SI, i.e., stronger suppression, and thus the tuning function in Figure 5*A* appears reversed compared with that in Figure 4*A* (larger SI at iso-orientation and smaller SI at orthogonal orientation). All tuning functions in the reminder of the article are expressed in this format. Figure 5*B–E* shows orientation tuning curves of near- and far-surround suppression for four additional representative V1 neurons at various laminar locations. For all cells in Figure 5, except the cell in Figure 5*E* (in layer 4Cβ), near-surround suppression was strongest at iso-orientation and weakest at orthogonal orientation. Similar results were obtained for near-surround suppression measured with either surround stimulus sizes (4° or 6° outer diameter). Far-surround suppression was significantly tuned for the layer 4B cell (Fig. 5*C*), but poorly tuned for all other cells (Fig. 5*A*,*B*,*D*,*E*). Despite diversity in the strengths of near- and far-surround suppression across these cells, for all cells far-surround suppression showed broader orientation tuning than near-surround suppression. To quantify this observation, we measured the ΔSI and CV for each cell (see Materials and Methods; values for each cell are reported in Fig. 5*A–E*). ΔSI is the difference in suppression index at iso-orientation versus at ortho-orientation, and thus has positive values when iso-orientation suppression is stronger than ortho-orientation suppression and negative values for stronger ortho- than iso-orientation suppression. The CV is a global measure of orientation selectivity, which can take values between 0, indicating no orientation selectivity, and 1, indicating that suppression occurs at only one surround orientation. Thus for example, for the layer 3B cell in Figure 5*A*, the ΔSI dropped from 0.36 for near-surround stimulation to 0.11 when only the far surround was stimulated, and the CV dropped from 0.24 to 0.09 (in the 6° near- and far-stimulus condition). For this cell, the broader tuning of far-surround suppression compared with near-surround suppression was due to an increase in the strength of ortho-orientation suppression, whereas iso-orientation suppression was unchanged. For the layer 5 and layer 4Cα cells (Fig. 5*B*,*D*), broader orientation tuning of the far surround, compared with the near-surround, resulted from both stronger ortho-orientation suppression and weaker iso-orientation suppression. Instead, for the layer 4B cell (Fig. 5*C*), the strength of iso-orientation suppression was markedly reduced for far-surround stimulation compared with near-surround stimulation, but ortho-orientation suppression was unchanged. Finally, the cell in layer 4Cβ (Fig. 5*E*) showed poor orientation tuning of both near- and far-surround suppression, with slightly weaker far-surround suppression at all

orientations. These differences in orientation tuning of near- and far-surround suppression across cells were reflective of laminar-specific differences we observed across the V1 population. These laminar differences are analyzed in a later section of the Results. In the next section, we first describe the V1 population data regardless of the neurons' laminar location, i.e., pooling neuronal responses across V1 layers.

Figure 5*F* shows the average tuning curves for near- and far-surround suppression for our V1 cell population, including only cells that showed surround suppression (defined as a mean response to center-surround orientation differences of 0° and 15° that was at least 1 SD below the center-only response at the optimal orientation). The ΔSI (0.28 ± 0.03) and CV (0.24 ± 0.02) for near-surround suppression measured using surround gratings of 4° outer diameter (near4° condition) were significantly higher than the ΔSI (0.13 ± 0.02) and CV (0.12 ± 0.01) for far-surround suppression measured with surround gratings of 4° inner diameter (far4° condition): $p < 10^{-5}$ for both comparisons (unpaired Student's *t* test). Similarly, ΔSI (0.30 ± 0.03) and CV (0.25 ± 0.01) for the near6° condition were significantly higher than ΔSI (0.13 ± 0.02) and CV (0.12 ± 0.01) for the far6° condition: $p < 10^{-8}$ for both comparisons (Student's *t* test). Thus, across the population of V1 cells with suppressive surrounds, far-surround suppression was more broadly tuned than near-surround suppression; this difference was due to significantly stronger ortho-orientation suppression (mean SI at center-surround orientation differences of 60°,75°, and 90° for near versus far suppression; $p < 0.0007$ for both 4° and 6° conditions, unpaired *t* test), and slightly weaker, but significant, iso-orientation suppression (mean SI at center-surround orientation differences of 0°,15°, and 30° for near versus far suppression; $p < 0.009$ for both 4° and 6° conditions, unpaired *t* test) in the far surround compared with the near surround.

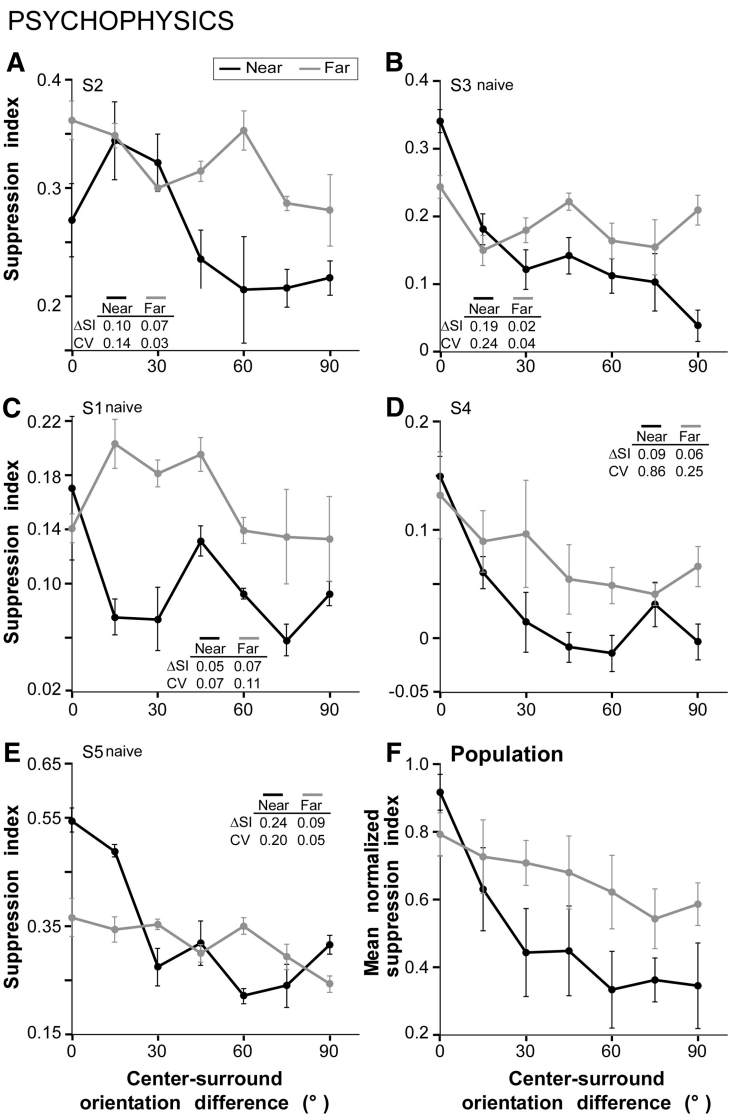

Figure 6. Orientation tuning of near- and far-surround suppression in human psychophysics. ***A–E***, Orientation tuning curves of near-surround (black) and far-surround (gray) suppression for five human subjects, of whom three were naive. Suppression index measures the strength of suppression of the perceived contrast of the center grating exerted by the surround stimulus. ***F***, Average tuning curve across the five subjects. Before averaging, the suppression index for each subject was normalized to the largest SI value for that subject. Mean ΔSI and CV were as follows: 0.13 ± 0.04 and 0.3 ± 0.14 (near; $n = 5$ subjects), 0.05 ± 0.01 and 0.09 ± 0.04 (far; $n = 5$ subjects).

Psychophysics

Figure 4*B* shows for one example subject (S3) the psychophysical data obtained using similar stimuli (Fig. 2*B*,*C*) as used for the electrophysiological experiments. Here the tuning curves are expressed as the perceived contrast of the center grating as a function of the difference in orientation between the center and surround gratings of the test stimulus. The purple line indicates the actual contrast of the center grating (20%). The same data for subject S3 are shown in Figure 6*B* plotted as SI versus center-surround orientation difference. SI was computed as for V1 cells (see Materials and Methods), but here responses (spike rates) were replaced with the corresponding perceived contrasts. Figure 6, *A* and *C–E*, shows the orientation tuning of surround suppression in each of the four remaining subjects. In all subjects, both near- and far-surround stimuli suppressed the perceived contrast of the center grating more strongly when the center and surround stimuli were of similar orientation; increasing the center-surround orientation difference decreased suppression strength. Thus, despite variability across subjects in suppression strengths and sharpness of orientation tuning, both near- and far-surround

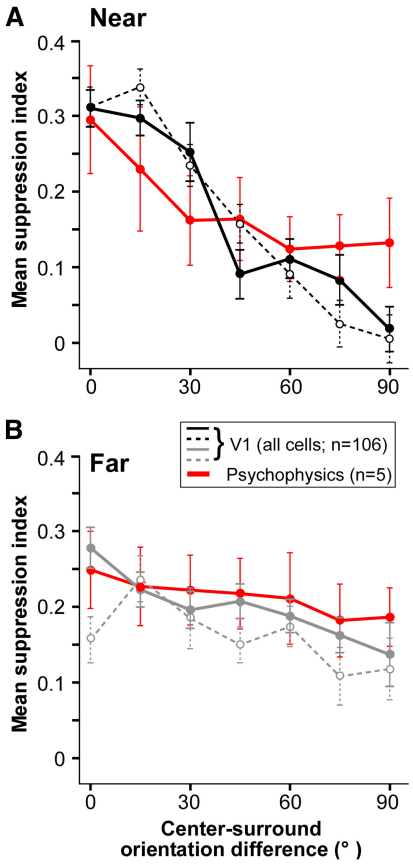

Figure 7. Comparison of orientation tuning of suppression in V1 cells and human psychophysics. ***A***, ***B***, Average population tuning curves of near-surround (***A***) and far-surround (***B***) suppression for all V1 cells ($n = 106$), including suppressive and nonsuppressive (black curves, near suppression; gray curves, far suppression), and for all human subjects ($n = 5$; red curves). Other conventions are as in Figures 5 and 6).

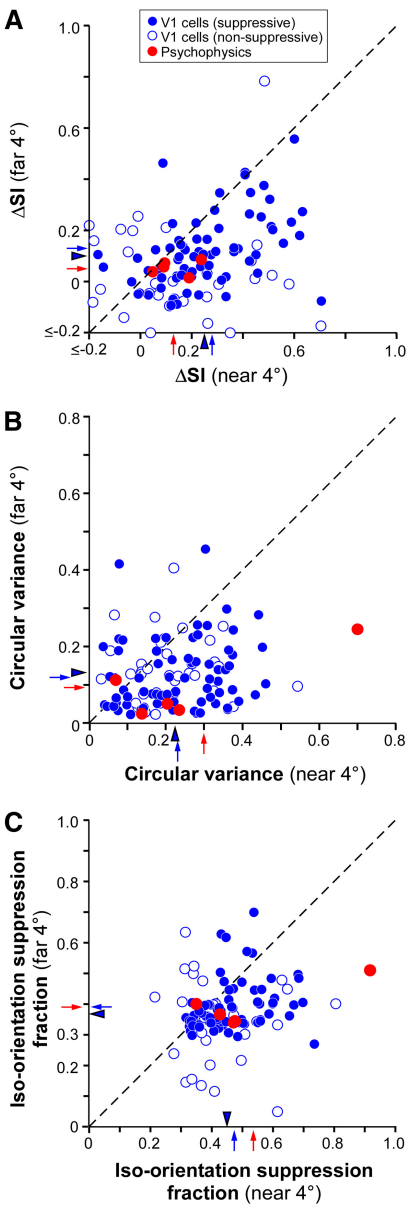

Figure 8. Comparison of orientation selectivity of suppression and iso-orientation suppression fraction in V1 cells and human psychophysics. ***A***, Scatterplot of the ΔSI of suppression in the near versus far surround. ***B***, Scatterplot of the CV of suppression in the near versus far surround. ***C***, Scatterplot of iso-orientation suppression fraction in the near versus far surround. Only near4° and far4° conditions are shown. Empty blue dots, V1 cells that showed no suppression in the near and far surround; solid blue dots, V1 cells that showed at least one form of suppression (near or far); red dots, psychophysics data; red arrows, means of psychophysics data; solid blue arrows, means of suppressive cells; arrowheads, means of all V1 cells (suppressive and nonsuppressive).

suppression were tuned for orientation (for all subjects ΔSI has positive values and CV >0). However, as the center-surround orientation difference increased, suppression strength decreased more rapidly in the near-surround compared with the far-surround condition, and this difference persisted when tuning curves were averaged across subjects (Fig. 6*F*). In Figure 6*F*, the data from individual subjects was first normalized to the largest SI value for that subject, to account for intersubject differences in surround suppression strengths, and then averaged over the subjects. The ΔSI (0.13 ± 0.04) and CV (0.30 ± 0.14) for near-surround suppression were significantly higher than the ΔSI (0.05 ± 0.01) and CV (0.09 ± 0.04) for far-surround suppression ($p < 0.05$, bootstrap test). As for V1 cells, in human perception the orientation tuning of the suppression was broader in the far compared with the near-surround, and this was due to surround orientations nearer to orthogonal exerting stronger suppression in the far than in the near surround.

Comparison of V1 neuronal responses and human psychophysics

In Figures 7 and 8, we compare the orientation tuning of near- and far-surround suppression in psychophysics and electrophysiology. It is important to emphasize that this comparison is qualitative because it is made between two different types of data.

In Figure 7, we compare the orientation tuning of near-surround (Fig. 7*A*) and far-surround (Fig. 7*B*) suppression in

macaque V1 cells and human observers. In contrast to the results reported above, here the suppression index was averaged across the whole population of V1 cells ($n = 106$), including suppressive and nonsuppressive cells, as we reasoned that all cells would likely contribute to the psychophysical results. The suppression index for the psychophysical data was averaged across the five human subjects without being normalized within each subject. In both V1 and human perception, the strength of near-surround suppression decreased steeply as the orientation difference between the stimuli in the center and surround increased (Fig. 7*A*). In the V1 cell population, the suppression index decreased from 0.31 (in both near4° and near6° conditions) at iso-orientation to 0.09 (near4°) and 0.16 (near6°), respectively, at a center-surround orientation difference of 45°. In human subjects, for the same change in center-surround orientation difference, the suppression index decreased from 0.29 to 0.16. However, suppression at 90° or near-90° orientation difference was modestly higher in human subjects compared with V1 cells. In both V1 cells and human subjects, far-surround suppression showed modest orientation tuning (Fig. 7*B*). In V1 cells, the suppression index decreased from 0.28 (far4°) and 0.16 (far6°) at iso-orientation, to 0.21 (near4°) and 0.15 (far6°) at a center-surround orientation difference of 45°. In human subjects, the corresponding decrease in suppression index was from 0.25 to 0.22. Thus, the orientation tuning of near- and far-surround suppression showed a similar trend in V1 neurons and human perception. In both, near-surround suppression was more sharply tuned than far-surround suppression, as measured by the ΔSI or by the CV. Specifically, for all V1 cells, the mean ΔSI for near4° (0.25 ± 0.03) and near6° (0.31 ± 0.03) was significantly higher than the mean ΔSI for far4° (0.1 ± 0.02) and far6° (0.08 ± 0.02), respectively, with $p < 10^{-8}$ for both comparisons (paired Student's t test). For the non-normalized psychophysical functions, the mean ΔSI for near (0.13 ± 0.04) and far (0.05 ± 0.01) suppression were significantly different, with $p < 0.05$ (bootstrap test). For all V1 cells, the mean CV for near4° (0.22 ± 0.01) and near6° (0.25 ± 0.01) was significantly higher than mean CV for far4° (0.13 ± 0.01) and far6° (0.16 ± 0.01), respectively, with $p < 10^{-9}$ for both comparisons. For the non-normalized psychophysical functions, the mean CV for near (0.3 ± 0.14) and far (0.09 ± 0.04) suppression were significantly different, with $p < 0.05$ (bootstrap test).

Figure 8*A* shows a scatterplot of ΔSI for near versus far-surround suppression for both V1 cells and human subjects. Only the near4° and far4° conditions are shown, but results were similar for the 6° near and far conditions. Most dots lie below the diagonal line indicating sharper orientation selectivity of near versus far-surround suppression (mean values and statistical significance of the difference are reported above or in Figs. 5*F*, 6*F*). Figure 8*B* shows a scatterplot of CV for near versus far-surround suppression for both V1 cells and human subjects. Most cells and four of five subjects are located below the diagonal line, again, indicating sharper orientation selectivity of near- than far-surround suppression for most single cells and human subjects (mean values and statistical significance of the difference are reported above or in Figs. 5*F*, 6*F*).

We also measured the fraction of suppression strength occurring at and near iso-orientation, a metric that, unlike ΔSI, is not affected by the absolute value of suppression strength. Unlike CV, which is a global measure of the shape of the tuning curve, the iso-orientation suppression fraction is a local measure of the sharpness of the tuning curve around its peak. The latter was calculated by first fitting a Gaussian function to the orientation tuning curve of surround suppression (i.e., the SI versus orientation-difference curves—e.g., Fig. 5) for each cell, and then measuring from these fits the area under the curve between 0° and 30° orientation difference as a fraction of the total area under the tuning curve. A higher fractional value indicates that a larger fraction of the suppression occurs between 0° and 30° center-surround orientation differences, indicating sharper orientation tuning. Figure 8*C* reports the results of this analysis in the form of a scatterplot of iso-orientation suppression fraction for near versus far surround, for both V1 cells and human subjects. Again only the 4° surround conditions are shown, but results for the 6° condition were similar. Most points lie below the diagonal, indicating that for most cells and human subjects a higher fraction of the total suppression occurs at iso-orientation in the near surround compared with the far surround, and thus that near-surround suppression is more sharply orientation-tuned than far-surround suppression. The mean iso-orientation suppression fraction for the near surround (0.45 ± 0.01 and 0.46 ± 0.01 for 4° and 6° surround sizes, respectively, including all cells) was significantly higher than for the far surround (0.37 ± 0.01 and 0.38 ± 0.01, respectively), with $p < 10^{-7}$ for both comparisons (paired t test). Similar results were seen in the psychophysics data. The mean iso-orientation suppression fraction was 0.52 ± 0.10 for the near surround and 0.38 ± 0.03 for the far surround, and this difference was statistically significant ($p < 0.01$, bootstrap test).

V1 laminar specificity in orientation tuning of near- and far-surround suppression

Different circuits have different laminar specificity, and there are pronounced differences in receptive field properties across V1 layers in macaque. Laminar-specific differences have also been observed in the spatial extent and strength of surround suppression that may reflect laminar differences in connectivity (Ichida et al., 2007; Shushruth et al., 2009). Thus, to make more direct comparison with anatomical data, we examined the tuning of near- and far-surround suppression across V1 layers. Figure 9 shows the tuning curves for the population of suppressive cells only (mean SI vs center-surround orientation difference) for both near- and far-surround suppression in each V1 layer. There were differences in orientation tuning and suppression strength across layers, but in all layers near-surround suppression was more sharply tuned than far-surround suppression. In all layers, the ΔSI and/or CV (values reported in Table 1) for near-surround suppression were significantly higher than for far-surround suppression in at least one surround size condition (4° or 6°) (ΔSI $p < 0.05$ for the near4°–far4°comparison in layers 3B, 4Cα, and 5–6, and for the near6°–far6° comparison in all layers except 2–3A and 4A). Although there was no significant difference in near versus far ΔSI in layers 2–3A, and 4A for either surround size condition, the CV for near- and far-surround suppression in these layers was significantly different in at least one condition ($p < 0.05$; unpaired t test).

In all layers, except 4A and 4Cβ, the broader tuning of far-surround suppression was due to stronger ortho-orientation suppression in the far than in the near surround. Iso-orientation suppression was of similar strength in the near and far surround in layers 2–3A, 4A, and 5/6. However in layer 3B, 4B, and 4Cα iso-orientation suppression was slightly weaker in the far than in the near surround, and this also contributed to the broader orientation tuning of far suppression in these layers.

Figure 10 shows the distribution of ΔSI and CV in different V1 layers. The same parameters are shown in Figure 11 in a scatterplot as a function of cortical depth. For near-surround suppression the ΔSI was higher (>0.3) in layers 3B, 4B, and 4Cα, and weakest in layer 4A and below 4Cα, and this differ-

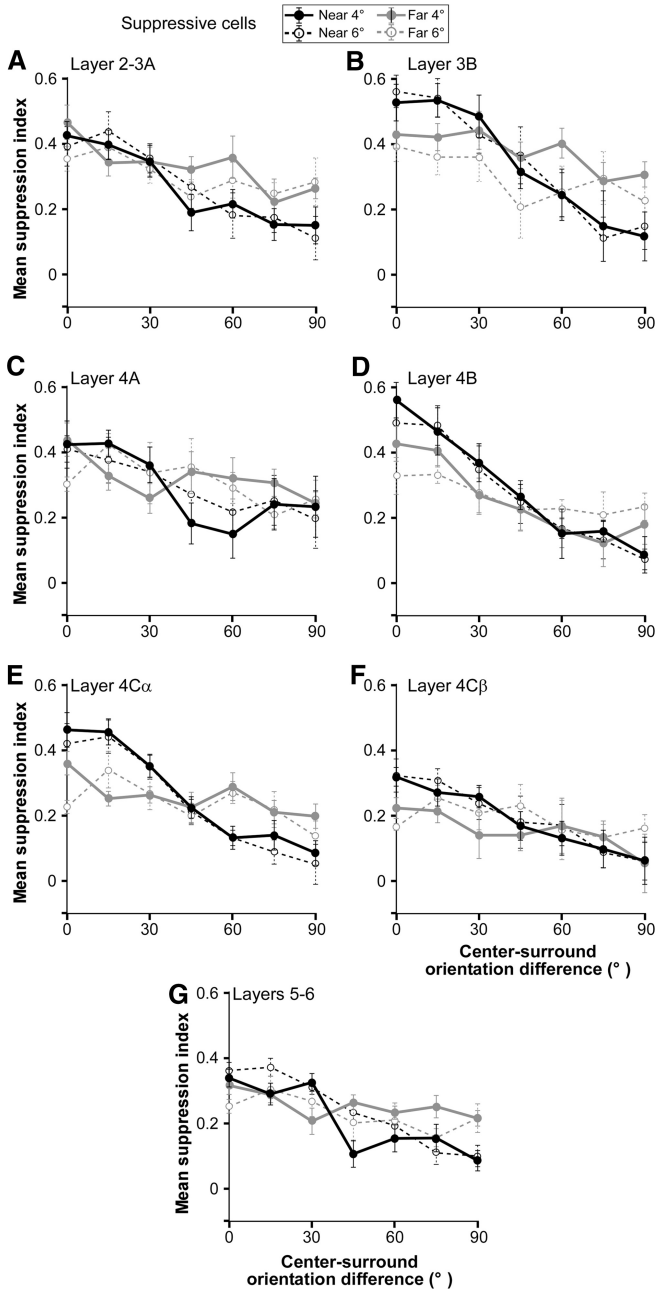

Figure 9. Orientation tuning of near- and far-surround suppression in different V1 layers. ***A–G***, Average orientation tuning curves of near-surround (black curves) and far-surround (gray curves) suppression for population of V1 neurons recorded in specific V1 layers (as indicated). Only cells that showed suppression in a given stimulus condition were included in the tuning curve for that condition. Conventions are as in Figure 5. Mean ΔSI and CV values for each layer are reported in Table 1.

ence was statistically significant ($p = 0.0031$, Kruskal–Wallis test). The CV of near-surround suppression was largest in layer 4Cα but not significantly different from that in other layers, indicating that near-surround suppression shows at least some tuning in all layers. The scatterplot of CV (Fig. 11*B*) shows a large spread of CV values across layers, with cells having CV around 0.4 located in most layers. For far-surround suppression the ΔSI was highest (>0.2) in layer 4B and weakest in layers 5/6, and the difference between these two layers was statistically significant ($p < 0.0036$, Kruskal–Wallis test corrected for multiple comparisons). The scatterplot in Figure 11*A* shows that cells with the largest values of ΔSI (near 0.4) were located in layers 4B and above (except for 4A). The CV of far-surround suppression was significantly larger in layer 4B and weaker in layers 5–6 compared with all other layers ($p = 0.04$, Kruskal–Wallis test), and cells with the lowest values of CV were located in layers 5–6. The difference in CV between layer 4B and 5/6 for far-surround suppression was highly statistically significant ($p < 0.002$, Kruskal–Wallis test corrected for multiple comparisons).

Discussion

We found that the orientation tuning of surround suppression depends on the spatial separation between center and surround stimuli in both macaque V1 and human perception. Specifically, the suppression caused by near-surround stimulation was more sharply orientation tuned than the suppression caused by far-surround stimulation. These results support the idea that the near and far surround are two distinct regions generated by different neural circuits with distinct orientation specificities. The similarity between electrophysiological and psychophysical results also point to an important relationship between surround suppression in V1 neurons and human perception. In V1, we additionally found laminar differences in the orientation tuning of both the near and far surround, suggesting laminar differences in the orientation specificities of their underlying circuitry.

Near- and far-surround suppression differ in orientation tuning

Far-surround suppression is weaker than near-surround suppression in both V1 (Levitt and Lund, 2002; Shushruth et al., 2009) and perception (Cannon and Fullenkamp, 1991; Saarela and Herzog, 2008), but these differences in suppression strength cannot explain the different orientation tuning of near- and far-surround suppression seen in our data. This is because far-surround suppression was stronger than near-surround suppression at near-ortho-orientations. A previous study in cat

Table 1. Orientation tuning of surround suppression in different V1 layers: mean ΔSI and mean CV

	Near surround (4°)			Near surround (6°)			Far surround (4°)			Far surround (6°)			
Layer	*N*	mean ΔSI	mean CV	*N*	mean ΔSI	mean CV	*N*	mean ΔSI	mean CV	*N*	mean ΔSI	mean CV	Figures
2/3A	14	0.26 ± 0.06	0.19 ± 0.03	13	0.27 ± 0.08	0.24 ± 0.04	13	0.16 ± 0.05	0.11 ± 0.02	12	0.11 ± 0.04	0.12 ± 0.02	9*A*, 10, 11
3B	11	0.40 ± 0.10	0.21 ± 0.04	10	0.42 ± 0.08	0.24 ± 0.04	10	0.13 ± 0.05	0.11 ± 0.02	7	0.12 ± 0.03	0.12 ± 0.03	9*B*, 10, 11
4A	6	0.19 ± 0.08	0.26 ± 0.05	7	0.17 ± 0.06	0.18 ± 0.03	7	0.11 ± 0.02	0.10 ± 0.02	7	0.13 ± 0.04	0.16 ± 0.04	9*C*, 10, 11
4B	7	0.39 ± 0.07	0.25 ± 0.04	8	0.38 ± 0.07	0.25 ± 0.04	8	0.27 ± 0.05	0.23 ± 0.05	6	0.11 ± 0.04	0.13 ± 0.04	9*D*, 10, 11
4Cα	8	0.35 ± 0.06	0.29 ± 0.04	9	0.36 ± 0.07	0.34 ± 0.05	6	0.10 ± 0.04	0.09 ± 0.03	7	0.11 ± 0.03	0.11 ± 0.03	9*E*, 10, 11
4Cβ	4	0.22 ± 0.04	0.25 ± 0.06	4	0.24 ± 0.01	0.24 ± 0.04	4	0.12 ± 0.04	0.16 ± 0.04	3	0.06 ± 0.02	0.19 ± 0.07	9*F*, 10, 11
5/6	17	0.19 ± 0.03	0.24 ± 0.03	16	0.26 ± 0.03	0.23 ± 0.02	16	0.07 ± 0.03	0.08 ± 0.01	11	0.09 ± 0.03	0.16 ± 0.02	9*G*, 10, 11

N, Number of cells.

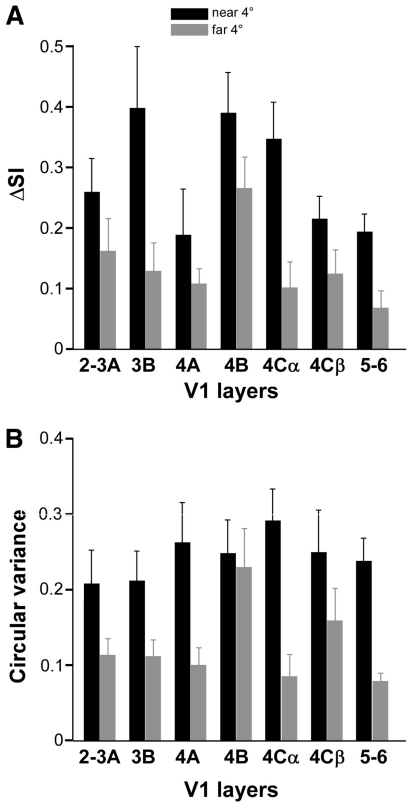

Figure 10. Orientation selectivity of near- and far-surround suppression in different V1 layers. ***A***, ***B***, Distribution of ΔSI (***A***) and CV (***B***) for near-surround (black) and far-surround (gray) suppression across V1 layers. Only the near4° and far4° stimulus conditions are included and only cells that showed surround suppression in each condition.

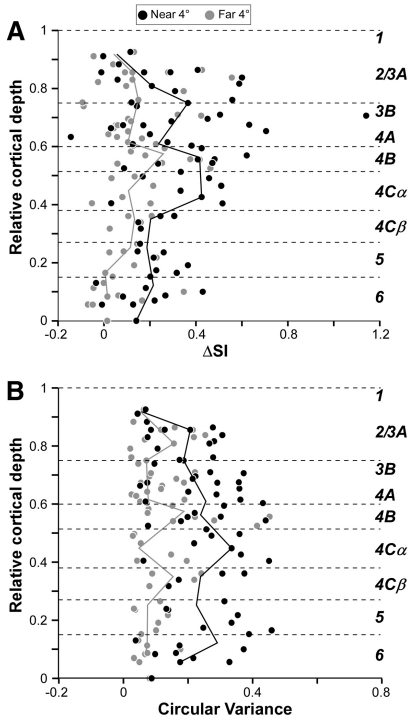

Figure 11. V1 laminar distribution of orientation selectivity of near- and far-surround suppression. ***A***, ***B***, Scatterplot of ΔSI (***A***) and CV (***B***) as a function of cortical depth for near-surround (black dots) and far-surround (gray dots) suppression for the population of V1 cells showing suppression in each condition (only near4° and far4° included). The dashed horizontal lines mark V1 layer boundaries, and the cortical layers are indicated to the right of the plots. Solid black and gray vertical lines: medians of the V1 cell sample calculated at intervals of 10% of total cortical depth.

V1 reported that the suppression caused by far-surround stimulation was more broadly orientation tuned than the suppression caused by full surround stimulation (near plus far) (Hashemi-Nezhad and Lyon, 2012). However, compared with full surround stimulation, far-surround stimulation resulted in weaker iso-orientation suppression, but similar ortho-orientation suppression strength. Thus, broader tuning of far-surround suppression, in this study, could have resulted from weaker far-surround suppression, an interpretation that cannot explain our findings. These different results are attributable to the different stimulus configurations used in the two studies. We compared near-surround versus far-surround stimulation, whereas Hashemi-Nezhad and Lyon (2012) compared near-surround versus full-surround stimulation, and thus did not isolate the tuning of suppression from the near surround. Polat and Sagi (1993) examined the effects on contrast detection of small Gabor patches placed at various distances from a target Gabor. They found both suppressive and facilitatory effects of flankers in the near surround (≤3° separation), whose orientation tuning resembled that of near-surround suppression in our psychophysical study. However, in their study, flankers in the far surround (~3.6° from the target) had no effect on target detection, likely due to the weak surround stimulation exerted by such small stimuli. In contrast, we used large gratings likely to have stronger effects. Mizobe et al. (2001), instead, using Gabor stimuli in cat V1 observed both near

and far (up to 12°) surround effects, but did not examine the tuning of far-surround suppression.

We found sharper tuning of near-surround suppression than previous studies. In our cell population, there was >90% decrease in suppression strength when the surround stimulus orientation was changed from iso-oriented to orthogonal. This contrasts with the 30–35% decrease found in previous studies (Cavanaugh et al., 2002; Hashemi-Nezhad and Lyon, 2012). Broader tuning of suppression in these studies was likely due to concomitant stimulation of the near and far surround, and is thus consistent with our findings.

Petrov et al. (2005) studied surround suppression of contrast detection with stimuli likely activating mainly the near surround of V1 neurons. They found that suppression was negligible for center-surround orientation differences ≥45°. In our psychophysical and electrophysiological data, near-surround suppression was still present at 45° orientation difference. This discrepancy is attributable to different center stimulus contrasts used in the two studies. Psychophysics (Nurminen et al., 2010) and single-cell recordings (Schwabe et al., 2010) have shown that suppression strength decreases at lower center contrast. Thus, it is likely that at the very low center contrast (at threshold) used by Petrov et al. (2005), weak suppressive effects from orthogonal surround stimuli disappear.

Cannon and Fullenkamp (1991), using eight cycles-wide surround stimuli, found that the strength of surround suppression decreases steeply between center-surround orientation differences of 0° and 15°, but more gradually at larger orientation differences. They concluded that surround suppression arises from two distinct mechanisms, one narrowly orientation tuned, the other broadly tuned. Our results are consistent with their hypothesis, but further indicate that the narrowly tuned mechanism is spatially restricted, while the broadly tuned mechanism is spatially widespread.

Correlation between human psychophysics and V1 physiology

Previous studies found positive correlations between contextual effects in human vision and the response of single V1 cells (Kapadia et al., 1995, 1999; Li et al., 2000). However, in those studies it was unclear whether the stimuli intended to activate the surround also encroached onto the RF (as defined in our study). Moreover, these studies compared the mean firing rates of V1 neurons to subjects' performance in detection and discrimination tasks. This is problematic because performance in these tasks relates to the noise level and slope of the underlying neural responses (Geisler and Albrecht, 1997). In contrast, we used stimuli clearly confined to the surround, and a contrast-matching task, which is better suited to compare mean neuronal firing rates with psychophysical performance, because performance in this task relates to the magnitude of the underlying neural response (Chen and Tyler, 2002). Although it is not straightforward to compare psychophysics and electrophysiological data, our results nevertheless demonstrate a striking similarity between the tuning of surround effects in human perception and V1 cells.

Anatomical circuits underlying the orientation tuning of near- and far-surround suppression

We previously suggested that near-surround suppression results predominantly from both untuned surround suppression of geniculocortical afferents and tuned suppression from intra-V1 horizontal connections, while far-surround suppression is generated exclusively by interareal feedback (Angelucci and Bressloff, 2006; Angelucci and Shushruth, 2013). Here, we have found that near-surround suppression is more sharply tuned than far-surround suppression, and is most narrowly tuned in layers 3, 4B, and 4Cα. Because the suppression contributed by geniculocortical afferents to V1 is untuned (Solomon et al., 2002; Webb et al., 2002; Bonin et al., 2005) or less tuned (Ozeki et al., 2009) for orientation than V1 suppression, orientation-tuned near-surround suppression in V1 is likely generated by intra-V1 horizontal connections. These connections, at least in V1 layers 2–3, are well suited to this task, because they link preferentially neurons of similar orientation preference (Malach et al., 1993; Bosking et al., 1997) and target both excitatory and inhibitory neurons (McGuire et al., 1991). The orientation specificity of horizontal connections in other V1 layers is unknown. However, long-range connections in layers 4B and upper-4Cα are "patchy" (Lund et al., 2003), whereas in layer 6 they are widespread and do not link domains of similar eye dominance (Li et al., 2003). Therefore, there appears to be a correlation between the sharpness of tuning of near-surround suppression across V1 laminae and the laminar location of patterned and orientation-specific horizontal connections. V1 layers with sharpest tuning of near-surround suppression also have stronger near suppression (Sceniak et al., 2001; Shushruth et al., 2009), except layer 4A, which despite strong suppression shows poor tuning. In contrast, there is no correlation between layers with sharpest orientation tuning of near-surround suppression and layers with sharpest orientation tuning of RF responses (Ringach et al., 2002).

Broader orientation tuning of far than near-surround suppression suggests that feedback connections, the presumed substrate for far-surround suppression, are more broadly orientation biased than horizontal connections. Feedback connections to V1 terminate in upper and lower layers, avoiding layer 4C (Salin and Bullier, 1995), and target both excitatory and inhibitory neurons (Anderson and Martin, 2009), but their orientation organization remains controversial. Specifically, there are reports of both anatomically widespread (Rockland and Pandya, 1979; Maunsell and van Essen, 1983; Rockland, 2003) and orientation-unspecific (Stettler et al., 2002) V2-to-V1 feedback connections, and patterned (Angelucci et al., 2002; Angelucci and Bressloff, 2006) and orientation-biased (Shmuel et al., 2005) feedback connections from V2 to V1 layers 2/3. The orientation organization of feedback to V1 from other extrastriate areas is unknown. It is likely that there are multiple feedback systems differing in functional specificities terminating in different V1 layers (Angelucci and Bressloff, 2006). In particular, sharper tuning of far suppression in layer 4B suggests greater orientation specificity of feedback connections to this layer, while weak tuning in layers 5/6 suggests orientation-unspecific feedback connections to these layers. In effect, feedback also contributes to the near surround (Fig. 1), but its effect is likely masked by the stronger tuned component of near-surround suppression. There is no correlation between the laminar distribution of the orientation tuning of far suppression and the laminar distributions of far-surround suppression strength (Shushruth et al., 2009) or RF orientation tuning (Ringach et al., 2002).

Two previous studies that examined the tuning of surround suppression, inferred two components to the underlying neural signal, one that is monocular and has very broad spatiotemporal tuning, likely originating in the LGN or input layers of V1, the other binocular and sharply tuned for orientation and spatiotemporal frequency, likely of long-range intracortical origin (Webb et al., 2005; Petrov and McKee, 2009). It is unlikely that the monocular and untuned suppression of these previous stud-

ies corresponds to the broadly orientation-tuned far-surround suppression of our study. In our study, the far-surround stimuli activated cortical regions well beyond the spatial spread of feedforward afferents, and thus likely recruited long-range intracortical connections. The untuned, monocular, and early suppression of these previous studies is likely confined to the near surround, and was likely masked by the tuned component of near-surround suppression in our stimulus protocol.

Role of near- and far-surround suppression in natural vision

The similarity of surround suppression in human and macaques suggests that this phenomenon reflects fundamental signal processing principles. A prominent hypothesis, stemming from efficient coding principles (Attneave, 1954; Barlow, 1961) and information theory (Shannon, 1948), suggests that the visual system is tuned to the statistics of natural images (Simoncelli and Olshausen, 2001; Geisler, 2008). In natural images, there is a statistical relation between edge orientation and distance between edges: nearby edges have higher probability than distant edges of being co-oriented and cocircular, and of belonging to the same physical contour (Geisler et al., 2001). The different orientation tuning of near- and far-surround suppression may reflect this statistical dependency in the visual environment. Accordingly, suppression should be narrowly orientation tuned for nearby edges, and more broadly tuned for distant edges. Such tuning would increase the coding efficiency of more frequently co-occurring contours, because the latter would evoke fewer spikes (due to tuned suppression) than less frequent contours. On the other hand, the same tuning results in increased saliency of less frequently co-occurring contours in natural images.

Perceptually, sharply orientation-tuned near-surround suppression may serve to detect small orientation differences in nearby edges, which is useful for local contour completion or figure–ground segregation (Lamme, 1995). Instead, broadly tuned far-surround suppression could serve to detect large orientation differences in distant edges, useful for perception of global contours and/or to direct saccades and/or attention to salient visual field locations that are markedly different from their surrounding (Petrov and McKee, 2006).

References

Albrecht DG, Hamilton DB (1982) Striate cortex of monkey and cat: contrast response function. J Neurophysiol 48:217–237. Medline

Alitto HJ, Usrey WM (2008) Origin and dynamics of extraclassical suppression in the lateral geniculate nucleus of the macaque monkey. Neuron 57:135–146. CrossRef Medline

Allman J, Miezin F, McGuinness E (1985) Stimulus specific responses from beyond the classical receptive field: neurophysiological mechanisms for local-global comparisons in visual neurons. Annu Rev Neurosci 8:407–430. CrossRef Medline

Anderson JC, Martin KA (2009) The synaptic connections between cortical areas V1 and V2 in macaque monkey. J Neurosci 29:11283–11293. CrossRef Medline

Angelucci A, Bressloff PC (2006) The contribution of feedforward, lateral and feedback connections to the classical receptive field center and extraclassical receptive field surround of primate V1 neurons. Prog Brain Res 154:93–120. CrossRef Medline

Angelucci A, Sainsbury K (2006) Contribution of feedforward thalamic afferents and corticogeniculate feedback to the spatial summation area of macaque V1 and LGN. J Comp Neurol 498:330–351. CrossRef Medline

Angelucci A, Shushruth S (2013) Beyond the classical receptive field: surround modulation in primary visual cortex. In: The new visual neurosciences (Chalupa LM, Werner JS, eds), in press. Cambridge: MIT.

Angelucci A, Levitt JB, Walton EJ, Hupe JM, Bullier J, Lund JS (2002) Circuits for local and global signal integration in primary visual cortex. J Neurosci 22:8633–8646. Medline

Attneave F (1954) Some informational aspects of visual perception. Psychol Rev 61:183–193. CrossRef Medline

Bair W, Cavanaugh JR, Movshon JA (2003) Time course and time–distance relationships for surround suppression in Macaque V1 neurons. J Neurosci 23:7690–7701. Medline

Barlow HB (1961) Possible principles underlying the transformation of sensory messages. In: Sensory communication (Rosenblith WA, ed), pp 217–234. Cambridge: MIT.

Blakemore C, Tobin EA (1972) Lateral inhibition between orientation detectors in the cat's visual cortex. Exp Brain Res 15:439–440. Medline

Bonin V, Mante V, Carandini M (2005) The suppressive field of neurons in lateral geniculate nucleus. J Neurosci 25:10844–10856. CrossRef Medline

Bosking WH, Zhang Y, Schofield B, Fitzpatrick D (1997) Orientation selectivity and the arrangement of horizontal connections in tree shrew striate cortex. J Neurosci 17:2112–2127. Medline

Bringuier V, Chavane F, Glaeser L, Frégnac Y (1999) Horizontal propagation of visual activity in the synaptic integration field of area 17 neurons. Science 283:695–699. CrossRef Medline

Cannon MW, Fullenkamp SC (1991) Spatial interactions in apparent contrast: inhibitory effects among grating patterns of different spatial frequencies, spatial positions and orientations. Vis Res 31:1985–1998. CrossRef Medline

Cavanaugh JR, Bair W, Movshon JA (2002) Selectivity and spatial distribution of signals from the receptive field surround in macaque V1 neurons. J Neurophysiol 88:2547–2556. CrossRef Medline

Chen CC, Tyler CW (2002) Lateral modulation of contrast discrimination: flanker orientation effects. J Vis 2:520–530. Medline

Chubb C, Sperling G, Solomon JA (1989) Texture interactions determine perceived contrast. Proc Natl Acad Sci U S A 86:9631–9635. CrossRef Medline

DeAngelis GC, Freeman RD, Ohzawa I (1994) Length and width tuning of neurons in the cat's primary visual cortex. J Neurophysiol 71:347–374. Medline

Ejima Y, Takahashi S (1985) Apparent contrast of a sinusoidal grating in the simultaneous presence of peripheral gratings. Vision Res 25:1223–1232. CrossRef Medline

Gallant JL, Connor CE, Van Essen DC (1998) Neural activity in areas V1, V2 and V4 during free viewing of natural scenes compared to controlled viewing. Neuroreport 9:2153–2158. CrossRef Medline

Geisler WS (2008) Visual perception and the statistical properties of natural scenes. Annu Rev Psychol 59:167–192. CrossRef Medline

Geisler WS, Albrecht DG (1997) Visual cortex neurons in monkeys and cats: detection, discrimination, and identification. Vis Neurosci 14:897–919. CrossRef Medline

Geisler WS, Perry JS, Super BJ, Gallogly DP (2001) Edge co-occurrence in natural images predicts contour grouping performance. Vis Res 41:711–724. CrossRef Medline

Girard P, Hupé JM, Bullier J (2001) Feedforward and feedback connections between areas V1 and V2 of the monkey have similar rapid conduction velocities. J Neurophysiol 85:1328–1331. Medline

Grinvald A, Lieke EE, Frostig RD, Hildesheim R (1994) Cortical point-spread function and long-range lateral interactions revealed by real-time optical imaging of macaque monkey primary visual cortex. J Neurosci 14:2545–2568. Medline

Hashemi-Nezhad M, Lyon DC (2012) Orientation tuning of the suppressive extraclassical surround depends on intrinsic organization of V1. Cereb Cortex 22:308–326. CrossRef Medline

Ichida JM, Schwabe L, Bressloff PC, Angelucci A (2007) Response facilitation from the "suppressive" receptive field surround of macaque V1 neurons. J Neurophysiol 98:2168–2181. CrossRef Medline

Kapadia MK, Ito M, Gilbert CD, Westheimer G (1995) Improvement in visual sensitivity by changes in local context: parallel studies in human observers and in V1 of alert monkeys. Neuron 15:843–856. CrossRef Medline

Kapadia MK, Westheimer G, Gilbert CD (1999) Dynamics of spatial summation in primary visual cortex of alert monkeys. Proc Natl Acad Sci U S A 96:12073–12078. CrossRef Medline

Lamme VA (1995) The neurophysiology of figure-ground segregation in primary visual cortex. J Neurosci 15:1605–1615. Medline

Levitt JB, Lund JS (1997) Contrast dependence of contextual effects in primate visual cortex. Nature 387:73–76. CrossRef Medline

Levitt JB, Lund JS (2002) The spatial extent over which neurons in macaque striate cortex pool visual signals. Vis Neurosci 19:439–452. Medline

Li H, Fukuda M, Tanifuji M, Rockland KS (2003) Intrinsic collaterals of layer 6 Meynert cells and functional columns in primate V1. Neuroscience 120:1061–1069. CrossRef Medline

Li W, Thier P, Wehrhahn C (2000) Contextual influence on orientation discrimination of humans and responses of neurons in V1 of alert monkeys. J Neurophysiol 83:941–954. Medline

Lund JS, Angelucci A, Bressloff PC (2003) Anatomical substrates for functional columns in macaque monkey primary visual cortex. Cereb Cortex 13:15–24. CrossRef Medline

Maffei L, Fiorentini A (1976) The unresponsive regions of visual cortical receptive fields. Vis Res 16:1131–1139. CrossRef Medline

Malach R, Amir Y, Harel M, Grinvald A (1993) Relationship between intrinsic connections and functional architecture revealed by optical imaging and in vivo targeted biocytin injections in primate striate cortex. Proc Natl Acad Sci U S A 90:10469–10473. CrossRef Medline

Maunsell JH, van Essen DC (1983) The connections of the middle temporal visual area (MT) and their relationship to a cortical hierarchy in the macaque monkey. J Neurosci 3:2563–2586. Medline

McGuire BA, Gilbert CD, Rivlin PK, Wiesel TN (1991) Targets of horizontal connections in macaque primary visual cortex. J Comp Neurol 305:370–392. CrossRef Medline

Mizobe K, Polat U, Pettet MW, Kasamatsu T (2001) Facilitation and suppression of single striate-cell activity by spatially discrete pattern stimuli presented beyond the receptive field. Vis Neurosci 18:377–391. CrossRef Medline

Nelson JI, Frost BJ (1978) Orientation-selective inhibition from beyond the classic visual receptive field. Brain Res 139:359–365. CrossRef Medline

Nurminen L, Kilpeläinen M, Laurinen P, Vanni S (2009) Area summation in human visual system: psychophysics, fMRI, and modeling. J Neurophysiol 102:2900–2909. CrossRef Medline

Nurminen L, Peromaa T, Laurinen P (2010) Surround suppression and facilitation in the fovea: very long-range spatial interactions in contrast perception. J Vis 10:9. CrossRef Medline

Ozeki H, Sadakane O, Akasaki T, Naito T, Shimegi S, Sato H (2004) Relationship between excitation and inhibition underlying size tuning and contextual response modulation in the cat primary visual cortex. J Neurosci 24:1428–1438. CrossRef Medline

Ozeki H, Finn IM, Schaffer ES, Miller KD, Ferster D (2009) Inhibitory stabilization of the cortical network underlies visual surround suppression. Neuron 62:578–592. CrossRef Medline

Petrov Y, McKee SP (2006) The effect of spatial configuration on surround suppression of contrast sensitivity. J Vis 6:224–238. CrossRef Medline

Petrov Y, McKee SP (2009) The time course of contrast masking reveals two distinct mechanisms of human surround suppression. J Vis 9:21.1–11. CrossRef Medline

Petrov Y, Carandini M, McKee S (2005) Two distinct mechanisms of suppression in human vision. J Neurosci 25:8704–8707. CrossRef Medline

Polat U, Sagi D (1993) Lateral interactions between spatial channels: suppression and facilitation revealed by lateral masking experiments. Vis Res 33:993–999. CrossRef Medline

Ringach DL, Shapley RM, Hawken MJ (2002) Orientation selectivity in macaque V1: diversity and laminar dependence. J Neurosci 22:5639–5651. Medline

Rockland KS (2003) Feedback connections: splitting the arrow. In: The primate visual system (Kaas JH, Collins CE, eds), pp 387–405: CRC.

Rockland KS, Pandya DN (1979) Laminar origins and terminations of cortical connections of the occcipital lobe in the Rhesus monkey. Brain Res 179:3–20. CrossRef Medline

Saarela TP, Herzog MH (2008) Time-course and surround modulation of contrast masking in human vision. J Vis 8:23.1–10. CrossRef Medline

Salin PA, Bullier J (1995) Corticocortical connections in the visual system: structure and function. Physiol Rev 75:107–154. Medline

Sceniak MP, Ringach DL, Hawken MJ, Shapley R (1999) Contrast's effect on spatial summation by macaque V1 neurons. Nat Neurosci 2:733–739. CrossRef Medline

Sceniak MP, Hawken MJ, Shapley R (2001) Visual spatial characterization of macaque V1 neurons. J Neurophysiol 85:1873–1887. Medline

Sceniak MP, Chatterjee S, Callaway EM (2006) Visual spatial summation in macaque geniculocortical afferents. J Neurophysiol 96:3474–3484. CrossRef Medline

Schwabe L, Ichida JM, Shushruth S, Mangapathy P, Angelucci A (2010) Contrast-dependence of surround suppression in macaque V1: Experimental testing of a recurrent network model. Neuroimage 52:777–792. CrossRef Medline

Sengpiel F, Sen A, Blakemore C (1997) Characteristics of surround inhibition in cat area 17. Exp Brain Res 116:216–228. CrossRef Medline

Shannon CE (1948) A mathematical theory of communication. The Bell System Technical J 27:379–423.

Shmuel A, Korman M, Sterkin A, Harel M, Ullman S, Malach R, Grinvald A (2005) Retinotopic axis specificity and selective clustering of feedback projections from V2 to V1 in the owl monkey. J Neurosci 25:2117–2131. CrossRef Medline

Shushruth S, Ichida JM, Levitt JB, Angelucci A (2009) Comparison of spatial summation properties of neurons in macaque V1 and V2. J Neurophysiol 102:2069–2083. CrossRef Medline

Shushruth S, Mangapathy P, Ichida JM, Bressloff PC, Schwabe L, Angelucci A (2012) Strong recurrent networks compute the orientation-tuning of surround modulation in primate primary visual cortex. J Neurosci 32:308–321. CrossRef Medline

Sillito AM, Grieve KL, Jones HE, Cudeiro J, Davis J (1995) Visual cortical mechanisms detecting focal orientation discontinuities. Nature 378:492–496. CrossRef Medline

Simoncelli EP, Olshausen BA (2001) Natural image statistics and neural representation. Annu Rev Neurosci 24:1193–1216. CrossRef Medline

Snowden RJ, Hammett ST (1998) The effects of surround contrast on contrast thresholds, perceived contrast and contrast discrimination. Vision Res 38:1935–1945. CrossRef Medline

Solomon JA, Sperling G, Chubb C (1993) The lateral inhibition of perceived contrast is indifferent to on-center/off-center segregation, but specific to orientation. Vision Res 33:2671–2683. CrossRef Medline

Solomon SG, White AJ, Martin PR (2002) Extra-classical receptive field properties of parvocellular, magnocellular, and koniocellular cells in the primate lateral geniculate nucleus. J Neurosci 22:338–349. Medline

Stettler DD, Das A, Bennett J, Gilbert CD (2002) Lateral connectivity and contextual interactions in macaque primary visual cortex. Neuron 36:739–750. CrossRef Medline

Walker GA, Ohzawa I, Freeman RD (1999) Asymmetric suppression outside the classical receptive field of the visual cortex. J Neurosci 19:10536–10553. Medline

Walker GA, Ohzawa I, Freeman RD (2000) Suppression outside the classical cortical receptive field. Vis Neurosci 17:369–379. CrossRef Medline

Webb BS, Tinsley CJ, Barraclough NE, Easton A, Parker A, Derrington AM (2002) Feedback from V1 and inhibition from beyond the classical receptive field modulates the responses of neurons in the primate lateral geniculate nucleus. Vis Neurosci 19:583–592. Medline

Webb BS, Dhruv NT, Solomon SG, Tailby C, Lennie P (2005) Early and late mechanisms of surround suppression in striate cortex of macaque. J Neurosci 25:11666–11675. CrossRef Medline

CHAPTER 3

SPATIO-TEMPORAL PROFILE OF INPUTS ACROSS LAYERS OF V1 BY STIMULATION OF NEAR- AND FAR-SUURROUND

3.1 Introduction

In Chapter 2, we showed that there are functional differences between near and far surround stimulation across layers of V1. Specifically, near surround is more sharply tuned in superficial layers (L) 3B, L4B, and L4Cα than deep layers. This result was also reported by Henry et al. (2013). However, far surround is more orientation selective in L4B compared to other layers (Shushruth et al., 2013). Generally, near surround shows higher selectivity to orientation than far surround reflecting that its underlying circuit is encoding sharp orientation differences.

In this dissertation, we examine how surround modulation is computed across layers of V1. We specifically ask whether the laminar anatomical connectivity patterns lead to functional distinction in response to stimulation of the two surround regions (near vs. far). Each layer has particular pattern of neuronal inputs and outputs, including intra-areal, feedforward and feedback connections (Lund, 1988). Geniculocortical afferents from lateral geniculate nucleus (LGN) terminate in L4C and L6 of V1 (Hendrickson et

al., 1978; Blasdel and Lund, 1983; Lund, 1988; Callaway, 1998). After complex intracortical processing, superficial layers (L2/3 and L4B) and, to some extent, deep layers (L6) send the processed information from V1 to the extrastriate cortex (V2 and MT, respectively (Callaway, 2004)). Deep layers (L5 and L6) send back the information to subcortical regions for motor control (Lund, 1973; Callaway, 2004). Remarkably, the axonal projections from higher visual cortices terminate in both upper and lower layers being prominent in L1/2A (Rockland and Pandya, 1979; Ungerleider and Desimone, 1986), L6 and L5B (Callaway, 2004; Federer et al., 2015) and only form sparse termination in L3 and L4B (Federer et al., 2015) while avoiding L4C. Moreover, horizontal connections are dense in L2/3, L4B and L5 (Angelucci et al., 2002). Based on the proposed model by Angelucci and colleagues (Angelucci and Bressloff, 2006) (Figure 1.5-B), we presume that near surround is mainly generated by horizontal connections, but the fast far surround suppression is mainly originated by feedback projections from the extrastriate cortex (V2, V3, and MT in anesthetized primates). To reexamine this hypothesis, one could investigate how layers having different anatomical connections would reflect the main substrates of near and far surround. In particular, what are the temporal dynamics of inputs generated by stimulation of near and far surround across layers?

Elaborating on this, we ask which layer receives the first input reflected in population current sinks? Single electrode recordings limited visual scientists to examining the spatio-temporal profile of surround modulation across layers because one layer was sampled at a time. A number of studies reported the timing profile of the cortical column in response to strong activation of thalamocortical afferents by full field

flashes of light while recording neuronal activities from all layers at the same time using linear microelectrode arrays (Schroeder et al., 1991; Schroeder et al., 1998). The timing of inputs are typically measured by subthreshold local field potentials that are representative of integrative dendritic inputs (Kajikawa and Schroeder, 2011). Current source density analysis applied on the LFP voltage traces provides a proper localization of current flow across cortical layers. Specifically, current sinks are markers of integrative excitatory flow to the neuronal ensembles (Mitzdorf and Singer, 1979; Mitzdorf, 1985; Kajikawa and Schroeder, 2011; Self et al., 2013). These studies reported that the fastest current sink in columnar RF stimulation was localized in the thalamocortical recipient layers L4C (Figure 3.1-D) (Schroeder et al., 1998). This pattern was also found in other primary sensory cortices such as auditory (Müller-Preuss and Mitzdorf, 1984; Steinschneider et al., 1992) and somatosensory areas (Kulics and Cauller, 1986; Schroeder et al., 1995). In addition, measuring the post synaptic spiking activity localized the fastest activity in L4C and L6 (Schroeder et al., 1991; Schroeder et al., 1998) consistent with canonical pathway and LGN collaterals in L6 (Callaway, 2004; Sincich and Horton, 2005).

There is no study reporting the temporal dynamics of inputs to the cortical columns caused by stimulation of the surround-only stimulus. Most of the previous studies investigated different sensory and cognitive tasks while activating the columnar receptive field by visual or auditory stimuli (Schroeder et al., 1991; Givre et al., 1994; Schroeder et al., 1998; Lakatos et al., 2007; Lakatos et al., 2008; Hansen et al., 2011; Hansen et al., 2012). Given the fact that there are distinct patterns of feedforward, feedback and horizontal connections across V1 layers, in this chapter, we examine the spatiotemporal

profile of inputs to V1 layers to stimuli that was designed to probe each surround region (i.e., near or far). We correlated the main underlying mechanisms based on the fastest input to the cortical column while noting there was no activation of the canonical pathway by columnar RF.

3.2 Methods

3.2.1 Experimental and Surgical Preparation

All experimental procedures complied with the guidelines of the National Institute of Health and were approved by the Institutional Animal Care and Use Committee of the University of Utah. Recordings were made from anesthetized and paralyzed macaque monkeys (*Macaca fascicularis*, 3-4 kg). Animals were anesthetized by isoflurane (0.5-1.5%) during the surgery and sufentanil (6-12 μg/kg/h) during the recordings. Paralytic (vercuronium bromide, 0.1- .3 μg/kg/h) was added just before the recording started. Animals were artificially respired with O_2 (100), or the mixture of O_2 and N_2O (70:30). The vital signs, including heart rate, end-tidal CO_2, temperature (rectal sensor), O_2 saturation, blood pressure, and lung pressure were monitored continuously. The pupils were dilated by topical atropine, the corneas were protected by plain or corrected contact lenses and the foveas were plotted on a tangent screen using reversible ophthalmoloscope prior to the recordings.

3.2.2 Electrophysiological Recordings and Data Acquisition

Extracellular recordings were made in parafoveal V1 (4-8° eccentricity) of six anesthetized and paralyzed macaque monkeys. Data used here, are selected from four

successful macaque experiments. We simultaneously recorded multiunit activity (MUA) and local field potentials (LFP) from all layers of V1 using multicontact linear arrays. 9 out of 10 (n = 4 monkeys) penetrations were recorded by V-Probe (24 contacts, Plexon) and one penetration was recorded by A32 (32 contacts, NeuroNexus). Contacts of both arrays were 100µm apart, spanning the whole cortical depth. The V-probe was 100 mm in length, 210µm in diameter, and there was 500µm from the tip of the probe to the first contact; its reinforcement tube was 18 mm in length and 640µm in diameter. Contacts were referenced to the probe shaft (V-Probe) or one recording contact (A32) and the ground was placed under wet skin touching the skull and the stereotaxic setup. A custom-made guide tube provided mechanical stability to the recording setup. Prior to probe insertion in the cortex, the probe shafts were coated with DiI to provide robust visualization of the lesion track in further histology.

Data were collected and amplified using a 128-channel Cerebus system (Blackrock Microsystems, Salt Lake City, UT). To obtain LFPs, the raw signal from either 24 or 32 contacts were band-pass filtered (1-100 Hz, second order butterworth filter) and down-sampled to 2,000 Hz. All LFP analyses were performed on the down-sampled version with 0.5ms time resolution. The MUA spikes were obtained by band-pass filtering (250 Hz-7.5 kHz,) the raw signal, which was continuously recorded at a sampling rate of 30 kHz. It was automatically thresholded by Cerebus software.

Visual stimuli were generated with MATLAB (MathWorks, Inc.) and presented on a calibrated Sony GDM-C520K CRT monitor (viewing distance 57cm, 100Hz frame rate) using the ViSaGe system (CRS, Cambridge, UK).

3.2.3 RF Mapping, Vertical Recordings and Tuning Properties of Cortical Column

It was crucial to make sure that all the penetrations were vertical to the cortical surface. To sample from a cortical column, prior to the electrode advancement, we had an estimate of the receptive field using topographical position of the probe relative to the horizontal and vertical meridian. Right after probe advancement in the cortex, we manually scanned the monitor by drifting gratings while listening to the neuronal responses from each contact (spike sounds). Then obtaining the course region of RF, we systematically mapped the receptive field of all contacts using small flashing squares reversing in contrast (Figure 3.2-A, 0.5º x 0.5º, stimulus presentation of 500ms), which covered at least three degrees of visual field (36 positions by a 0.5º square). The stimulus was presented randomly at each position interleaved with a blank stimuli. Using custom written MATLAB scripts, spike counts were obtained during stimulus (black square) and blank (mean luminance gray square) for each channel. The stimulus driven spike counts (0-200ms) minus blank (-200-0ms) was plotted for each location of the grid, and the geometric center that was strongly activated by stimulus evoked MUA was chosen as RF location for each contact (Figure 3.3-A). If stimulus-evoked spike-counts of all contacts showed similar hot spots in the grid, meaning they are all mapping on similar RF in the visual field, we continued the experiment for that penetration, otherwise, the probe was retracted and was readvanced in another cortical position. In addition to finding the Cartesian coordinates of RF for all channels, other V1 neuronal characteristics such as orientation, spatial frequency, and temporal frequency were characterized via measuring the tuning curves of all contacts across the cortical column using sinusoidal drifting gratings. Specifically, orientation-tuning curves showed if the sampled penetration was

from a V1 orientation column (such as in Figure 3.3-B). Obtaining the preferred properties of all contacts across layers, we chose the orientation, spatial frequency and temporal frequency that were optimal for most contacts. Then we measured area summation of all contacts with the chosen parameters using a circular drifting grating patch at 100% contrast that was centered over the geometric center of the grid hot spot. The patch diameter expanded from 0.1 to 26° with smaller steps up to 2 degrees and larger ones beyond that. We plotted the size-tuning curve for each contact after (i.e., firing rate vs. stimulus size) the block of stimuli was finished and chose the RF size for the column.

3.2.4 Visual Stimuli

The near surround was probed by the same flashing square stimuli covering nearby RF (< 1° from the center of RF, which was at 500ms stimulus presentation and 500ms blank). Two criteria were met; first, near surround evoked less than 50% spiking activity compared to RF location (Figure 3.4-F). Second, thalamocortical recipient layer 4C was not the first layer activated in time obtaining the CSD profile (Figure 3.4-B). The far surround was probed by 2° annular static gratings (Figure 3.2-B) that were moving from the edge of RF outward for 500 ms following by 750 ms blank. The surround inner diameter (beyond 2° from RF center) was chosen when the annular grating was not evoking spiking activity, which is consistent with previous studies (Ichida et al., 2007; Shushruth et al., 2013). Similar to the near surround, far surround did not evoke earliest current sink in L4C (Figure 3.4-D and 3.4-H).

3.2.5 Current Source Density Analysis

Current source density was applied on the trial averaged LFP using the kernel CSD toolbox (Potworowski et al., 2012). CSD is the second spatial derivative approximation of the LFP signal, which reflects the net local transmembrane currents that generate LFP. CSD was computed as:

$$\text{CSD (x)} = -\sigma * \frac{v(x-h)-2v(x)+v(x+h)}{h^2} \quad (3.1)$$

in which, v is the voltage (μV), x is the point in the extracellular medium that CSD is calculated at, h is the spacing between recording contacts of the linear probe (here 100μm), and σ is the connectivity of the cortical tissue (0.4 S/m)(Logothetis et al., 2007).

To estimate CSD across layers, we interpolated the CSD every 10μm. CSD provides information about current flow in the extracellular medium (Nicholson and Freeman, 1975; Mitzdorf and Singer, 1979; Mitzdorf, 1985). Specifically, it localizes current sources and sinks across cortical layers that receive afferent inputs. Current sink in the extracellular medium usually occurs before the cell depolarizes (Schroeder et al., 1998), and the outward current in the extracellular medium becomes negative (current sink). The recurrent flow coming out of the cell causes the source localization in the extracellular space (positive current)(Buzsaki et al., 2012). Thus the current sink is a signature of integrated subthreshold inputs at the postsynaptic dendrites. Current sink and sources are well localized in the extracellular medium by the contribution of asymmetric neurons such as pyramidal cells with long distal dendrites (Buzsaki et al., 2012). The current flow into the distal dendrites localizes the current sinks in the medium further away from the recurrent source close to the soma. But, in those symmetrical neurons that do not have an open field, such as stellates, the current sink will be balanced by other sinks/sources in

other directions. However, all the dendrites in spherical cells are not active at the same time, thus, small dipoles would be still generated. In addition, the amplitude of the sink and source drops with distance from their neuronal origins (Buzsaki et al., 2012).

Due to the fact that surround stimuli does not activate spiking activity (i.e., it is close to the baseline), we measure the timing of current sinks that are not masked by spiking activity and aim to understand the temporal profile of inputs to different layers.

3.2.5.1 Z-score of CSD

In order to increase signal to noise ratio, CSD was baseline corrected (Z-scored). In particular, we normalized the CSD of each profile to the standard deviation of the baseline (200ms prior to stimulus onset) after its mean was subtracted.

$$\text{Z-CSD}(t) = \frac{CSD_{st}(t) - mean(CSD_b)}{std\ (CSD_b)} \tag{3.2}$$

where, $CSD_{st}(t)$ is the computed CSD at each time point (every 0.5ms) after stimulus onset, and CSD_b is the computed CSD during blank (-200-0ms).

3.2.5.2 Laminar borders

CSD that is recorded vertically across cortical layers is known to provide a good landmark of L4C boundaries in primary sensory cortices (Figure 3.1-D) (Mitzdorf and Singer, 1979; Schroeder et al., 1991; Schroeder et al., 1998), and is used for the identification of laminar borders. In particular, the CSD profile that corresponded to the hot spot of the RF grid (mapped by MUA, Figure 3.3-A) was used to localize the border caused by both current sinks in L4C and current sources in L5. This polarity reversal of current is a robust measure of border boundaries (Schroeder et al., 1998). Also, the depth

of the cortex was obtained by comparing the CSD profile with spiking activity. In particular, the fastest L4C was compared with the fastest onset of spiking activity in response to RF stimulation. Usually, as it is shown in Figure 3.4-E, the first stimulus onset occurs at the top of L4C (4Cα, magnocellular pathway) and L6 due to LGN collateral terminations. Also, using spiking activity, we had an estimate of L1 and white matter that do not evoke supra-threshold action potentials. Based on previous studies (Lund, 1973, 1988), the thickness of L4C was assigned to be 200-300μ; infragranular (IG) layers from bottom of cortex encompass 500-600μ and supragranular (SG) layers from the top of cortex cover 600-750μ. In addition, results of the CSD method were confirmed with histology, allowing for identification of cortical layers and sublayers specifically L4C (Lund, 1988).

3.2.5.3 CSD alignment

Obtaining the border of L4C based on CSD and MUA, we aligned penetrations together. For most of the vertical penetrations the border of L4C and L5 was at the depth of 1.05/1.15 and total V1 depth was 1.45-1.6. Taking into account the cortical thickness variations (1.45-1.6), we were able to align all L4C to each other manually (0.75-1.05). This method is in line with one study (Self et al., 2013), but instead of aligning to a reference penetration, we aligned all penetrations based on their L4C borders.

3.2.5.4 Grand averages

To obtain grand averages of Z-CSD (Figure 3.5 Panels A-D), we half-wave rectified all the aligned Z-CSD profiles to their negative values (discarding the positive source

values) and then normalized them between -1 and 0, so that the penetration that had the largest Z-CSD amplitude did not weight the grand average. After normalized rectification, the average Z-CSD of each specific stimuli (RF, near, near-far border and far surround) was obtained, and this is called the "grand average".

3.2.6 Latency Analysis of CSD

The onset latency of CSD was measured for each depth by finding the earliest time bin after stimulus onset in which the CSD amplitude was at least 3-6 SD below the baseline. In order to avoid threshold crossings due to noise, the CSD signal was required to remain below the threshold for at least three consecutive 5 ms bins before a threshold crossing was logged. The time of the first bin was taken as the signal onset. For some stimulus set, due to the nature of weak visual signal (i.e., far surround) the threshold was set higher (i.e., 5, 6, or 7 SD). Consistent with previous studies (Schroeder et al., 1990; Tenke et al., 1993; Givre et al., 1994; Schroeder et al., 1997), and since negative deflections in LFP and CSD signals (termed current sinks) are assigned to net local depolarization, we use them as latency of inputs.

3.3 Results

Stimulation of columnar RF evokes the fastest current sink happening in L4C representing termination of thalamocortical afferents from LGN (Schroeder et al., 1991). The localization of current sink is followed by SG and IG layers (Figures 3.1-D, 3.4-A and 3.5-A). This pattern of L4C activation is also in line with the evoked postsynaptic spiking activity in L4C and L6 (Figure 3.4-E) driven by collaterals. The sink in L6 is not

strong enough due to strong recurrent source in L5, possibly masking the current sink in L6.

Activation of near surround by small flashing squares (0.5˚) outside the RF evokes the fastest current sink in SG (mainly L2/3) and IG (mainly upper IG) layers at the same time, followed by delayed L4C. This pattern of activation is consistent with involvement of horizontal connection in the aforementioned layers (Figures 3.4-B and 3.5-B). It is important to remember that surround stimuli by itself (in the absence of RF stimulation), does not activate spiking activity (Hubel and Wiesel, 1965). Thus, LFP and its corresponding CSD represent the population dendritic inputs in the extracellular medium. As shown in Figure 3.4-F, MUA activity is decreased markedly in amplitude compared to RF stimulation (Figure 3.4-E), confirming that the postsynaptic spiking activity is diminished considerably and the CSD is truly reflecting dendritic input.

Stimulation of the far surround (beyond 2˚ from the center of RF) by annular gratings (2˚ width) localizes the earliest response in L1/2A and low IG (L6) but significantly delayed in SG (L2/3) and top IG (L5A) layers. Similar to near surround, far surround does not evoke postsynaptic spiking activity (Figure 3.4-H).

In addition, stimulating the near-far-border region evokes L1/2A, low IG, and L2/3 while top IG is delayed. This could be explained by involvement of feedback terminations in L1/2A and low IG with a small delay of monosynaptic horizontal connections in L2/3 and larger delay in top IG.

Figure 3.5 represents grand averages where each rectified profile (negative values are kept) is normalized and then averaged with other penetrations for each condition (i.e., RF, near, near-far border and far surround, see **3.2.5.3**). Panels A-D essentially show

similar patterns of activation as the example penetration in Figure 3.4.A-D. Since the grand average profile is rectified, there is less variability during blank; hence, we used SD=7 to pick the corresponding latencies.

The difference in the laminar pattern activated by the near and far surround is in line with our hypothesis that feedback connections from higher visual cortical areas, that terminate prominently in L1/2A and lower IG layers, are the main substrate of far surround modulation, while the near surround is mainly generated by intra-V1 horizontal connections that are dense in L2/3 and top IG and to some extent by feedback (fast L1/2A and low IG) or interlaminar connections.

3.3.1 Latency Distribution of Near and Far Surround

Similar to the example penetration (Figures 3.4-A), all vertical penetrations (n =10) show similar time profiles of current inputs across layers in response to stimulation of near and far surround. Because of the topographical location of the penetrations, that is, sampling from an orientation column or a pinwheel, there was a large variation in the absolute latencies between recordings in each specific layer. To compensate for this, the minimum latency of each profile (i.e., RF, near or far) was subtracted from the fastest latencies in each layer. The value is called "delta-latency=DL." The closer DL to 0, the faster the latency. Figure 3.6 shows the distribution of DL in each layer in response to different stimuli (RF, near, near-far border and far surround). Consistent with previous studies, the fastest stimulus onset is happening in L4C (DL =0) in response to stimulation of columnar RF (n =17 conditions). Applying the Kruskal-Wallis nonparametric test with Bonferroni corrections, L4C is significantly faster than L1/2A (p =0.0021), L2/3 (p =

0.002) and low IG (p = 0.0484), except L4B (p = 0.1449) and top IG (p = 0.1040). The large variation in low IG could represent involvement of thalamocortical collaterals terminating in lower IG (L6). But it is not always there due to the cancelations of weak current sinks by stronger current sources in top IG.

In the near surround (Figure 3.6-B, n =16 conditions), all the layers, except L4B, were significantly different from L4C being the latest (L1/2A, p = 0.0013; L2/3, p =0 .0023; top IG, p <0.0001; low IG, p =0.0239). However, there were no significant pairs across L1/2A, L2/3, top and low IG. These results can imply that in the near surround both horizontal and feedback connections are involved as it is proposed in earlier studies (Angelucci and Sainsbury, 2006)). Nevertheless, due to the larger RF size of higher visual areas, near surround stimulated by small squares (0.5˚ from the center of RF) might engage monosynaptic horizontal axons more strongly than weak feedback terminations.

In the surround region, referred to near-far-border (Figure 3.6-C, n =4 conditions), there are still no significant pairs among L2/3, L1/2A, top and low IG. The main difference with near surround is that L1/2A and low IG are receiving inputs a little faster than L2/3 and top IG. Remarkably, the distribution median of low IG is faster than the distribution median of top IG in near-far-border surround (0 ms vs. 17.25ms; Figure 3.6-C), which is not the case in the near surround (4.5 ms vs. 0 ms; Figure 3.6-B).

In the far surround (Figure 3.6-D, n =9 conditions), DL of L2/3 and top IG were considerably delayed, while L1/2A and low IG remain very fast. Applying the same nonparametric test (Kruskal-Wallis) with multiple comparison correction (Bonferroni), on four layers including L1/2A, L2/3, top and low IG, delta latencies in L1/2A were

significant from top IG (p = 0.0215) and close to significant from L2/3 (p = 0.0653), but not significant from low IG (p >0.5). Similar results were preserved for low IG (vs. L2/3, p = 0.0049; top IG, p = 0.0011). This suggests that feedback terminations, being prominent in L1/2A and low IG (L5B and L6) (Federer et al., 2015), are the main substrate for far surround and provide the first inputs to the V1 cortical column. The variations in the distribution of DL in L1/2A could exist due to the weak engagement of neuronal response by 2° annuli in the far surround. Figure 3.6-E shows the mean and standard error of delta latency in response to RF, near, near-far border and far surround stimuli.

3.4 Discussion

In this chapter, we have examined the temporal dynamics of inputs across V1 layers in response to stimulation of near and far surround. Since termination of feedforward, feedback, and intrinsic horizontal connections across V1 layers show distinct patterns (Chapter 1; Figure 1.3-B), we questioned whether the latency of inputs probed by near and far surround stimulation would reflect the underlying circuit of different surround regions.

A number of studies reported the temporal profile of current inputs to the cortical column by measuring the latency of current sink, which is a robust marker of net synaptic inputs to the extracellular neuronal ensemble. These studies reported the spatiotemporal profile of V1 column in response to color stimuli (Givre et al., 1995), diffuse flashes of lights (Schroeder et al., 1991; Schroeder et al., 1998), square-wave (Schroeder et al., 1991) or sine-wave gratings (Hansen et al., 2012) while activating the columnar RF. Schroeder et al.(1998) showed that diffuse flashes of light evoked the feedforward stream

localizing the fastest current sink in granular layers, followed by extragranular layers in area V1 and V2, which is consistent with previous reports (Mitzdorf and Singer, 1979; Maunsell and Gibson, 1992; Givre et al., 1994; Givre et al., 1995). Recently, Hansen et al.(2012) reported that the trial-to-trial correlated variability varies across layers, being weaker in granular layers and stronger in output layers, including supra- and infra-granular ones. In their study, they also used a 5° static sinusoidal grating implying that the columnar RF and near surround were stimulated.

Others (Self et al., 2013) studied the spatiotemporal pattern of V1 layers in a figure-ground segregation task in awake behaving primates. When the figure was overlapping the columnar RF, a pattern similar to stimulating the canonical pathway across layers of V1 was observed (fastest current sink in L4C followed by other layers). In the later part of the response (after 100ms from stimulus onset) there were sustained activities in L1/2A and L5 that is claimed to present involvement of feedback inputs in region filling task. They also used the spatiotemporal profile of inputs to the cortical column and related that to feedback terminations.

In the aforementioned studies, activation of columnar RF in primary sensory cortices drove excitatory postsynaptic spikes first in thalamocortical recipient layer 4C leading to firing action potentials in supra and infra granular layers. This activation of recurrent laminar networks would mask the effect of current inputs even if the surround region was stimulated. Hence, in order to study the temporal dynamic of inputs caused by near and far surround stimulation, we did not present any stimuli inside the columnar RF to prevent the flow of postsynaptic activity across layers. Using small flashing squares reversing in contrast, we probed the near surround which was 0.25-1° away from the edge

of columnar RF (Figures 3.2-A and 3.3-A). The first inputs by near surround were observed out of granular layers and were simultaneously localized in both supra- and infra-granular layers. L4C was significantly delayed from L1/2A, L2/3, and IG layers ($P < 0.05$, Figure 3.6-B). This pattern of activation is consistent with dense horizontal projections in L2/3 and top IG (Angelucci et al., 2002). However the fast activation of L1/2A and low IG as it was observed in top IG and L2/3 (Figure 3.6-B) suggests that feedback might also be engaged in the near surround. There is anatomical evidence (Guillery and Sherman, 2002) showing that there are routes from subcortical structures to the extrastriate cortex while bypassing V1 that have modulatory roles. In addition, studying the latency of current sinks across dorsal and ventral visual pathways by laminar recordings, Schroeder et al. (1998) claimed that V4 showed earlier onset latencies than spiking activity of supragranular layers in V1 that are the source of feedforward inputs to V4. These latencies were correlated with hyperpolarizing modulatory signals while the driving excitatory signals measured by the latency of post synaptic spiking activity emerged later in L4C of V4 after SG layers of V1 (Maunsell and Gibson, 1992; Givre et al., 1995). In sum, this studies reveal the possibility of involving the fast feedback connections in the near surround as was also proposed in the initial model by Angelucci and colleagues (Angelucci and Bressloff, 2006).

Using 2° static annular gratings encompassing beyond the edge of the RF, we probed the far surround. Former studies characterized the extent of the far surround beyond 2° from the center of RF (Ichida et al., 2007; Shushruth et al., 2009; Shushruth et al., 2012). These stimuli localized the fastest current sink in L1/2A and deep IG followed by delayed L2/3 with top IG and granular layers suggesting that feedback connections terminating to

L1/2A and low IG are the main substrate of far surround. However, in some penetrations the far surround was further away from the center of RF (beyond 3° in radius), and we could observe closer regions that engaged both horizontal and feedback connections (Figure 3.6-C, n =4). The grand average of this region, which was called near-far border, showed delayed top IG but still fast L2/3 with a small delay relative to L1/2A and low IG. Presumably, this region is involving feedback from the extrastriate cortex but still could engage monosynaptic horizontal connections of V1.

There are a couple of limitations in this study: one is, we probed near and far surround using different stimuli (i.e., small flashing squares vs. 2° annular gratings). Closer annular gratings to RF (<1°) were found to activate columnar RF, so we used small flashes of light to isolate monosynaptic horizontal connections that could also address the asymmetry in the surround (Walker et al., 1999). In particular, in identical distances from center of geometric RF, some positions evoked spikes in granular layers while others did not. The second caveat was that the strength of LFP and the following CSD were weak in response to far surround stimulation although we were using large annular gratings. Thus, we chose higher SD to pick up the latency of current sinks from ongoing brain oscillations observed during blank.

In sum, these results shed light on distinct underlying mechanisms of near and far surround by linking the temporal profile of inputs across layers with the known anatomical connections. The significance of the results of this chapter reveals how local field potential and its spatial derivatives can be employed to study the neuronal behaviors in response to any task or stimuli that has modulatory but not driving role. Future studies, such as optogenetic manipulation, can selectively activate or inactivate different

connections in each layer to study their causal role in generating different properties of near and far surround. Furthermore, there is a little known about the role of different layers in processing natural images. One can correlate the properties of natural images encompassing near and far surround across V1 layers.

3.5 References

Angelucci A, Bressloff PC (2006) The contribution of feedforward, lateral and feedback connections to the classical receptive field center and extra-classical receptive field surround of primate V1 neurons. Prog Brain Res 154:93-121.

Angelucci A, Sainsbury K (2006) Contribution of feedforward thalamic afferents and corticogeniculate feedback to the spatial summation area of macaque V1 and LGN. J Comp Neurol 498:330-351.

Angelucci A, Levitt JB, Walton E, Hupé JM, Bullier J, Lund JS (2002) Circuits for local and global signal integration in primary visual cortex. J Neurosci 22:8633-8646.

Blasdel GG, Lund JS (1983) Terminations of afferent axons in macaque striate cortex. J Neurosci 3:1389-1413.

Buzsaki G, Anastassiou CA, Koch C (2012) The origin of extracellular fields and currents--EEG, ECoG, LFP and spikes. Nat Rev Neurosci 13:407-420.

Callaway EM (1998) Local circuits in primary visual cortex of the macaque monkey. Ann Rev Neurosci 21:47-74.

Callaway EM (2004) Feedforward, feedback and inhibitory connections in primate visual cortex. Neural Networks 17:625-632.

Federer F, Merlin S, Angelucci A (2015) Anatomical and functional specificity of V2-toV1 feedback circuits in the primate visual cortex. Soc Neurosci Abstr Online.

Givre S, Arezzo JC, Schroeder C (1995) Effects of wavelength on the timing and laminar distribution of illuminance-evoked activity in macaque V1. Visual Neurosci 12:229-239.

Givre SJ, Schroeder CE, Arezzo JC (1994) Contribution of extrastriate area V4 to the surface-recorded flash VEP in the awake macaque. Vision Res 34:415-428.

Guillery R, Sherman SM (2002) Thalamic relay functions and their role in corticocortical

communication: generalizations from the visual system. Neuron 33:163-175.

Hansen BJ, Eagleman S, Dragoi V (2011) Examining local network processing using multi-contact laminar electrode recording. J Vis Exp.

Hansen BJ, Chelaru MI, Dragoi V (2012) Correlated variability in laminar cortical circuits. Neuron 76:590-602.

Hendrickson AE, Wilson JR, Ogren MP (1978) The neuroanatomical organization of pathways between the dorsal lateral geniculate nucleus and visual cortex in Old World and New World primates. J Comp Neurol 182:123-136.

Henry CA, Joshi S, Xing D, Shapley RM, Hawken MJ (2013) Functional characterization of the extraclassical receptive field in macaque V1: contrast, orientation, and temporal dynamics. J Neurosci 33:6230-6242.

Hubel DH, Wiesel TN (1965) Receptive fields and functional architecture in two nonstriate visual areas (18 and 19) of the cat. J Neurophysiol 28:229-289.

Ichida JM, Schwabe L, Bressloff PC, Angelucci A (2007) Response facilitation from the "suppressive" receptive field surround of macaque V1 neurons. J Neurophysiol 98:2168-2181.

Kajikawa Y, Schroeder CE (2011) How local is the local field potential? Neuron 72:847-858.

Kulics A, Cauller L (1986) Cerebral cortical somatosensory evoked responses, multiple unit activity and current source-densities: their interrelationships and significance to somatic sensation as revealed by stimulation of the awake monkey's hand. Exp Brain Res 62:46-60.

Lakatos P, Chen CM, O'Connell MN, Mills A, Schroeder CE (2007) Neuronal oscillations and multisensory interaction in primary auditory cortex. Neuron 53:279-292.

Lakatos P, Karmos G, Mehta AD, Ulbert I, Schroeder CE (2008) Entrainment of neuronal oscillations as a mechanism of attentional selection. Science 320:110-113.

Logothetis NK, Kayser C, Oeltermann A (2007) In vivo measurement of cortical impedance spectrum in monkeys: implications for signal propagation. Neuron 55:809-823.

Lund JS (1973) Organization of neurons in the visual cortex, area 17, of the monkey (Macaca mulatta). J Comp Neurol 147:455-496.

Lund JS (1988) Anatomical organization of macaque monkey striate visual cortex. Ann Rev Neurosci 11:253-288.

Maunsell JH, Gibson JR (1992) Visual response latencies in striate cortex of the macaque monkey. J Neurophysiol 68:1332-1344.

Mitzdorf U (1985) Current source-density method and application in cat cerebral cortex: investigation of evoked potentials and EEG phenomena: Am J Physiol

Mitzdorf U, Singer W (1979) Excitatory synaptic ensemble properties in the visual cortex of the macaque monkey: a current source density analysis of electrically evoked potentials. J Comp Neurol 187:71-83.

Müller-Preuss P, Mitzdorf U (1984) Functional anatomy of the inferior colliculus and the auditory cortex: current source density analyses of click-evoked potentials. Hearing Res 16:133-142.

Nicholson C, Freeman JA (1975) Theory of current source-density analysis and determination of conductivity tensor for anuran cerebellum. J Neurophysiol 38:356-368.

Potworowski J, Jakuczun W, Leski S, Wojcik D (2012) Kernel current source density method. Neural Comput 24:541-575.

Rockland KS, Pandya DN (1979) Laminar origins and terminations of cortical connections of the occipital lobe in the rhesus monkey. Brain Res 179:3-20.

Schroeder C, Mehta A, Givre S (1998) A spatiotemporal profile of visual system activation revealed by current source density analysis in the awake macaque. Cereb Cortex 8:575-592.

Schroeder C, Seto S, Arezzo JC, Garraghty P (1995) Electrophysiological evidence for overlapping dominant and latent inputs to somatosensory cortex in squirrel monkeys. J Neurophysiol 74:722-732.

Schroeder C, Tenke C, Givre S, Arezzo JC, Vaughan H (1991) Striate cortical contribution to the surface-recorded pattern-reversal VEP in the alert monkey. Vision Res 31:1143-1157.

Schroeder CE, Tenke CE, Givre SJ, Arezzo JC, Vaughan HG, Jr. (1990) Laminar analysis of bicuculline-induced epileptiform activity in area 17 of the awake macaque. Brain Res 515:326-330.

Schroeder CE, Javitt DC, Steinschneider M, Mehta AD, Givre SJ, Vaughan HG, Jr., Arezzo JC (1997) N-methyl-D-aspartate enhancement of phasic responses in primate neocortex. Exp Brain Res 114:271-278.

Self MW, van Kerkoerle T, Super H, Roelfsema PR (2013) Distinct roles of the cortical layers of area V1 in figure-ground segregation. Curr Biol 23:2121-2129.

Shushruth S, Ichida JM, Levitt JB, Angelucci A (2009) Comparison of spatial summation properties of neurons in macaque V1 and V2. J Neurophysiol 102:2069-2083.

Shushruth S, Mangapathy P, Ichida JM, Bressloff PC, Schwabe L, Angelucci A (2012) Strong recurrent networks compute the orientation-tuning of surround modulation in primate primary visual cortex. J Neurosci 4:308-321.

Shushruth S, Nurminen L, Bijanzadeh M, Ichida JM, Vanni S, Angelucci A (2013) Different orientation-tuning of near and far surround suppression in macaque primary visual cortex mirrors their tuning in human perception. J Neurosci 33:106-119.

Sincich LC, Horton JC (2005) The circuitry of V1 and V2: integration of color, form and motion. Ann Rev Neurosci 28:303-326.

Steinschneider M, Tenke CE, Schroeder CE, Javitt DC, Simpson GV, Arezzo JC, Vaughan HG (1992) Cellular generators of the cortical auditory evoked potential initial component. Electroencephalogr Clin Neurophysiol /Evoked Potentials Section 84:196-200.

Tenke CE, Schroeder CE, Arezzo JC, Vaughan HG, Jr. (1993) Interpretation of high-resolution current source density profiles: a simulation of sublaminar contributions to the visual evoked potential. Exp Brain Res 94:183-192.

Ungerleider LG, Desimone R (1986) Cortical connections of visual area MT in the macaque. J Comp Neurol 248:190-222.

Walker GA, Ohzawa I, Freeman RD (1999) Asymmetric suppression outside the classical receptive field of the visual cortex. J Neurosci 19:10536-10553.

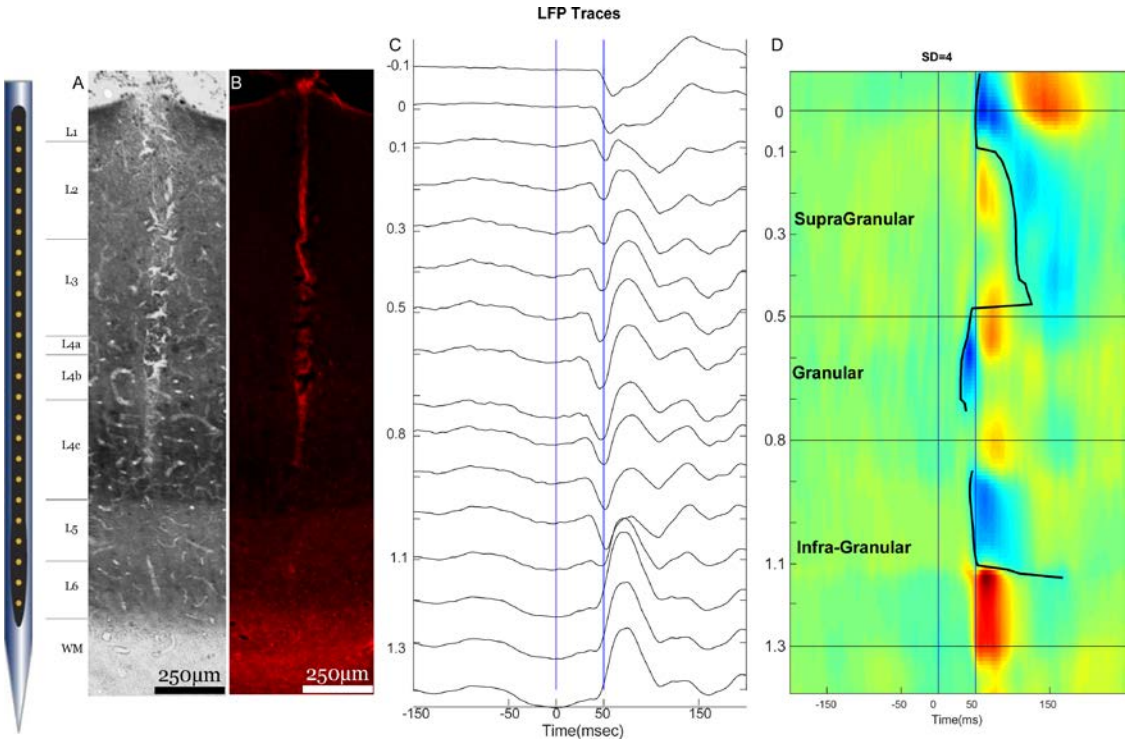

Figure 3.1: Example penetration A) is the CO stained section B) shows the DiI track of the probe C) LFP traces recorded from all channels (See methods). D) The computed CSD from LFP traces in panel C, sink is shown in blue and source is shown in red. In both C and D blue vertical lines show stimulus onset and 50ms delay. The black line overlayed on the CSD heatmap is the computed latency of current sink, which was obtained by 4 SD above the blank response.

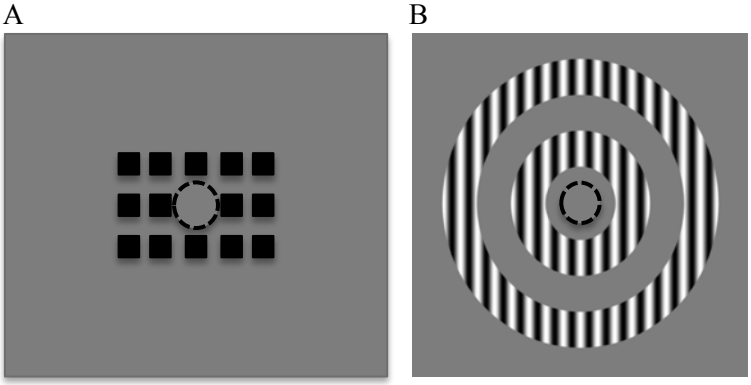

Figure 3.2: The visual stimuli to probe A) near and B) far surround. The dashed circles in both panels show the presumed RF extent.

Figure 3.3: Receptive field (A) and orientation (B) mapping across every other contacts for similar penetration as in Figure 3.1. A) Represents the RF mapping using MUA, for most of the contacts receptive fields are aligned with 1 degree precision in the visual field, each square covers 0.5° in the visual field. B) Represents the orientation tuning curves using MUA for similar contacts as in panel A. The red traces are obtained by least square methods fitting summation of two Gaussians.

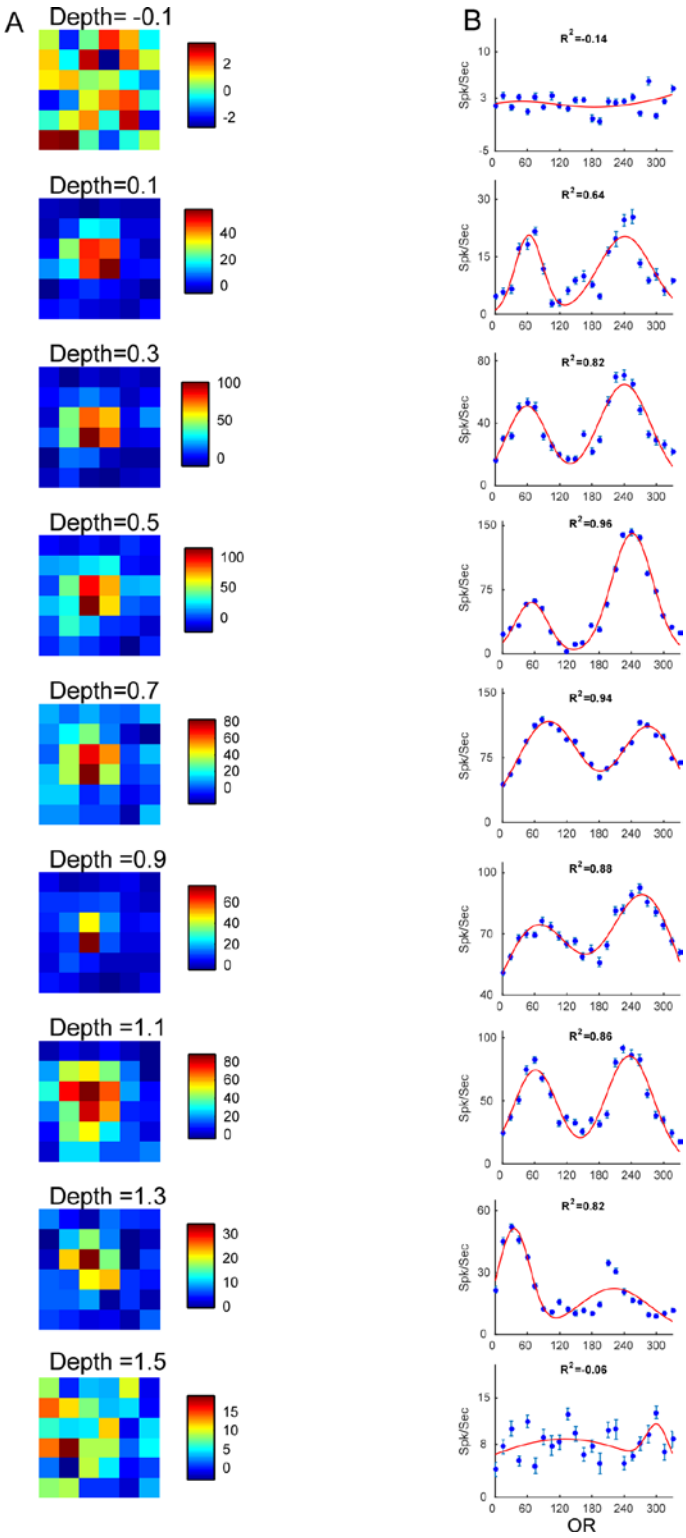
A
Depth= -0.1
2
0
-2
Depth=0.1
40
20
0
Depth=0.3
100
50
0
Depth=0.5
100
50
0
Depth=0.7
80
60
40
20
0
Depth =0.9
60
40
20
0
Depth =1.1
80
60
40
20
0
Depth =1.3
30
20
10
0
Depth =1.5
15
10
5
0
B
R²=-0.14
R²=0.64
R²=0.82
R²=0.96
R²=0.94
R²=0.88
R²=0.86
R²=0.82
R²=-0.06
Spk/Sec
0 60 120 180 240 300
OR

Figure 3.4: The CSD heat map and MUA PSTH for an example penetration. A-D) the rectified Z-score of CSD in response to columnar A) RF, B) near, C) near-far border and D) far surround. Layers are separated by horizontal black lines. The black contour overlaid on each is the latency computed by SD=6 for each panel. E-H) is the PSTH of MUA for similar conditions (on the left). All PSTH are normalized to the maximum of panel E. E) shows that the fastest postsynaptic activity is localized in 4Ca and L6 consistent with the canonical terminations. F-H) shows the spiking activity is diminished dominantly by stimulation of the surround only.

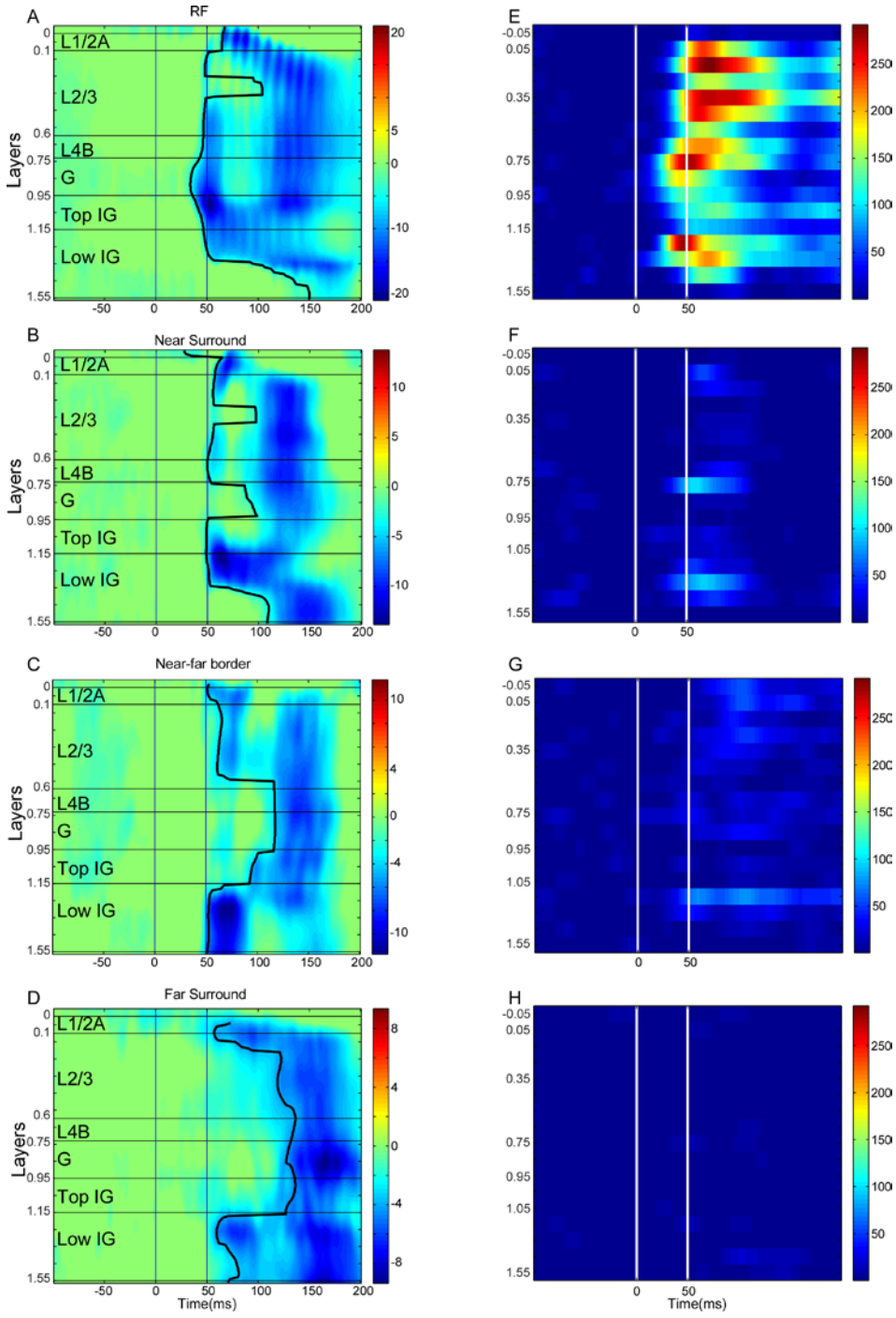
A
RF
B
Near Surround
C
Near-far border
D
Far Surround
E
F
G
H
L1/2A
L2/3
L4B
G
Top IG
Low IG
Layers
Time(ms)

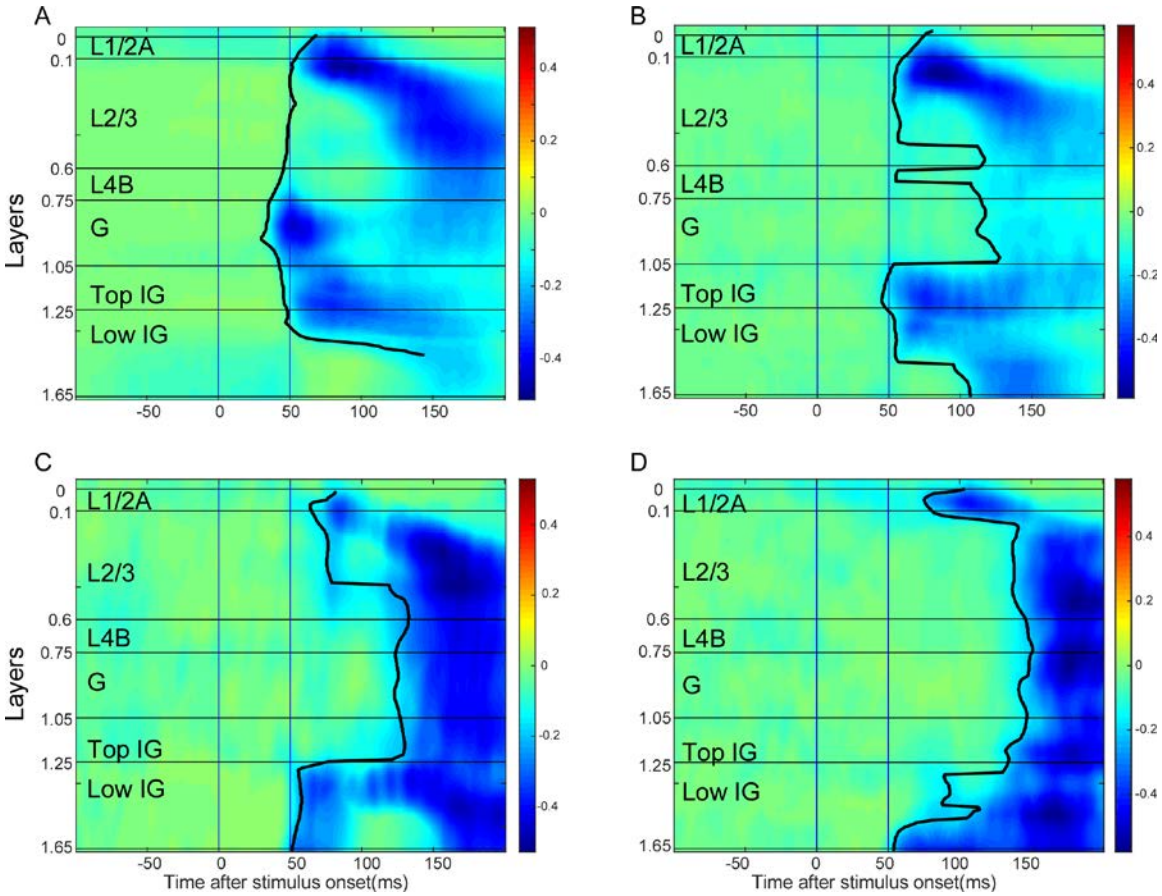

Figure 3.5: Indicates the grand averages of rectified and normalized Z-CSD of all penetrations for each corresponding stimuli superimposed by latency profiles (black contours). SD=7 is chosen for the grand averages. In A-D layer borders are shown in horizontal black lines.

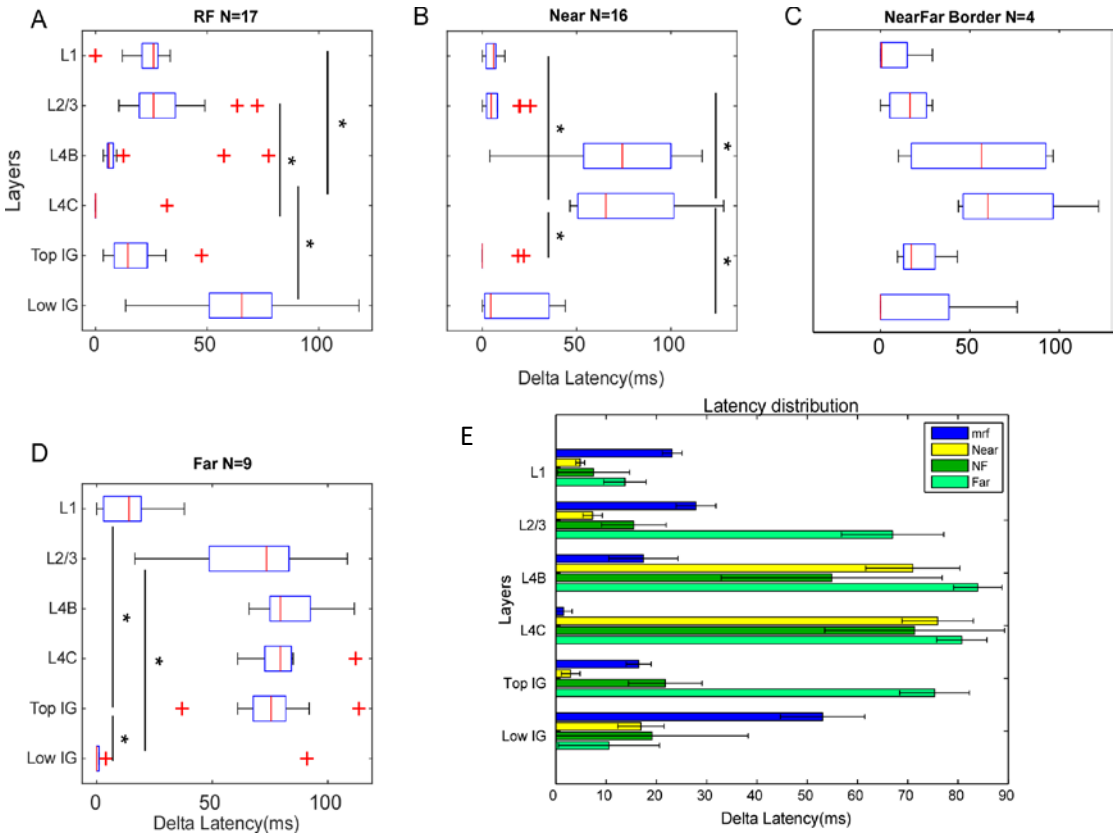

Figure 3.6: Distribution of delta latency in response to RF, near and far surround. A) Shows the distribution of DL for RF activation, L4C was significantly faster than L2/3, L1, top IG and low IG, (See results for statistical values). B) Represents the DL distribution in response to near surround. L4C was significantly later than all other layers but not from L4B. C) DL distribution for Near-far border. D) The DL distribution results that L1 and low IG were significantly different from L2/3 and top IG but not from each other. D) Shows the mean distribution of DL for the 4 different stimuli with corresponding SEM. All latencies are computed by 5 SD from the blank on the nonrectified version of each profile.

CHAPTER 4

TEMPORAL DYNAMICS OF UNTUNED AND ORIENTATION-TUNED SURROUND SUPPRESSSION ACROSS LAYERS OF THE PRIMARY VISUAL CORTEX

4.1 Introduction

In Chapter 3, we studied the spatiotemporal profile of inputs caused by near and far surround stimulation. Consistent with the original model by Angelucci and colleagues (Angelucci and Levitt, 2002; Angelucci and Bullier, 2003; Angelucci and Bressloff, 2006; Angelucci and Sainsbury, 2006), and the results from Chapter 3, distinct temporal dynamics across layers suggested two different neuronal mechanisms underlying near and far surround: that near surround is mainly generated by LGN afferents and horizontal connections, while far surround is mainly generated by feedback from higher visual centers such as V2, V3, and MT in anesthetized primates (Figure 1.5). In this chapter, we examine how the temporal dynamics of outputs (postsynaptic spiking activity) vary across layers of V1 and is related to the inputs' profile.

In particular, to study the postsynaptic targets affected by the surround, we measure the spiking rate to stimulation of both RF and surround regions (i.e., near and far). As mentioned in Chapter 1, surround modulation (SM) in V1 occurs when neuronal response

(spikes) to stimulation of the receptive field (RF) of a neuron is modulated by simultaneous stimulation outside of the receptive field. The receptive field surround by itself cannot evoke neuronal responses but can modulate responses to stimulation of the RF (Blakemore and Tobin, 1972; Maffei and Fiorentini, 1976; Nelson and Frost, 1978; Allman et al., 1985). It has been proposed that SM is a powerful representation of visual contextual modulation (Bair et al., 2003) and plays an important role in figure-ground segregation (Lamme, 1995), detection of salient targets (Petrov et al., 2005), and texture pop-out mechanisms (Knierim and Van Essen, 1992).

As it is previously outlined SM has various functional properties. (1) It is contrast sensitive; specifically when RF is of high contrast, independent of surround contrast it would be usually suppressive (DeAngelis et al., 1994; Cavanaugh et al., 2002a; Shushruth et al., 2009). (2) It is orientation selective; suppression is likely to be strongest when RF and surround gratings are iso-oriented and weakest when they are cross-oriented (DeAngelis et al., 1994; Sillito et al., 1995; Cavanaugh et al., 2002a). Recently, it is shown that this characteristic is preserved even when the RF and surround are stimulated by suboptimal orientation for a given V1 cell (Sillito et al., 1995; Shushruth et al., 2012). (3) It is distant dependent, suppression is stronger in the nearby regions of RF (near surround) and becomes weaker by increasing distance from RF (far surround) (Sceniak et al., 2001; Cavanaugh et al., 2002a; Bair et al., 2003; Shushruth et al., 2009). (4) It is tuned to spatial frequency, being strongest in low frequencies (Webb et al., 2005). In addition, similar spatial frequency of RF and surround cause suppression.

Here, we focus on spatial extent and orientation selectivity of SM. There are numerous studies supporting the idea that different spatial extents of SM (near and far surround in

this dissertation) mirror distinct underlying circuits. Essentially, the proposal is based on both anatomical extent of monosynaptic horizontal connections (Angelucci et al., 2002) and their slow conduction velocity (Girard et al., 2001), suggesting that polysynaptic horizontal projections are slower than fast far surround modulation (Grinvald et al., 1994; Nowak and Bullier, 1997; Girard et al., 2001; Slovin et al., 2002). However, fast inter-areal connections (2-6 m/s) between V1 and the extrastriate areas (Girard et al., 2001) could serve as the main substrate for modulation from far surround (12.5° from the RF center) that is shown to have 9-60ms latency relative to RF onset in the parafoveal V1(Bair et al., 2003). Bair and colleagues (2003) also showed that the time of surround suppression does not increase with distance from the RF, and is not consistent with the involvement of time consuming polysynaptic chains of horizontal connections (see Chapter 1, section 1.3.2 and 1.3.3)

Furthermore, it is noteworthy that SM has two components, one is fast and orientation insensitive, while the other one emerges later in time and is orientation selective (Bair et al., 2003; Webb et al., 2005). Using reverse correlation, Xing and colleagues (2005) measured the latency of tuned and untuned suppression with the stimuli covering h-sRF and a larger one covering two to five times larger than h-sRF. They observed stronger and more persistent orientation selectivity by larger stimuli. In addition, the time to peak for tuned suppression emerged 17ms later than the time of excitation while the untuned suppression was as fast as RF excitation. This observation was later revisited by Henry and colleagues (2013) using different measures of latency. Computing the cumulative spike counts and taking into account trial variability, they reported that the untuned suppression emerged in the first 25ms after stimulus onset and can be as fast as RF onset, while the

tuned suppression (the difference between iso-oriented RF-surround and cross-oriented RF-surround) emerged in the second 25ms after RF onset. These two studies, along with other reports (Cavanaugh et al., 2002a; Webb et al., 2005; Alitto and Usrey, 2008) suggest that the fast untuned suppression might have a subcortical origin such as LGN, while the tuning is initiated by intracortical processing, possibly by orientation-tuned horizontal or feedback connections.

Most of the aforementioned studies investigated the tuned and untuned components in near surround. In the Chapter 2, we tested the orientation tuning of different spatial extent of surround modulation (near and far), so we investigated the two properties of SM (orientation tuning as well as spatial extent). Pooling all the data together from all layers we observed that, in general, near surround was more sharply orientation-tuned than far surround. But we were interested to examine if there is any functional difference between near and far surround across V1 layers. Taking advantage of histological reconstructions, we have found that near surround was more sharply tuned in layer (L) 3B, L4B, and L4Cα, where horizontal connections are known to be patchy, while far surround was only tuned in layer 4B. Later on Henry and colleagues (2013), also noticed similar results as our findings that near surround is more tuned in L2/3 and L4B, providing more support that near and far surround have different underlying circuits mirrored across layers.

These studies by our group (Shushruth et al., 2013), and Henry and colleagues (2013) were limited by single electrode recordings; thus, they were not able to determine the emergence of untuned and tuned components of surround regions simultaneously across layers. Using laminar microelectrodes that allowed us to measure the neuronal responses from all layers simultaneously, in this chapter, we reexamined the emergence (temporal

covariations) of tuned and untuned elements of near and far SM. By costimulating RF and surround that evokes postsynaptic spiking activity, we will answer the following questions:

1. In which layer does the earliest **untuned** surround suppression emerge in response to costimulation of RF and near / far surround?

2. In which layer does the **tuned** component of surround suppression emerge first?

4.2 Methods

All recordings are made in anesthetized macaques as described in detail in section 3.2.1. Surgical preparations, electrophysiological recordings, RF mapping, and other tuning properties are also explained in sections 3.2.2 and 3.2.3.

4.2.1 Visual Stimuli

To characterize the surround modulation and the temporal profile of tuned and untuned SM, both RF and surround regions were costimulated by static gratings with optimal parameters for the cortical column. In detail, the RF orientation was fixed to be optimal for most of the contacts if the penetration was not sampling an orientation column (50μ), while it was a vertical recording for as a RF column (1-2mm). The spatial frequency was chosen to most effectively drive all of the contacts across layers; in most cases, a low frequency (0.5-1.5 cycles/°) was chosen since we were recording from parafoveal V1 (4-8 ° eccentricities) (see section 3.2.3). The size of RF was chosen after the size-tuning curve was obtained for each contact during experiment. The RF size was selected as a tradeoff between smallest and largest h-sRF across contacts to probe near surround as well as not activating excitatory regions of larger RFs. To probe the surround elements two different

configurations were used: 1) A large disk encompassing both near and far surround from the size-tuning experiment, which was presented at optimal orientation of the RF covering 20˚ of the visual field (i.e., radius=10˚). 2) A center circular grating patch matched to the columnar RF diameter that was surrounded by 2˚ degree annular grating presented in different distances from the edge of RF ranging from 0.5˚ to 5.5° (Figure 4.1 A and C, respectively). The main difference between these two stimuli is that there is a gap (matched to mean luminance gray of the screen defined as blank) between the edge of columnar RF and the surround inner radius in the latter. As the annular grating moves out the gap size increases. Near surround configuration was presumably encompassing the extent of V1 neurons' horizontal and feedforward connections (Figure 4.1-A and B), while far surround configuration, which was selected beyond 2˚ (in radius) from the center of RF (Figure 4.1-C and D), supposedly engaged beyond monosynaptic horizontal connections and LGN afferents (Angelucci et al., 2002; Sceniak et al., 2006; Alitto and Usrey, 2008). In contrast to the RF and annular gratings, the large grating disk would possibly engage all connections including LGN afferents, intra-V1 horizontal connections and feedback projections. To address the temporal emergence of tuned suppression, the same stimuli was used as second configuration above (annular gratings), but the surround grating was randomly presented at iso-oriented or cross-oriented relative to columnar preferred orientation (RF orientation; Figure 4.1.A vs. 4.1.B or Figure 4.1.C vs. 4.1.D).

4.2.2 MUA Analysis

Data were collected and amplified using a 128-channel Cerebus system (Blackrock Microsystems, Salt Lake City, UT). The MUA spikes were obtained by band-pass filtering

(250 Hz-7.5 kHz,) the raw signal, which was continuously recorded at a sampling rate of 30 kHz. The MUA was thresholded automatically by a built-in software in the Cerebus system that was based on the energy of the signal passing a threshold.

4.2.3 Latency Analysis of MUA

The peri-stimulus time histogram (PSTH) was obtained by convolving a Gaussian filter (10ms bandwidth) with MUA raster plots using chronux toolbox (Bokil et al., 2010). This analysis provides spike rates with 2ms resolution. The mean of blank response was subtracted from the whole curve. The latency of suppression comparing the trial-averaged MUA in response to RF and the MUA responses to either iso-oriented surround or cross-oriented surround, was measured as following: First, the absolute value of the signal change (subtracted RF and RF-surround) was obtained; Second, the local minima and maxima of the change was measured (minima=0 means the two curves intersect) and third, after the minimum of local extremums and center onset, the algorithm identified those consecutive bins (20 ms width) that the suppression index was 15% in each and the next bin (shifted by one sample) had larger area under its curve than the current bin. The last criterion means there is larger differences between the two curve in the next bin compared to the current one (integral of the change should be increasing). If these criteria were held for three consecutive bins, then the first bin was chosen as the time of suppression. Essentially, time of suppression was equal or larger than time of center onset. We will refer to this method as divergence method or the first method (Figure 4.1-E). The center (RF) onset was obtained using the 10% of the peak value of the center PSTH as it was defined in other studies (Henry et al., 2013). The same method (divergence method) was used for the tuned

suppression, however, instead of comparing the RF and RF-surround responses, we compared the response to RF-surround at iso-oriented and cross-oriented (orthogonal) configurations. The time of tuned suppression had to be after the minimum of the suppression time computed by RF-surround at iso-oriented and RF-surround at cross-(ortho) oriented stimuli. Also, instead of searching for the bins with 15% suppression index, since we were comparing the PSTH of iso- and cross-oriented conditions, orientation specific suppression index (OSSI) had to reach 10%. We chose positive values of OSSI which means that the iso-oriented condition was suppressing more than cross-oriented one. We just applied all this analysis on those contacts that were at least suppressive for 15% (SI measured in the first 150ms from stimulus onset) at either iso- or ortho-configurations.

4.2.3.1 Second method for measuring latency

We also computed latency by taking into account the trial variability. Similar to Henry et al. (2013), the cumulative spike counts during stimulus presentation were compared between RF-only versus RF-surround stimulation. The cumulative spike counts were generated by bootstrap resampling (with replacement, 5000 iteration) from the population of trials at each time bin (10ms width). The time bin was chosen as the latency, if the corresponding RF spike count was larger than spike count of RF-surround for at least 95% of the time. Also two consecutive bins had to satisfy this condition. This method was applicable to those conditions that the change (difference between any two conditions) was large, but it was not the best method for those conditions that suppression or the differences in tuning were small. Specifically, for far surround that the response is weakly suppressive

or tuned, the latency will grow. Also for those contacts that are strongly suppressive the latency computed by bootstrapping is much larger than the divergence method. For example in Figure 4.1.F the time of suppression is 161ms and 131ms after stimulus onset for iso- and cross-oriented gratings, respectively that is more delayed than in Figure 4.1-E (44ms and 40ms). In addition due to small differences between iso-and cross-oriented conditions the second method did not find any value for the tuned latency while the divergence between the average MUA is happening at 52ms. The drawbacks of the second method is discussed in detail by Bair et al. (2003). In particular, the bootstrapped method fails to pick the tuned time for those contacts that show transient tuning (e.g., Figure 4.1-E). This was more common in the population and it could be due to stimulation by static gratings, which resulted in adaptation after 150-200ms in all conditions including RF. In both panels (Figure 4.1-E and 4.1-F) the center onset is the 10% of the peak response during stimulation of columnar RF.

4.2.4 Suppression Index (SI) and Orientation Specific Suppression Index (OSSI)

The suppression index was computed as below:

$$SI(\theta) = 1 - \frac{R_{CS}}{R_C} \tag{4.1}$$

where θ is the surround orientation for the condition, R_C is the mean of MUA PSTH to the RF only stimulus in the first 150ms after stimulus onset, and R_{CS} is the mean of MUA PSTH to the RF-surround stimulus again in the first 150ms. 0<SI<1 means for the given θ suppression occurred compared with RF activation. While the negative values of SI means there was facilitation. If the signal is strongly suppressed, that is, R_{CS} obtains negative

values compared to baseline, the SI would take larger values than 1.

The orientation-specific suppression index was computed as below (Self et al., 2014) :

$$OSSI = \frac{R_{cross} - R_{iso}}{R_{cross} + R_{iso}} \quad (4.2)$$

R_{cross} and R_{iso} are the similar responses as above for cross- and iso-oriented surround, respectively. This selectivity index shows how the cell was tuned. In the latency analysis for the tuning, the OSSI in each bin had to reach above 10% for further analysis.

4.3 Results

In this section, we investigated the dynamics of surround modulation specifically surround suppression by measuring the latency of MUA across all layers while stimulating both center and surround regions with static sinusoidal gratings (section 4.2.1). We examined whether there are relations between inputs (that were probed in Chapter 3) and outputs that encode surround suppression across V1 layers. As previously described in the method section, for near surround we used 2˚ annuli, in which the distance between the inner radius of the annulus and the center of columnar RF was less than 2˚ (1.4-1.9), instead of small flashing squares (used in Chapter 3 to study the inputs). Horizontal connections were better isolated by small flashing squares (0.5°) rather than symmetrical annuli. However, the flashing squares do not evoke strong suppression in the spiking activity, thus, we used annular gratings to stimulate near surround. For far surround, the distance between the inner radius of the annulus and the center of columnar RF was larger than two degrees (2.4-5˚).

4.3.1 Latency of Near and Far Surround Suppression for the Average PSTH

For each contact, the time of surround suppression is defined to be the point that average MUA (across trials, will be referred as MUA) in response to costimulation of RF and surround diverges from the average MUA in response to RF only stimulation (e.g., green trace vs. blue trace in Figure 4.2-A, respectively). In particular, we chose the iso-oriented surround, due to the fact that it usually evokes the maximum suppression from V1 cells and is also comparable with the iso-oriented large grating disk. Additional criteria are that in each time bin the suppression index should reach 15% to be picked up as the onset of suppression, and the suppression onset is equal or larger than the center onset of the corresponding contact. Figure 4.2 shows the normalized MUA that are averaged across all contacts located in layers 2/3, L4B/4Cα, middle 4C, top IG and low IG (possibly 5b/6). Near surround (n=4 penetrations; a total of 56 contacts; Figure 4.2A-E) evokes the first suppression in the top of IG and L4B/4Cα (24 and 28 ms, respectively, green vertical lines) followed by delayed L2/3 (50 ms), L4C (64 ms) and low IG (76 ms). Since the average of normalized MUA by iso-oriented grating causes facilitation in L5, we suspected maybe near surround is still in the region of sRF. To check this, for two penetrations we included near surround that is further away from RF center (1.9° instead of 1.4°, Figure 4.3.A-E). The latency result remains the same except L4C is suppressed as fast as L2/3 at (48 ms vs. 46 ms), but is still later than L4B/4Cα (26 ms) and top IG (24 ms). Far surround stimulation (Figure 4.2.F-J; n=6 penetrations; a total of 87 contacts), evokes the fastest suppression in top IG (52 ms; Figure 4.2-I green vertical line) followed by L2/3 (58 ms), L4B/4Cα (60 ms), L4C (60 ms) and low IG (70ms).

In addition, the fast untuned suppression in near surround arises as fast as RF onset in some layers, such as L4B/4Cα and top IG (Figure 4.2-B 4.2-D). The untuned suppression in L4B/4Cα can likely be generated by magnocellular afferents terminating in L4Cα contacting on a thin layer of horizontal connections in upper part of this layer as well as L4B horizontal axons (Lund, 1988). Proceeding L4B/4Cα, near surround suppression occurs in L2/3 and might likely arise by existing horizontal connections in this layer (suppression onset – center onset=10ms). Moreover, middle of L4C and low IG that have weaker suppression show the latest suppression onset. We have found a negative correlation between suppression strength and the latency of suppression, that is, the weaker the suppression the slower the suppression onset would be (Figure 4.4-A; r=-.031, p=0.04, n=45). This in agreement with a former report by Bair et al. (2003). However, we do not observe the same behavior in far surround (Figure 4.4-B; r=0.17, p=0.18, n=65).

We then computed the Pearson correlation between the latency of iso-oriented RF-near surround and the latency of iso-oriented RF-far surround for the penetrations that both near and far stimulation were available (n=4 penetrations). Contacts that have latency values for both near and far surround are included (n=37 contacts, i.e., nonNan). Figure 4.4-C represents a high positive correlation between the two populations (r=0.65, p<0.001, n=37). This suggests that for a given contact if near surround is delayed, far surround is also delayed. Essentially, the suppression from far surround could be as fast and variable as near surround.

4.3.2 Latency of Tuned Suppression for the Average PSTH

Then we examine the temporal dynamics of orientation-tuned SM which is thought to play an important role in the perception of edges (Knierim and Van Essen, 1992). We computed the latency of tuned-SM similar to untuned latency. Instead, the time of divergence between iso-oriented and cross-oriented stimuli is obtained (e.g., green curve versus red curve in Figure 4.2-A). In addition, the orientation specific suppression index (OSSI) of corresponding time bin should reach 10%. The fastest orientation-tuned SM (black lines) by near surround stimulation is located in top IG (24ms) followed by L4B/4Cα (46 ms), L2/3(74 ms), low IG, and L4C (144 and 146, respectively). Note that the tuning is weaker in L4C (OSSI=-0.08) and low IG (OSSI=0.03) than SG layers specifically L4B/4Cα (OSSI=0.32), consistent with the result from Chapter 2 and Henry et al. (Henry et al., 2013; Shushruth et al., 2013). In far surround (Figure 4.3 F-J), the tuning is stronger in L4B/4Cα (OSSI=0.12) and L2/3 (OSSI=0.1) and weaker in all other layers. The time of tuned component is fastest in L4B/4Cα (74 ms) and top IG (78 ms) followed by low IG (88 ms), L2/3 (94 ms) and L4C (144 ms). In general, and in accordance with single electrode recordings from Chapter 2 (Shushruth et al., 2013), far surround is weakly tuned (and sharply tuned in L4B) comparing with near surround, showing later temporal dynamics. Considering the second distance of near surround (dist=1.9) for two penetrations the OSSI becomes stronger for the average L2/3, top, and low IG. Additionally, the latency of tuned-SM becomes faster in L2/3 (46 ms, Figure 4.3-A), L4C (68 ms, Figure 4.3-C) and low IG (102, Figure 4.3-E) comparing to closer distances in Figure 4.2 (similar panels). In particular, tuning in L2/3 is larger (OSSI=0.29 vs. 0.13) and likely reaches 10% much earlier in time than in Figure 4.2-A; so the stronger tuning could explain the difference

(16ms) in the latencies.

Applying similar correlation analyses between the strength of tuning (OSSI) and latency of tuning, we observed that again there is a negative correlation in both near surround (Figure 4.4-D; r=-0.32, p=0.07, n=33), which was not significant, and far surround (Figure 4.4-E; r=-0.29, p=0.046, n=48). The clear result here is that far surround tuned latency shows large variability in the variance (heteroscedastic behavior) at different OSSI levels. One reason is at low OSSI (in the region of 0-0.1) the variance is larger than higher OSSI values. Measuring the correlation between tuned latency of near and far surround for those contacts that have latency values, led to no correlation between the two regions (Figure 4.4-F, r=-0.06, p=0.78, n=26). However, the strength of orientation selectivity (OSSI) is statistically different between near and far surround (Wilcoxan rank sum test, p = 0.0061, Figure 4.5-C).

4.3.3 Suppression Index and Orientation Selectivity

We have also quantified the suppression strength for the iso-oriented RF-surround and orientation selectivity between iso- and cross-oriented gratings. Contacts that showed suppression at iso-orientation were selected (i.e., 0=<SI<1). Also their OSSI is between 0 and 1, meaning that iso-oriented condition is more suppressed than cross-oriented condition; so there is no negative OSSI and iso-oriented grating does not decrease cell's firing rate to negative values leading to OSS>1. For this analysis, we included the contacts with mentioned criteria for SI and OSSI, but did not take into account if there was any value for latency or not. Thus, the sample number for each condition is larger than in Figure 4.4 (where there was value for latencies other than Nan).

Figure 4.5-A shows that near surround is suppressed stronger than far surround (Wilcoxan rank sum test, p=0.0003). Comparing the SI across layers with Kruskal-Wallis test (least significant difference correction) shows that L4B/4Cα (n=8) had stronger SI than L4C (n=6, p=0.0007) and low IG (n=8, p=0.0044) in near surround (red bars). This result is consistent with a former study (Shushruth et al., 2009) that using annular gratings L3B/4A had larger suppression strength than other layers. In far surround, there are no significant pairs across layers.

We found that there is significant differences between near and far surround in L2/3 (Wilcoxan rank sum test, p= 0.007) and L4B/4Cα (p=0.0003) but not in L4C and IG layers. This could be due to stronger suppression in SG layers in near surround compared to far surround while there is weaker suppression in IG and L4C in both near and far surround (Figure 4.5-B).

Near surround (n=38) is more orientation-tuned than far surround (n=61; ranksum, p= 0.0061), confirming the result of Chapter 2 (Figure 4.5-C). We do not find significant differences across layers in near surround that could be due to small sample number in each layer. However, L4B/4Cα and top IG seem to be more orientation-tuned than other layers in near surround. In response to far surround stimulation, L4B/4Ca (n=8) is more orientation-tuned than L4C (n=10), but is not different from other layers (Kruskal-Wallis, multiple comparison, p=0.011). This result is also replicated in Chapter 2, although we used delta SI (SI cross – SI iso) as a measure of tuning.

4.3.4 Latency Distribution of Untuned Suppression by Stimulation of Near and Far Surround

Similar to Figure 3.6, to combine latency measures from all penetrations, we subtracted the fastest latency among all layers from latencies of other contacts in each layer in each profile (i.e., RF, near and far surround). This difference value is called delta latency (DL). Then the distribution of delta latencies of all contacts pooled from all penetrations in each layer is plotted. Figure 4.6-B shows the distribution of DL for the untuned near surround (latency of iso-oriented grating versus RF computed by divergence method). Applying nonparametric (Kruskal-Wallis) test with least significant difference corrections, L4B/4Cα (n=8) is significantly faster than L2/3 (n=21, p=0.0018), L4C (n=9, p= 0.0082), top IG (n=6, p=0.0291), and low IG (n=10, p= 0.0162). The untuned suppression by far surround leads to L4C as the latest from all layers except top IG. L4C (n=14) is significantly later than low IG (n=17, p=0.005), L4B/4Cα (n=11, p=0.0425) and L2/3 (n=32, p=0.0209) and is close to significant from top IG (n=11, p=0.0533). Essentially, 42% of contacts (n=6/14) in L4C of far surround do not have latency values (equal to Nan) because the latency algorithm does not find the point in which the iso-oriented condition is different from RF; one reason is far surround stimulation leads to weaker suppression in L4C, being consistent with a previous report (Ichida et al., 2007).

As another alternative, weakly suppressed contacts result in later latency measures (after 150ms from stimulus onset generating Nan values) comparing to strongly suppressed contacts (Figure 4.2-H). We approached this issue by replacing all Nan values with the maximum value of latency distribution in the corresponding layer (Figure 4.7). In this case L4C is again significantly slower than most layers in far surround except top IG (vs. L2/3,

p=0.0005; L4B/4Cα, p= 0.0011; low IG, p= 0.0006; Figure 4.7-B), and L4B/4Cα is the fastest in near surround (vs. L2/3, p=0.0012; L4C, p= 0.0025; top IG, p=0.0273; low IG, p= 0.0067; Figure 4.7-A).

We also measured the latency of suppression using a large sinusoidal drifting grating patch that was used to characterize the size-tuning curve. This 20˚ disk (in diameter) was encompassing the RF, near and far surround regions at the same time with no gray annular gap that was used in our main stimuli. To extract the latency of suppression, we compared the MUA traces in response to the 20˚ large disk versus the peak of the size-tuning curve for each penetration (diameter ranged from 0.4-1.5˚). As Figure 4.6-A demonstrates L4C (n=13) is significantly faster than L2/3 (n=32, p=0.0289) and low IG (n=16, p=0.0079). In addition, L4B/4Cα (n=11) was significantly faster than L2/3 (p=0.0027) and low IG (p=0.0007). Since there is no gap in this stimulus the thalamocortical afferents might play a dominant role in generation of SM (Angelucci et al., 2002; Sceniak et al., 2006; Alitto and Usrey, 2008). Interestingly, both L4B/4Cα and middle of L4C are fast and do not differ from each other, which is in contrast to near surround stimulation with a gray gap (Figure 4.6-B). This suggests that when all connections are engaged, thalamocortical afferents likely take over in time and carry the first suppressed signal to the cortex consistent with earlier reports (Ozeki et al., 2004; Webb et al., 2005; Alitto and Usrey, 2008). However, due to stimulation by drifting gratings, to characterize the size-tuning curve, there is a large variability in the latency values across penetrations (n=6), specifically in the middle of L4C.

4.3.5 Latency Distribution of Orientation-Tuned Suppression by Stimulation of Near Surround

To study the latency distribution of orientation-selective SM we looked into the tuning by the stimulation of near surround. Recently, we showed that generally near SM is more orientation-tuned than far SM (Shushruth et al., 2013)(Chapter 2). Figure 4.6-D shows the distribution of delta latency across layers, which was computed between the MUA traces in response to iso-oriented static gratings versus cross-oriented ones. We notice that L4B/4Cα (n=8) is significantly faster than L2/3 (n=21, p=0.0257), L4C (n=9, p=0.0042), and low IG (n=10, p= 0.0485). Comparing the two panels 4.6-B and 4.6-D, suggests that the suppression might arise from horizontal or LGN afferents in near surround taking place first in L4B/4Cα but the tuning possibly arise from the horizontal connections that receive the first input from LGN. There is a weak possibility that tuning emerges from LGN, but, based on previous studies, the LGN cells are weakly orientation-tuned (Ozeki et al., 2004; Bonin et al., 2005; Webb et al., 2005). Additionally, orientation-tuned latency in top IG is not different from L4B/4Cα and that could be due to existence of horizontal connections in this layer (L5). Also, comparing the untuned suppression by the large disk and near surround stimulated by the annular gratings (Figures 4.6-B and 4.6-A), implies that even in near surround the untuned suppression might not arise from thalamic afferents since there is no fast activation in the middle of L4C.

Replacing the Nan values with the maximum of latency distribution in each layer in near surround (Figure 4.7-C) still results in L4B/4Cα faster than L2/3 (p=0.0154), L4C (p=0.0008) and low IG (p=0.0119). Applying the same analysis on the tuned latency (Figure 4.7-D) of far surround (which is more variable and less tuned) leads to L4C being

later than L4B/4Cα (p= 0.0483) and top IG (p= 0.017).

We also measured the latencies by the second method that takes into account the trial variability (refer to section 4.2.3). Figure 4.8 represents the latency distribution of DL computed by bootstrap method. Panels A-D represent the untuned near surround, untuned far surround, tuned near surround and tuned far surround, respectively. The untuned suppression (Figure 4.8-A) in near surround shows that L4B/4Cα is significantly different from top IG (p=0.02) and low IG (p=0.0014) but not from L4C and L2/3, which is also observed using the first method (Figure 4.6-B). The untuned suppression (Figure 4.8-B) in far surround is significantly later in L4C compared with L4B/4Cα (p= 0.0157) and L2/3 (p=0.0053) but not from low IG that is only extracted by the first method (Figure 4.6-C).

Measuring the tuned latency by bootstrapping spike counts across trials in near surround (refer to section 4.2.3, Figure 4.6-C) leads to faster L4B/4Cα compared with L2/3 (p= 0.021), L4C (p= 0.0486), and low IG (p= 0.0009). This significance outcome replicates the result by the first method (Figure 4.6-D). In far surround, top IG has just one value, but L4C is later than L4B/4Cα (p=0.0239). As discussed earlier (section 4.2), this method results in larger latencies with larger variances in each layer; because when the change in signal between any two curves is small, which is more common between iso- and cross-oriented stimuli (e.g., in tuned conditions), the variability across trials reaches significance level in later time points (possibly after 150ms which results to Nan values). Thus, we observe lots of Nans in the population of each layer in both untuned and tuned suppression.

Following on the latencies obtained by the bootstrapped method and setting the Nan values equal to the maximum of each layer, the untuned suppression conditions leads to

L4B/4Cα faster than other layers as observed in Figure 4.6-B and slower L4C than L2/3, L4B/4Cα and top IG in far surround. In the tuned near surround, L4B/4Cα is faster than others but not from L4C. However, the tuned far surround did not lead to any significant pairs across layers. To avoid complicated graphs, these results are not shown.

4.3.6 Latency of Untuned SM versus Orientation-Tuned SM

To investigate whether the untuned and orientation-tuned SM are served by similar circuits or not, we subtracted latency of untuned SM from the orientation-tuned SM (called SL). Essentially, in our algorithm, the time of suppression is equal or larger than center onset for each contact. In addition, the tuned component is also equal or larger than the faster untuned suppression between iso-and cross-oriented suppression. This criterion assured that the tuned suppression (neglecting any divergence due to fast facilitation) was measured.

We realize a population subset, in which tuning emerges as fast as untuned SM. Figure 4.9.B and 4.9.C represent the scatter plots of absolute latency of untuned versus absolute latencies of orientation-tuned SM of all contacts (pooled across layers) for near and far surround, respectively. In near surround about 47% of the cells have SL=0, the same percentage 47% (~ n=20) has SL>0, while 6% does not have latency value for either suppressed or tuned suppression so the SL=Nan. However, in far surround, 38% and 50% have SL=0 and SL>0, respectively, with 11% Nan values. This analysis is applied to those contacts that their 0<SI<1 so that they are suppressive. Also, the same population is plotted in Figure 4.4-A and B. In each condition (i.e., near or far surround) .the distribution of SL=0 is significantly different from SL>0ms (Wilcoxan rank sum test for near surround,

$p<0.0001$; Far surround, $p<0.0001$, Figure 4.9.A shows the histogram).

Two thresholds are used to summarize the subtracted latencies (SL>10 ms and SL>25 ms) and are shown as green and red lines in the Figure 4.9-B and 4.9-C; using the 25 ms threshold, in near surround 72 % has SL<25 ms and 21% has SL>25 ms, while in far surround ~ 58% and ~30% of the whole population has SL <25 ms and SL>25 ms, respectively. The distributions of near and far SL are not significant from each other. In each condition (i.e., near or far surround) the distribution of SL smaller than 25 ms is significantly different from SL larger than 25 ms (Wilcoxan rank sum test for both near and far surround, $p<0.0001$). Consistent with the monosynaptic delay we also used a threshold at 10 ms to divide SL values. The percentages are changed to 62% (SL<10 ms) versus 32 % (SL>10 ms) for the near, and 47% versus 41% for far surround. This suggests that close to half of the cells might have the same mechanisms for tuned suppression as untuned SM, while the tuning for 32-41% of the population might arise by the chain of neuronal synapses after suppression is conveyed. Again, in each condition the distribution of SL below 10 ms was significantly different from SL larger than 10 ms (Wilcoxan rank sum test for near surround, $p<0.0001$).

4.3.7 Latency of Untuned SM versus Orientation-Tuned SM Across Layers

Additionally, we divided contacts based on their location in each layer and quantified the subtracted latencies across layers. Figure 4.10 shows the average of SL in each layer for the near (black bars) and far (cyan bars) surround conditions. As it is observed, there are large standard errors in each group that could be due to small sample numbers. But the

general trend is that far surround has larger SL than near surround which is also observed comparing panel B and C of Figure 4.9. There is no significant difference between the SL populations across layers in neither near nor far surround (Kruskal-Wallis test). Furthermore, comparing the SL distributions of near and far surround in each layer (Wilcoxan rank sum test), no significant pairs are obtained, although in some layers such as L4B/4Cα the tuning in far surround emerges much later (mean SL=28 ms, median =8 ms) than untuned suppression compared with the fast tuning in near surround (mean SL=10 ms, median = 1 ms).

Similar plots, comparing the absolute untuned and tuned latencies in each layer for near (Figure 4.11) and far surround (Figure 4.12) are depicted. We find that the distribution of SL=0 is significantly different from SL>0 in near surround in L2/3 (p<0.0001) and L4B/4Cα (p=0.0286). Also in far surround, the two distributions are significant from each other in L2/3 (p<0.0001), L4B/4Cα (p=0.0121), and low IG (p<0.0001)

Applying the same statistical analysis on 10ms threshold leads to significant result between the distribution of SL>10 ms (n=6) and SL<10 ms (n=13) in L2/3 of near surround (rank sum, p<0.0001). In far surround, the SL>10 ms is significantly different from SL<10ms in L2/3 (n=12 vs. n=15, respectively, p<0.0001), L4B/4Cα (n=6 vs. n=5, p=0.0043), L4C (n=5 vs. n=2, p=0.0286), and low IG (n=9 vs. n=5 p<0.0001).

In sum, the results of this chapter, suggest that the untuned near SM first emerges in L4C, but the tuned near surround suppression and far SM emerge out of L4C in time suggesting cortical origins. In addition, the tuned suppression is likely generated by two different mechanisms. It could emerge by the same circuit that computes suppression or recruits multi-synapses that takes longer time than suppression.

4.4 Discussion

Numerous studies reported distinct specificities in the physiological properties of cortical layers. They showed that orientation selectivity (Ringach et al., 2002), spatial extent of RF, spatial frequencies, and temporal frequencies vary across layers. Recently, there is a growing literature on studying how laminar circuits contribute in processing simple visual stimuli. For instance, how neuronal correlations in the presence and absence of the visual stimuli vary (Smith et al., 2013; Snyder et al., 2014). One study reported that trial-to-trial correlated variability is weaker in input layers and stronger in output layers of V1 (Hansen et al., 2012). Yet, linking the functional role with structural connectivity across layers is still to be achieved.

The main aim of this dissertation is to understand how surround modulation, a fundamental property of V1 cells' responses, and thought to serve in many perceptual phenomena (Knierim and Van Essen, 1992; Lamme, 1995; Zipser et al., 1996; Lamme et al., 1999), is computed across layers of V1. In Chapter 3, we showed that near and far surround stimulation evoke distinct spatiotemporal profile of neuronal inputs to V1 layers that was consistent with the termination pattern of horizontal and feedback axons, respectively. This suggests and confirms that response modulation in near surround is mainly generated by intrinsic horizontal connections, while far surround modulation arises by top-down signals from the extrastriate cortex. However, in near surround thalamic afferents and feedback are also involved.

In this chapter, costimulating the columnar RF along with the surround regions (near vs. far), allows us to measure the neuronal outputs via measuring postsynaptic spiking activity across V1 layers. We asked: *In which layer the untuned and orientation-tuned*

surround modulation are first originated? *Do SM and its orientation selectivity emerge in the layers consistent with the input layers activated by the near and far surround?*

First, we quantified the emergence of suppression across layers. Using an expanding grating disk we measured the latency of suppression comparing the large stimulus (20˚ diameter) with the stimulus at the peak of size tuning curve (selected as the h-sRF) for the column. We found that the suppression emerged first in L4C, L4B/4Cα, and top IG followed by L2/3 and lower IG. Both L4B/4Ca and middle of L4C were significantly faster than L2/3 and lower IG. Using the grating covering RF, near and far surround at the same time should theoretically engage suppression from LGN, horizontal, and feedback (Angelucci et al., 2002; Bonin et al., 2005; Webb et al., 2005; Angelucci and Bressloff, 2006). Because there was no gap between RF and the surround regions (i.e., near and far), it is likely that the earliest suppression was dominated by LGN afferents that are more spatially restricted and terminate in L4C and L4Cα, followed in time by cortical circuits such as horizontal and feedback (Webb et al., 2005; Xing et al., 2005; Angelucci and Shushruth, 2013).

In complement to this stimulus, we stimulated the RF and near surround by static annular gratings with a gap in between (mean luminance gray) that was supposedly masking the effect of spatially strict thalamocortical afferents from LGN (Angelucci et al., 2002; Angelucci and Sainsbury, 2006). Essentially, the RF grating was fixed at preferred orientation while the orientation of the surround annuli changed between iso-and orthogonal (referred to cross in this chapter) relative to the RF orientation. Our sample includes both tightly orientation-tuned column and broader columns similar to pinwheel; based on former study by Shushruth et al. (2012) and earlier studies (Sillito et al., 1995;

Cavanaugh et al., 2002b), iso-oriented stimuli (regardless of being preferred or not) at RF and surround, suppresses cells as far as the RF stimulus evokes neuronal responses from the cell. This means the RF and surround are selective to the relative orientation between them rather than preferred orientation of cells. Considering this effect, if the recorded column was not an orientation column we measured the time of suppression while all the cells were stimulated simultaneously by iso-oriented grating close to dominant orientation for the majority of cells in the recorded column. We observed that the fastest suppression emerged in those contacts located on the border of L4B and 4C grouped as L4B/4Cα. Fast suppression in L4B/4Cα could be originated through existing horizontal connections in L4B and upper L4Cα contacting the fast conducting magnocellular inputs in upper 4C (Lund, 1988). Another possibility is that the noted suppression is the result of LGN afferents in near surround. Feedback and horizontal inputs to L4B, due to activation of near surround (refer to Chapter 3), are another alternative circuit generating the fast suppression in this layer.

Similar to previous section, the time of suppression for far surround was measured in response to iso-oriented center gratings and the 2˚ annulus was located beyond 2.4˚(minimum) from the center of RF. Under these conditions, we have found that L4C was delayed relative to other layers. In Chapter 3, we observed that the first inputs by far surround stimulation are localized in L1/2A and lower IG. Based on the known anatomical studies, the apical dendrites of L5 pyramids can project to L1/2A, and could be activated by feedback axons following far surround stimulation. Thus, we speculate that the fast suppression in the top IG (L5) could arise from their distal dendrites integrating feedback inputs to L1/2A. In addition, lower IG is also receiving the early inputs following far

surround stimulation and is also suppressed here faster than L4C. Moreover, top IG (L5) cells have basal dendrites in low IG and could integrate information from that layer too (unpublished data from Angelucci lab). Also, some of L4B and L2/3 might be contacted by feedback axons via their distal dendrites in L1/2A.

Another interesting result is that in both near and far surround L4C is delayed. We show that L4C responses were weakly suppressed in response to stimulation of different surround regions (Figure 4.2-C and 4.2-H), consistent with previous studies(Ichida et al., 2007) . In line with Bair et al.(2003), we also found the weaker the suppression, the later the time of suppression in near surround (negative correlation), but not in far surround. Furthermore, the latency of suppression in near surround was positively correlated with latency of suppression in far surround (Figure 4.4-C, see result section for significant p values). The similar latencies of suppression by the near and far surround stimulation admits similar behaviors of their underlying circuits. For example, they vary together and fast far surround suppression is observed consistent with high conducting feedback terminals (Girard et al., 2001; Angelucci et al., 2002). In addition, the strength of suppression was significantly larger in near surround than far surround, confirming the result of many previous findings (Cavanaugh et al., 2002a; Bair et al., 2003; Ichida et al., 2007; Shushruth et al., 2009; Schwabe et al., 2010; Shushruth et al., 2013).

In Chapter 2, we showed that near surround is more orientation sensitive than far surround in a population of V1 cells, a result that was assimilated in human subjects using a contrast matching task (Shushruth et al., 2013). These findings suggest that there are different orientation selectivity mechanisms for near and far surround suppression. Elaborating on this, we looked into orientation selectivity of near and far surround across

layers. We and others (Henry et al., 2013; Shushruth et al., 2013), found that near suppression is more orientation-tuned in L3B, L4B, and 4Cα while far surround was tuned in L4B. Because in these studies, recordings were made with single electrodes in each layer, it was previously not possible to measure the temporal covariations of tuned-surround suppression across V1 layers. Here, measuring the time of divergence between iso- and cross-oriented gratings we have found that in near surround L4B/4Cα and upper IG were faster than other layers. This result suggests that the orientation tuning of near surround does not emerge from LGN afferents even if they are contributing to suppression. Furthermore, orientation tuning of LGN suppression has been previously debated (Sillito et al., 1993; Bonin et al., 2005) and Ozeki et al. (2009) showed that geniculate surround suppression is markedly less orientation sensitive than V1 cells. Alternatively, this tuning might have intra cortical origins, emerging via horizontal connections in L4B/4Cα and upper IG that are also receiving the first inputs by near surround stimulation (See Chapter 3).

Far surround is generally less orientation-tuned than near surround (discussed in Chapter 2, Figure 4.5-C), thus measuring the propagation of tuning across layers would be prone to error. However, we observed that orientation specific suppression index was larger in L4B/4Ca than other layers following far surround stimulation (Figure 4.5-D, yellow bars), a result that was also observed in distribution of delta SI in Chapter 2 (our single electrode study). This suggests feedback to this layer is selective to orientation, probably influenced by dense axonal termination of direction/orientation-selective MT cells in L4B of V1(Rockland and Knutson, 2000).

To measure the latency, another method was utilized to take trial variability into

account; Figure 4.8 shows that in near surround L4B/4Ca was faster than upper and lower IG (Figure 4.8-A), and in far surround (Figure 4.8-B) L4C was slower than L4B/4Ca and L2/3. This method, as discussed previously (4.2.3), is very prone to the magnitude of the change between the two signals. We believe that the divergence method (Figure 4.6) extracts robust values that corresponds to true contact's behavior in a given condition.

We also compared the absolute latencies of suppression vs tuned suppression. It is however crucial to state that tuned latency has the constraint that it must be equal or larger than the latency of suppression. With this constraint we would not observe any cell being suppressed or tuned before center onset, (as noted in other studies (Muller et al., 2003)). A subpopulation showed suppression as fast as center onset consistent with a previous study (Muller et al., 2003), while reported suppression latencies by Bair and colleagues (2003) is 10-30 ms after center onset . In addition, close to half of the contacts in near surround showed no delay between suppressed and tuned components of surround while the other half showed delayed tuned components. This observation suggests that there are two different mechanisms across V1 cells, a fast tuning versus slow tuning. Fast tuning is possibly computed by the same circuit as suppression, while the slow tuning could be due to chains of di/poly-synaptic networks. To investigate in more depth, we applied a threshold of 10ms between the absolute latency of suppression and tuning, which is common as monosynaptic delay and found that more contacts in both near (62% vs. 32%) and far surround (47% vs. 41%) were showing the fast tuning and less demonstrate slow tuning characteristics. We did not observe any significance result between near and far surround. This denotes that surround suppression in some neurons becomes tuned as fast as suppression, while for others there is more complicated neuronal interactions to convey

tuning. For example, SG layers that have later center onset than granular layers get suppressed very quickly, while the suppression is already tuned. This could be due to existing horizontal connection in L2/3.

We then looked into layers to examine whether there is any correlation between layers with regard to tuned versus untuned latencies, although we had small number of samples in some layers. We observed that the two mechanisms are almost existing in all layers. This suggest that the slow tuning might engage recurrent network across layers.

Overall, the presented results in this chapter suggest that the inputs caused by any surround elements are employed by inter- or intra-laminar circuitry to generate suppression and its orientation selectivity. By investigating the absolute latencies of suppression and tuned suppression, we propose that there are two different mechanisms for generating the tuning of suppression: in some neurons the tuning is computed through same circuit as computes suppression, while in others there are involvement of di/polysynaptic connections to convey tuning property of SM.

These results need to be studied in more detail by future studies. For example, probing orientation column by optical imaging and then recording from those columns would help understanding the tuning circuits across layers with higher accuracies. Optogenetic inactivation of feedback areas separately, will also shed light on the circuits of untuned and tuned suppression. For instance, does silencing MT terminals remove the tuning of far surround in L4B? Answering this question is absolutely fundamental to understanding how SM is computed in the visual cortex.

4.5 References

Alitto HJ, Usrey WM (2008) Origin and dynamics of extraclassical suppression in the lateral geniculate nucleus of the macaque monkey. Neuron 57:135-146.

Allman J, Miezin F, Mc Guinness E (1985) Stimulus specific responses from beyond the classical receptive field: Neurophysiological mechanisms for local-global comparisons in visual neurons. Ann Rev Neurosci 8:407-430.

Angelucci A, Levitt JB (2002) Convergence of color, motion and form pathways in macaque V3. Soc Neurosci Abstr Online Program No. 658.2.

Angelucci A, Bullier J (2003) Reaching beyond the classical receptive field of V1 neurons: horizontal or feedback axons? J Physiol (Paris) 97:141-154.

Angelucci A, Bressloff PC (2006) The contribution of feedforward, lateral and feedback connections to the classical receptive field center and extra-classical receptive field surround of primate V1 neurons. Prog Brain Res 154:93-121.

Angelucci A, Sainsbury K (2006) Contribution of feedforward thalamic afferents and corticogeniculate feedback to the spatial summation area of macaque V1 and LGN. J Comp Neurol 498:330-351.

Angelucci A, Shushruth S (2013) Beyond the classical receptive field: surround modulation in primary visual cortex. The New Visual Neurosciences 1:425-444.

Angelucci A, Levitt JB, Walton E, Hupé JM, Bullier J, Lund JS (2002) Circuits for local and global signal integration in primary visual cortex. J Neurosci 22:8633-8646.

Bair W, Cavanaugh JR, Movshon JA (2003) Time course and time–distance relationships for surround suppression in macaque V1 neurons. J Neurosci 23:7690-7701.

Blakemore C, Tobin EA (1972) Lateral inhibition between orientation detectors in the cat's visual cortex. Exp Brain Res 15:439-440.

Bokil H, Andrews P, Kulkarni JE, Mehta S, Mitra PP (2010) Chronux: a platform for analyzing neural signals. J Neurosci Methods 192:146-151.

Bonin V, Mante V, Carandini M (2005) The suppressive field of neurons in lateral geniculate nucleus. J Neurosci 25:10844-10856.

Cavanaugh JR, Bair W, Movshon JA (2002a) Nature and interaction of signals from the receptive field center and surround in macaque V1 neurons. J Neurophysiol 88:2530-2546.

Cavanaugh JR, Bair W, Movshon JA (2002b) Selectivity and spatial distribution of signals

from the receptive field surround in macaque V1 neurons. J Neurophysiol 88:2547-2556.

DeAngelis GC, Freeman RD, Ohzawa I (1994) Length and width tuning of neurons in the cat's primary visual cortex. J Neurophysiol 71:347-374.

Girard P, Hupé JM, Bullier J (2001) Feedforward and feedback connections between areas V1 and V2 of the monkey have similar rapid conduction velocities. J Neurophysiol 85:1328-1331.

Grinvald A, Lieke EE, Frostig RD, Hildesheim R (1994) Cortical point-spread function and long-range lateral interactions revealed by real-time optical imaging of macaque monkey primary visual cortex. J Neurosci 14:2545-2568.

Hansen BJ, Chelaru MI, Dragoi V (2012) Correlated variability in laminar cortical circuits. Neuron 76:590-602.

Henry CA, Joshi S, Xing D, Shapley RM, Hawken MJ (2013) Functional characterization of the extraclassical receptive field in macaque V1: contrast, orientation, and temporal dynamics. J Neurosci 33:6230-6242.

Ichida JM, Schwabe L, Bressloff PC, Angelucci A (2007) Response facilitation from the "suppressive" receptive field surround of macaque V1 neurons. J Neurophysiol 98:2168-2181.

Knierim JJ, Van Essen D (1992) Neuronal responses to static texture patterns in area V1 of the alert macaque monkey. J Neurophysiol 67:961-980.

Lamme VAF (1995) The neurophysiology of figure-ground segregation in primary visual cortex. J Neurosci 15:1605-1615.

Lamme VAF, Rodriguez-Rodriguez V, Spekreijse H (1999) Separate processing dynamics for texture elements, boundaries and surfaces in primary visual cortex of the macaque monkey. Cereb Cortex 9:406-413.

Lund JS (1988) Anatomical organization of macaque monkey striate visual cortex. Ann Rev Neurosci 11:253-288.

Maffei L, Fiorentini L (1976) The unresponsive regions of visual cortical receptive fields. Vis Res 16:1131-1139.

Muller JR, Metha AB, Krauskopf J, Lennie P (2003) Local signals from beyond the receptive fields of striate cortical neurons. J Neurophysiol 90:822-831.

Nelson JI, Frost B (1978) Orientation selective inhibition from beyond the classical visual receptive field. Brain Res 139:359-365.

Nowak LG, Bullier J (1997) The timing of information transfer in the visual system. In: Extrastriate cortex in primates (Rockland KS, Kaas JH, Peters A, eds), pp 205-241. New York: Plenum Press.

Ozeki H, Finn IM, Schaffer ES, Miller KD, Ferster D (2009) Inhibitory stabilization of the cortical network underlies visual surround suppression. Neuron 62:578-592.

Ozeki H, Sadakane O, Akasaki T, Naito T, Shimegi S, Sato H (2004) Relationship between excitation and inhibition underlying size tuning and contextual response modulation in the cat primary visual cortex. J Neurosci 24:1428-1438.

Petrov Y, Carandini M, McKee S (2005) Two distinct mehcnaisms of suppressioni in human vision. J Neurosci 25:8704-8707.

Ringach DL, Shapley RM, Hawken MJ (2002) Orientation selectivity in macaque V1: diversity and laminar dependence. J Neurosci 22:5639-5651.

Rockland KS, Knutson T (2000) Feedback connections from area MT of the squirrel monkey to areas V1 and V2. J Comp Neurol 425:345-368.

Sceniak MP, Hawken MJ, Shapley RM (2001) Visual spatial characterization of macaque V1 neurons. J Neurophysiol 85:1873-1887.

Sceniak MP, Chatterjee S, Callaway EM (2006) Visual spatial summation in macaque geniculocortical afferents. J Neurophysiol 96:3474-3484.

Schwabe L, Ichida JM, Shushruth S, Mangapathy P, Angelucci A (2010) Contrast-dependence of surround suppression in macaque V1: Experimental testing of a recurrent network model. Neuroimage 52:777-792.

Self MW, Lorteije JA, Vangeneugden J, van Beest EH, Grigore ME, Levelt CN, Heimel JA, Roelfsema PR (2014) Orientation-tuned surround suppression in mouse visual cortex. J Neurosci 34:9290-9304.

Shushruth S, Ichida JM, Levitt JB, Angelucci A (2009) Comparison of spatial summation properties of neurons in macaque V1 and V2. J Neurophysiol 102:2069-2083.

Shushruth S, Mangapathy P, Ichida JM, Bressloff PC, Schwabe L, Angelucci A (2012) Strong recurrent networks compute the orientation-tuning of surround modulation in primate primary visual cortex. J Neurosci 4:308-321.

Shushruth S, Nurminen L, Bijanzadeh M, Ichida JM, Vanni S, Angelucci A (2013) Different orientation-tuning of near and far surround suppression in macaque primary visual cortex mirrors their tuning in human perception. J Neurosci 33:106-119.

Sillito AM, Cudeiro J, Murphy PC (1993) Orientation sensitive elements in the corticofugal influence on centre-surround interactions in the dorsal lateral geniculate nucleus. Exp Brain Res 93:6-16.

Sillito AM, Grieve KL, Jones HE, Cudeiro J, Davis J (1995) Visual cortical mechanisms detecting focal orientation discontinuities. Nature 378:492-496.

Slovin H, Arieli A, Hildesheim R, Grinvald A (2002) Long-term voltage-sensitive dye imaging reveals cortical dynamics in behaving monkeys. J Neurophysiol 88:3421-3438.

Smith MA, Jia X, Zandvakili A, Kohn A (2013) Laminar dependence of neuronal correlations in visual cortex. J Neurophysiol 109:940-947.

Snyder AC, Morais MJ, Kohn A, Smith MA (2014) Correlations in V1 are reduced by stimulation outside the receptive field. J Neurosci 34:11222-11227.

Webb BS, Dhruv NT, Solomon SG, Taliby C, Lennie P (2005) Early and late mechanisms of surround suppression in striate cortex of macaque. J Neurosci 25:11666-11675.

Xing D, Shapley RM, Hawken MJ, Ringach DL (2005) Effect of stimulus size on the dynamics of orientation selectivity in Macaque V1. J Neurophysiol 94:799-812.

Zipser K, Lamme VA, Schiller PH (1996) Contextual modulation in primary visual cortex. J Neurosci 16:7376-7389.

Figure 4.1: Visual stimuli and different latency methods. A) and B) Near surround stimuli at iso- and cross-oriented surround C) and D) far surround stimuli at iso- and cross-oriented surround, respectively. E) The PSTH of an example contact. The blue, green and red curves are the MUA PSTH to RF, RF-iso-oriented surround and RF-cross oriented surround, respectively. F) The cumulative spike count for the same cell. The vertical blue line in both E and F is the center onset, which is 10% of the peak. The vertical green and red lines in E and F are the computed latency for iso- and cross-oriented suppression computed by divergence method (E) versus bootstrapped spike count method (F). The black vertical lines in both panels are the time of tuned suppression between the red and green curves or cumulative spike counts of iso- and cross-oriented surround.

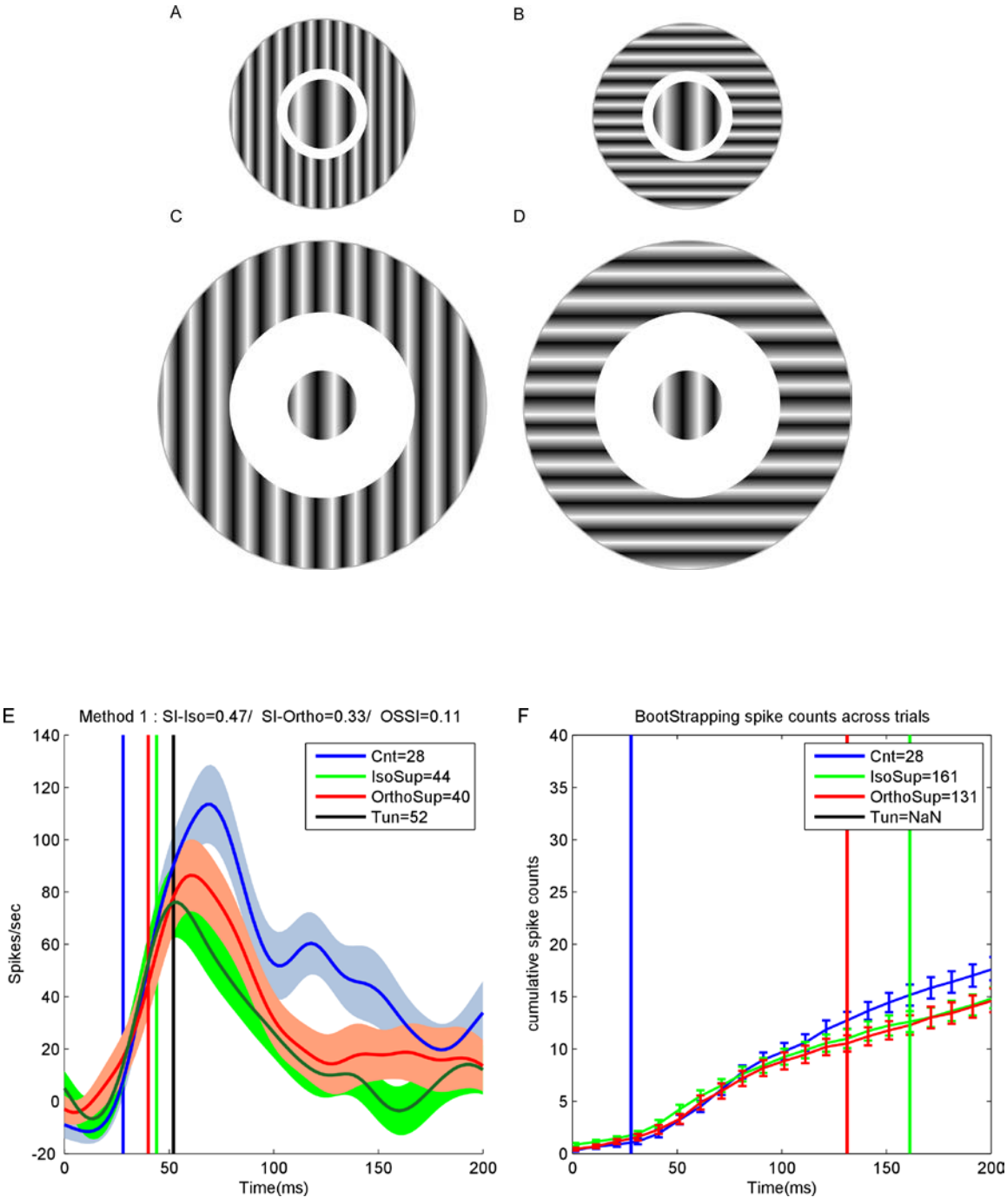
A
B
C
D
E
Method 1 : SI-Iso=0.47/ SI-Ortho=0.33/ OSSI=0.11
Cnt=28
IsoSup=44
OrthoSup=40
Tun=52
Spikes/sec
Time(ms)
F
BootStrapping spike counts across trials
Cnt=28
IsoSup=161
OrthoSup=131
Tun=NaN
cumulative spike counts
Time(ms)

Figure 4.2: Average normalized PSTH to near and far surround grouped in different layers. A-E) represent near surround in L2/3, L4B/4Ca, middle of L4C, top IG and low IG. F-J) represent far surround. In all 10 panels the blue curve is the response to RF stimulation, green and red curves are the response to RF+iso- and RF+cross oriented surround stimulation. The shaded lines are 1SD above and below the mean across all contacts. The blue, green, and red vertical lines are the center onset, latency of untuned iso-suppression and latency of untuned cross-oriented suppression. The black line is time of tuned suppression. On top of each panel the SI of iso-and cross conditions as wells as OSSI are stated.

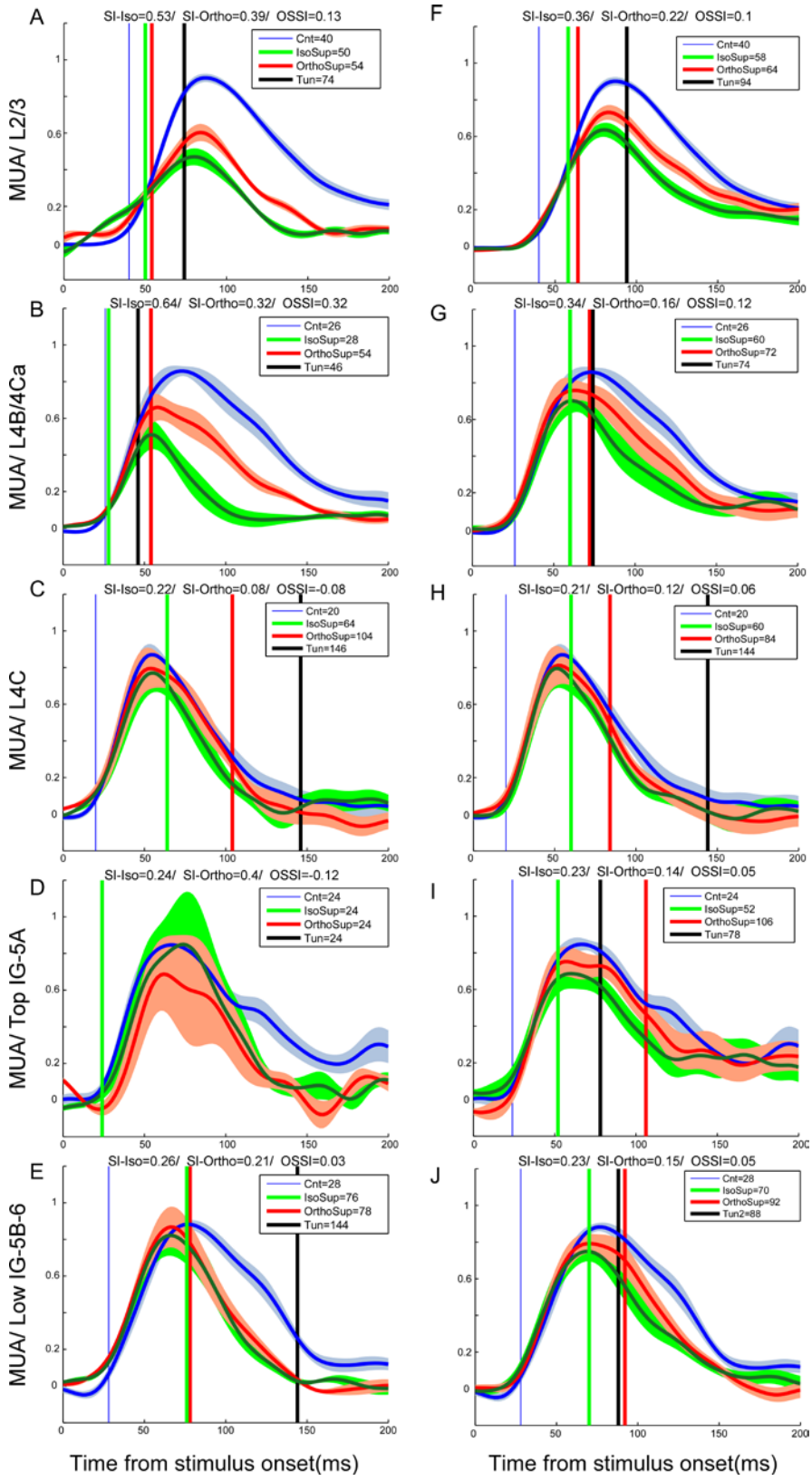
A
SI-Iso=0.53/ SI-Ortho=0.39/ OSSI=0.13
Cnt=40
IsoSup=50
OrthoSup=54
Tun=74
MUA/ L2/3
F
SI-Iso=0.36/ SI-Ortho=0.22/ OSSI=0.1
Cnt=40
IsoSup=58
OrthoSup=64
Tun=94
B
SI-Iso=0.64/ SI-Ortho=0.32/ OSSI=0.32
Cnt=26
IsoSup=28
OrthoSup=54
Tun=46
MUA/ L4B/4Ca
G
SI-Iso=0.34/ SI-Ortho=0.16/ OSSI=0.12
Cnt=26
IsoSup=60
OrthoSup=72
Tun=74
C
SI-Iso=0.22/ SI-Ortho=0.08/ OSSI=-0.08
Cnt=20
IsoSup=64
OrthoSup=104
Tun=146
MUA/ L4C
H
SI-Iso=0.21/ SI-Ortho=0.12/ OSSI=0.06
Cnt=20
IsoSup=60
OrthoSup=84
Tun=144
D
SI-Iso=0.24/ SI-Ortho=0.4/ OSSI=-0.12
Cnt=24
IsoSup=24
OrthoSup=24
Tun=24
MUA/ Top IG-5A
I
SI-Iso=0.23/ SI-Ortho=0.14/ OSSI=0.05
Cnt=24
IsoSup=52
OrthoSup=106
Tun=78
E
SI-Iso=0.26/ SI-Ortho=0.21/ OSSI=0.03
Cnt=28
IsoSup=76
OrthoSup=78
Tun=144
MUA/ Low IG-5B-6
J
SI-Iso=0.23/ SI-Ortho=0.15/ OSSI=0.05
Cnt=28
IsoSup=70
OrthoSup=92
Tun2=88
Time from stimulus onset(ms)
Time from stimulus onset(ms)

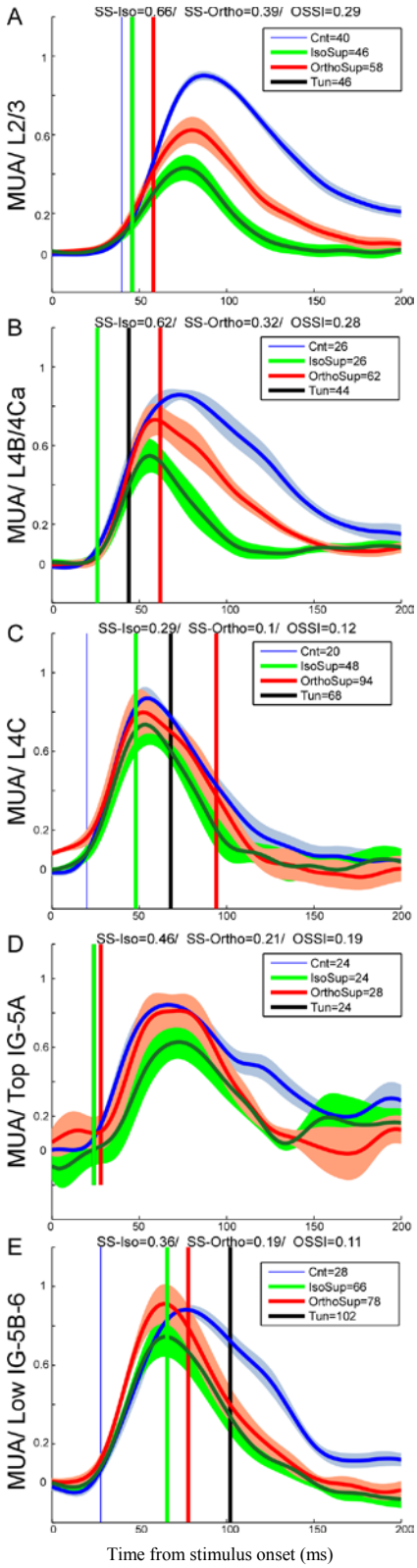

Figure 4.3: The average normalized MUA for near surround using two further distance for 2 penetrations. Descriptions are as in Figure 4.2.

Figure 4.4: Correlation plots. A and B) Latency of iso-oriented grating suppression versus SI for near- and far-surround, respectively. The black lines represent fitted values using linear regression. The correlation results are stated on top of each panel. C) The latency of iso-oriented suppression of near (x axis) versus far surround (y axis). The red line is the unity line and the black line is again the regressed fitted lines. D) and E) show the latency of tuned suppression versus OSSI and F) depicts latency of tuned suppression in near surround versus far surround for those contacts that had non-Nan values for both. Again the red line is the unity line and the black lines show the fitted regressions. In all 6 panels, the magenta and red squares represent mean and median of the presented values, respectively.

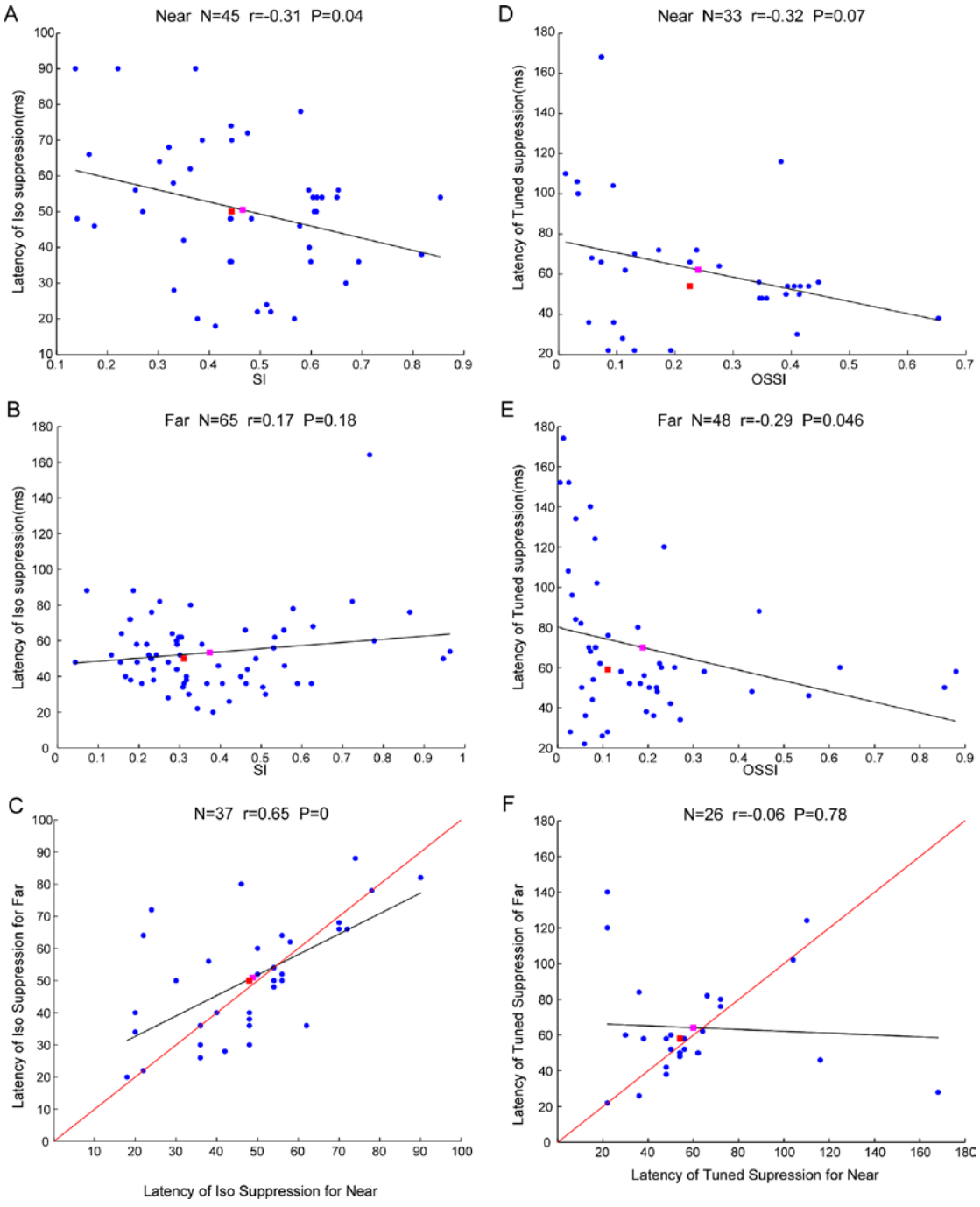
A
Near N=45 r=-0.31 P=0.04
Latency of Iso suppression(ms)
SI
D
Near N=33 r=-0.32 P=0.07
Latency of Tuned suppression(ms)
OSSI
B
Far N=65 r=0.17 P=0.18
Latency of Iso suppression(ms)
SI
E
Far N=48 r=-0.29 P=0.046
Latency of Tuned suppression(ms)
OSSI
C
N=37 r=0.65 P=0
Latency of Iso Suppression for Far
Latency of Iso Suppression for Near
F
N=26 r=-0.06 P=0.78
Latency of Tuned Suppression of Far
Latency of Tuned Supression for Near

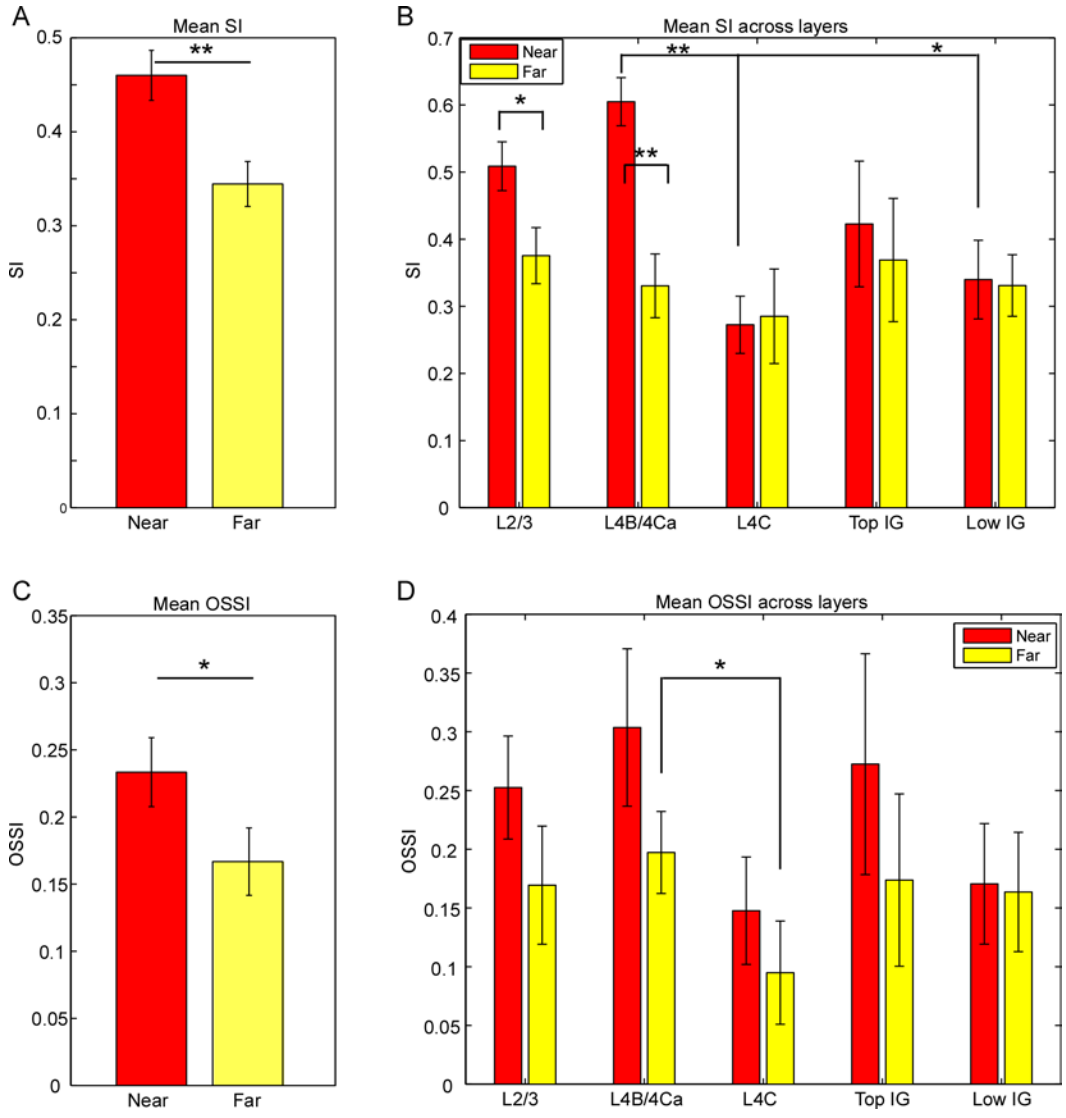

Figure 4.5: Suppression index (SI) and orientation specific suppression index (OSSI). A) SI from all contacts for near (red bars) and far surround (yellow bars), 0<SI<1. B) SI across layers. C) and D) Represent the OSSI of all contacts and across all layers, respectively, 0<OSSI<1.

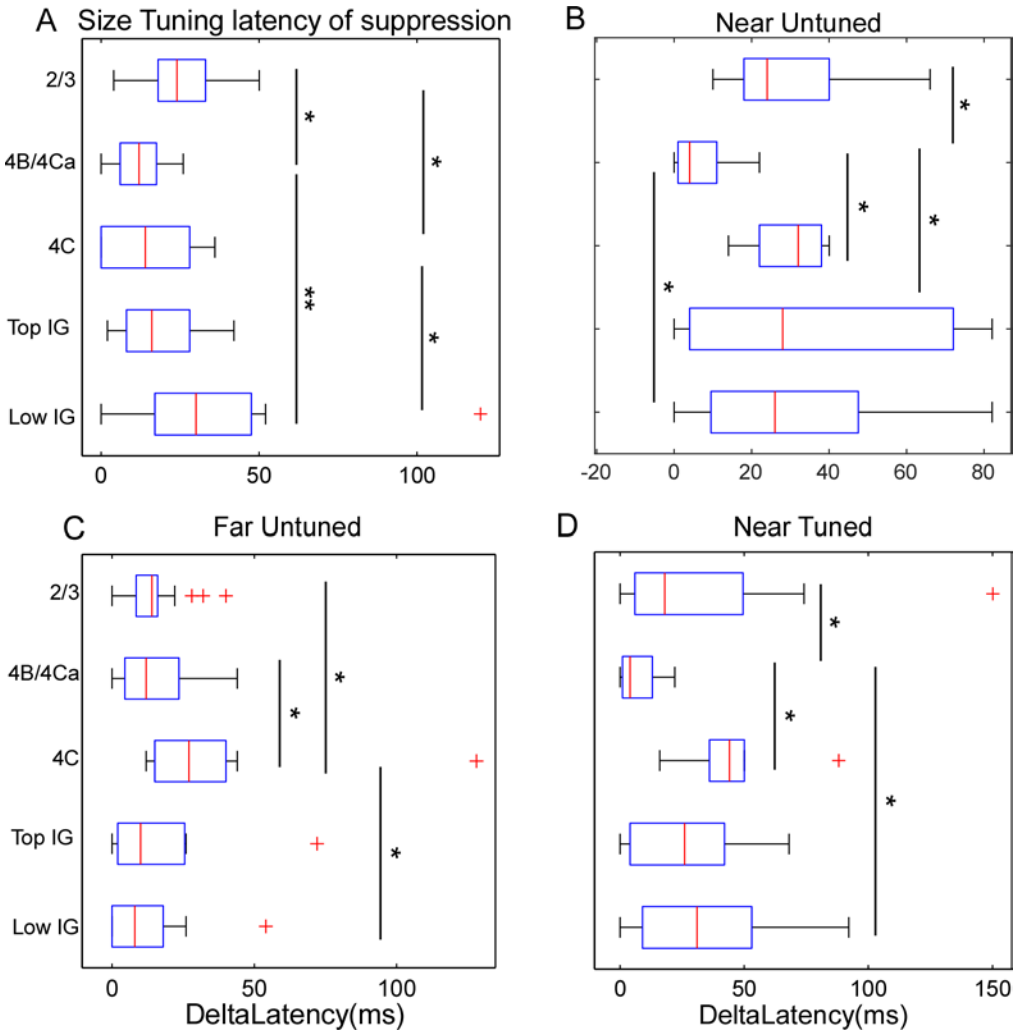

Figure 4.6: Distribution of delta latencies with divergence method for A) large disk, B) and C) Represent the distribution of the latency of untuned suppression in the near and far surround, respectively. D) Represent the distribution of tuned suppression in near surround. Significance values are stated as asterisks.

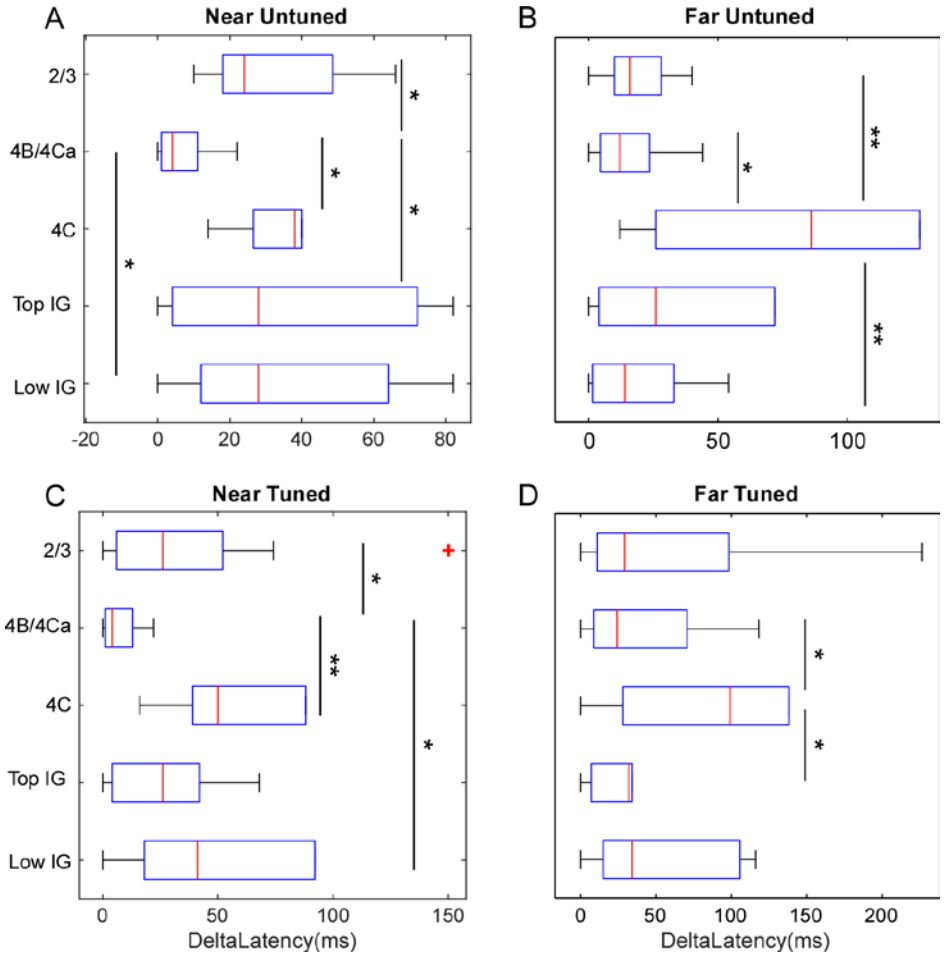

Figure 4.7: Distribution of delta latencies that the Nan values are set to the maximum of each layer. A) and B) represent the distribution of the latency of untuned suppression in the near- and far surround, respectively. C) and D) represent the distribution of tuned suppression in near and far surround.

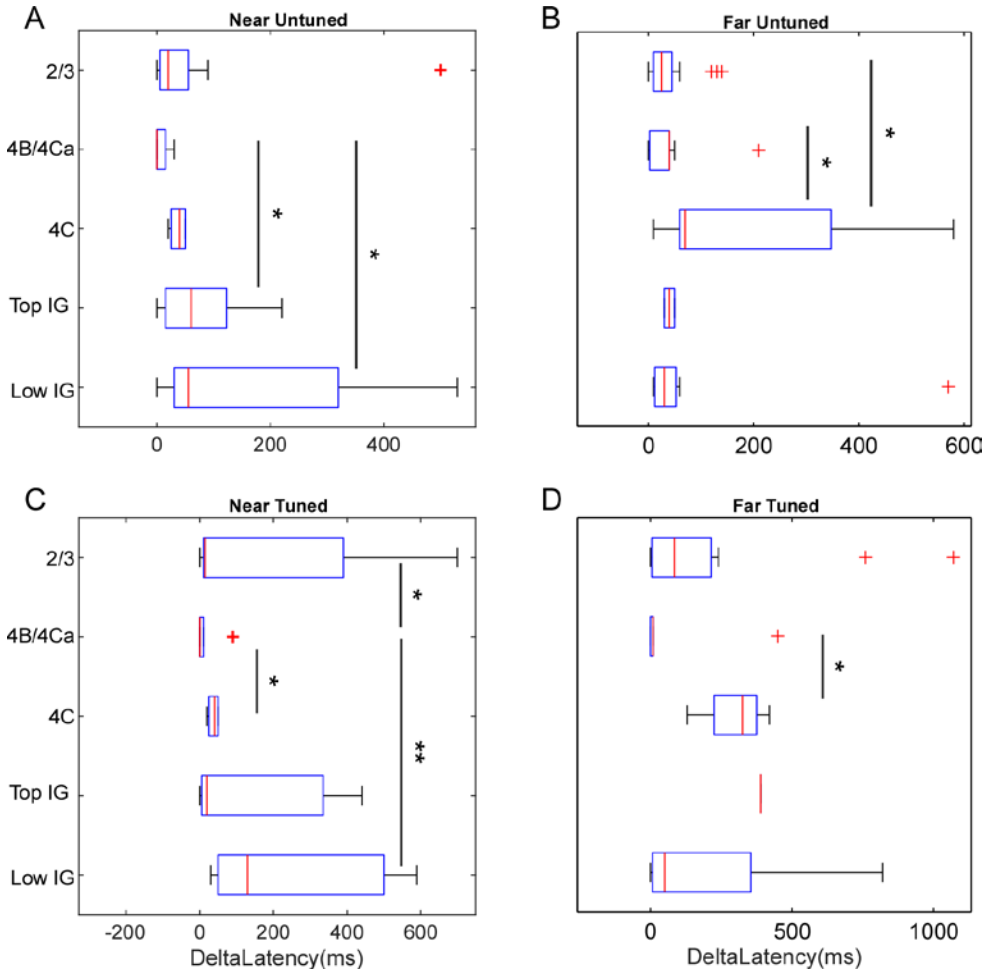

Figure 4.8: Distribution of DL computed by bootstrapped spike counts across trials. A) and B) represent the distribution of the latency of untuned suppression in the near and far surround, respectively. C and D) represent the distribution of tuned suppression in near and far surround.

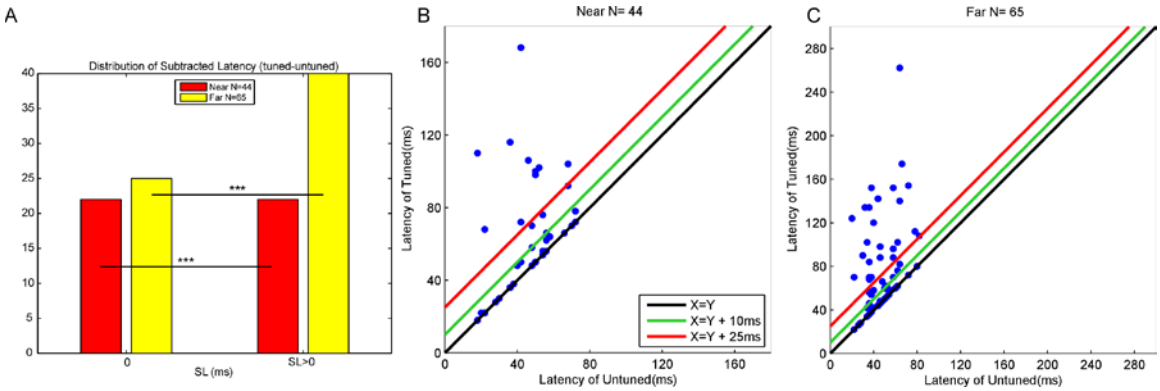

Figure 4.9: Untuned latencies versus tuned latencies for those contact that 0<SI<1. A) Histogram of the SL=0 and SL>0 for near (red bars) and far surround (yellow bars). B and C) absolute latencies of untuned vas tuned latencies for near- and far surround. Red and green lines show that 10 and 25 ms thresholds.

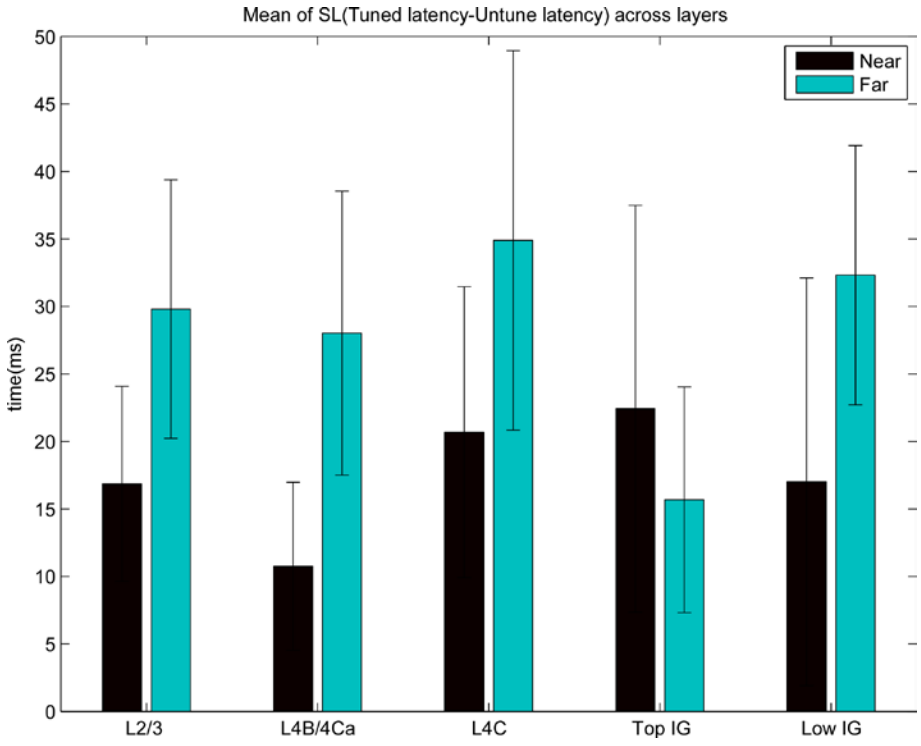

Figure 4.10: Mean of SL across layers for near (black) and far (cyan) surround.

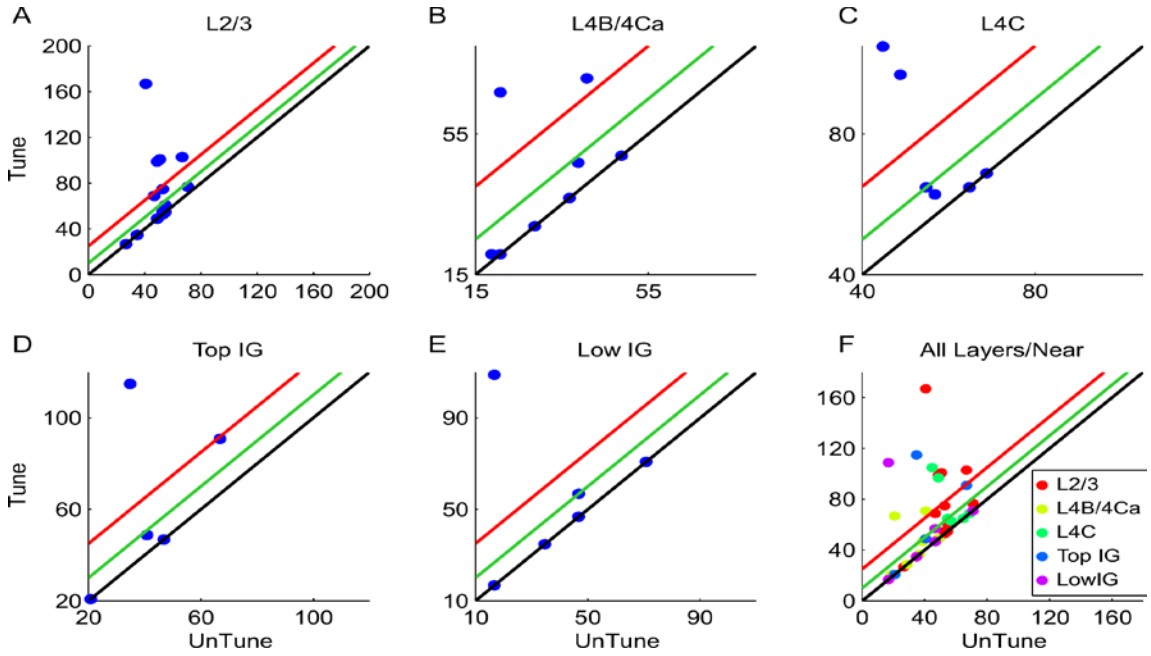

Figure 4.11: Latency of untuned and tuned suppression in each layer for near surround. A-E) represent the data in each layer with two thresholds green (10 ms) and red lines (25 ms). Panel F represents all data, which is similar to 4.9 B.

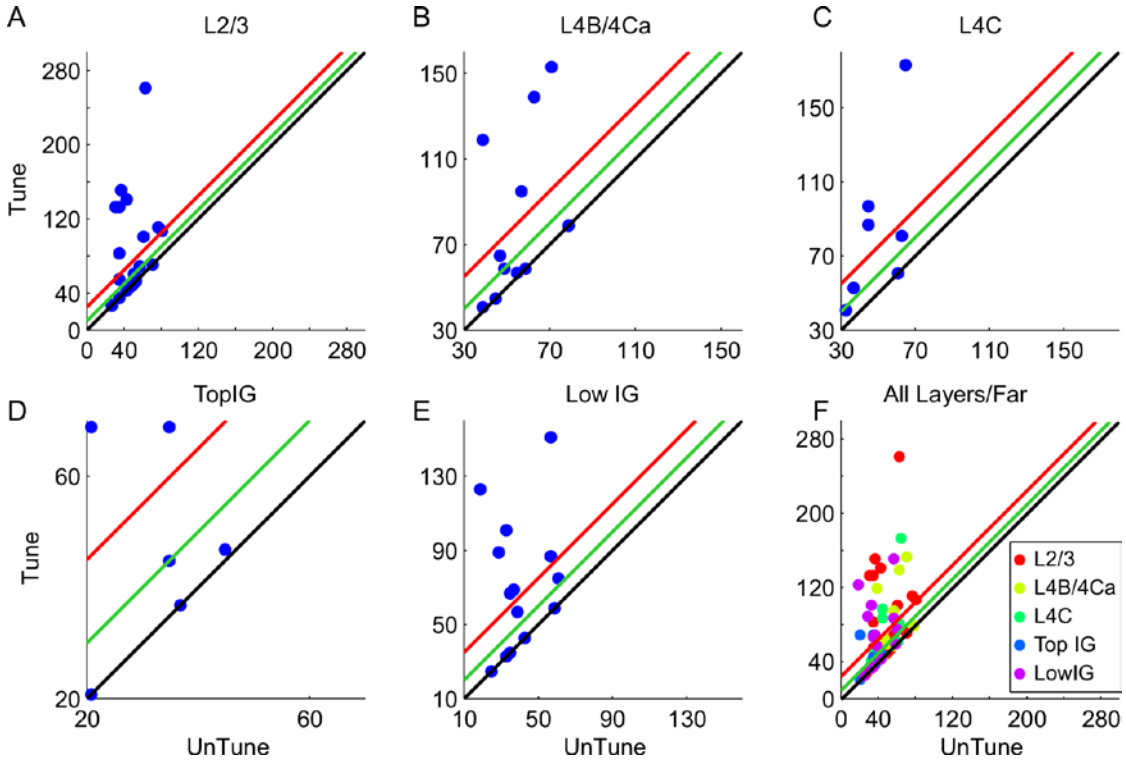

Figure 4.12: Latency of untuned and tuned suppression in each layer for far surround. A-E) represent the data in each layer with two thresholds green (10 ms) and red lines (25 ms). Panel F represents all data which is similar to 4.9C.

CHAPTER 5

BRAIN OSCILLATIONS AS A MARKER OF COLLINEAR HORIZONTAL ANDFEEDBACK CONNECTIONS INVOLVED IN CONTOUR COMPLETION

5.1 Introduction

Perception of an object from its background or detection of object boundaries is bound to the context in which the object is observed (Kapadia et al., 1995). Based on Gestalt principles, specific attributes of the visual image, such as contour continuity, makes objects "pop out" from their background (Hess and Field, 1999). As previously stated in Chapter1 (section 1.5), it is thought that surround modulation contributes to contour integration, which is useful for detection of object boundaries. Former studies (Kapadia et al., 1995; Polat et al., 1998) showed that when low contrast bars or Gabor patches of the same orientation were positioned inside and outside the RF along an axis collinear with a cell's preferred orientation, the neuronal response was enhanced, compared to when the stimuli in the surround were presented along the orthogonal axis (Figure 5.1-A). Moreover, collinear stimuli in the surround reduced the detection threshold in human observers (Kapadia et al., 1995). However, the facilitation decreased with increasing distance of the collinear surround stimuli from the stimulus inside RF

(Kapadia et al., 1995; Polat et al., 1998).

Polat et al. (1998) stimulated the RF and surround with iso-oriented and cross-oriented patches presented on axis collinear with the cell's preferred orientation in cat V1 (Figure 5.1-B). The surround patches were presented at high contrast, while the contrast of the center patch in the RF was varied. Similar to the former study, Polat et al. (1998) reported that when the center patch was at low contrast (less than or equal to twice the cell's contrast threshold) they observed facilitation, whereas suppression dominated when the center contrast was more than nine times higher than the threshold. However, 40% of the population showed response facilitation even at high center stimulus contrast. Interestingly, when the surround patches were presented at the orientation orthogonal to that preferred by the cell along the collinear axis, suppression was observed for 82% of the cells.

Later, other groups (Sceniak et al., 1999; Cavanaugh et al., 2002) speculated that this result was obtained because the l-sRF (which is two times larger than the h-sRF, see section 1.2.5) was activated by the bar stimuli in the near surround. Moreover, weak stimuli, such as small bars or Gabor patches, in the RF and surround do not sufficiently drive the inhibitory cells up to their threshold, thus, the surround stimuli cause excitation (Fitzpatrick, 2000). However, Kapadia et al. (1995) showed that an elongated bar on the collinear axis covering both the RF and the near surround did not cause facilitation, and they suggested that the stimulation of the gap between the center and the flanker stimuli might drive the inhibitory zones. Moreover, adding more collinear lines embedded in cluttered stimuli evoked higher spike discharges, which means the facilitation was increased (Figure 5.2-A). In summary, this effect would suggest that there exist a

mechanism that has specific preference for encoding collinear stimuli.

In Chapter 3, we used LFP signal to investigate the temporal dynamics of the surround inputs to the RF center; In particular, studying the latency of current sinks localized the LFP signal in the extracellular medium. We correlated the spatiotemporal profiles of V1 layers' activation with the termination of feedforward, feedback, and horizontal connections. In addition to reflecting input dynamics, other roles of LFP oscillations, which are low frequency signals (1-200Hz)(Berens et al., 2008a), in various sensory, motor, and cognitive tasks have been the subject of studies in recent years. For instance, it is thought that the oscillations in the theta frequency band play a clock-like role in the hippocampus, and are correlated with mnemonic neuronal representations (Jensen et al., 2007). Numerous studies have reported increases in gamma power (30-150 Hz) during sensory stimulation (Fries et al., 2002), feature binding (Singer and Gray, 1995) and attention tasks (Gregoriou et al., 2009).

These studies showed specifically that gamma power increases during stimulation of V1 cells' RFs. Although there are lots of controversial reports, it is agreed that these LFP oscillations (30-80 Hz) are tuned to stimulus orientation, direction, temporal frequency, contrast, and spatial frequency (Henrie and Shapley, 2005; Berens et al., 2008a, b; Jia et al., 2011; Lashgari et al., 2012). Oscillations in the gamma band also increase with surround suppression in V1. Gieselmann and Thiele (2008) found that while the MUA spiking activity was suppressed in response to grating patches of intermediate size (4° in diameter), gamma power kept increasing with stimulus size. This study suggested that inhibitory-induced oscillations may be an important player in generation of sustained gamma activity.

An important question is: what are the main sources of gamma activation? These rhythms most likely originate in local microcircuits, and involve both pyramidal and inhibitory interneuron activity (Fries et al., 2007). Modeling work suggested that inhibitory interneurons are the main origin of the oscillations (Traub et al., 1996; Wang and Buzsáki, 1996). In particular, fast spiking GABA-A basket cells are thought to be the main source of lateral inhibition in the neocortex (Galarreta and Hestrin, 1999; Markram et al., 2004; Cardin et al., 2009). However, the pyramidal cells contacting inhibitory cells via their long-range connections are the strongest contributors to LFP dipoles. The most recent proposal is that gamma oscillations are the result of local recurrent connections between excitatory and inhibitory cells, with the inhibitory interneurons generating and maintaining rhythmic inhibition on the pyramids' membrane potential (Bartos et al., 2007; Fries et al., 2007). Initially, the inhibitory cells are driven by strong excitation. The inhibition-excitation recurrent loop that has been observed in both the hippocampus and neocortex is the best candidate as a gamma generator.

It is noteworthy that collinear facilitation reflects the properties of long-range V1 horizontal connections. In particular, these connections, which arise from pyramidal cells, preferentially link columns of similar orientation along an axis collinear in space with the cell's preferred orientation (Gilbert and Wiesel, 1989; Malach et al., 1993; Bosking et al., 1997). Also, their patchy termination patterns make it possible for discontinuous collinear stimuli to evoke excitatory responses from these pyramids with less inhibition in between. Moreover, horizontal connections do not just contact excitatory cells, but also inhibitory cells, and can thus generate suppression, engaging the recurrent loop required for the generation of gamma oscillations. Recent studies showed that feedback

connections from V2 to V1 are also patchy and orientation specific (Schmidt et al., 1997; Angelucci et al., 2002; Shmuel et al., 2005; Angelucci and Bressloff, 2006; Federer et al., 2015), although others have reported contrasting results (Maunsell and Van Essen, 1983; Stettler et al., 2002). As it is discussed in previous chapters, feedback is likely contributing to far SM and might provide top-down signal to V1 for contour completion tasks (Polat et al., 1998). One hypothesis is that feedback contacting both inhibitory and excitatory cells (Anderson and Martin, 2009) might also be a player in the generation of rhythmic oscillations.

Most of the former reports observed collinear facilitation while they were stimulating the RF center at low contrast. But in the study reported in this chapter we recorded LFPs and its frequency content in response to collinear and noncollinear patches activating the surround in the absence of RF stimulation (similar to the stimuli used for the study in Chapter 3). We hypothesize that if the patchy horizontal and feedback connections are aligned in an anisotropic fashion and are the substrate of the contour completion, we might be able to observe their effects in the LFP oscillations, specifically in the gamma band. Although a former study by Gieselmann showed that stimulation of the surround alone did not evoke gamma increase, we predict that stimulating the patchy connections, via grating patches at distinct positions, might engage recurrent connections evoking LFP oscillations.

We probed the near and far surround using small static circular grating patches on the collinear and orthogonal axes relative to the cell's preferred orientation, while we recorded through the layers of V1. We measured the increase in different frequency bands to stimulation of different surround elements in collinear and noncollinear

configurations (Figure 5.2).

5.2 Methods

All the recordings are made from V1 of two anesthetized macaques (n=5 penetrations) as described in detail in section 3.2.1. Surgical preparations, electrophysiological recordings, RF mapping, and other tuning properties are also as described in sections 3.2.2 and 3.2.3.

5.2.1 Visual Stimuli

We stimulated the cortical column with iso-oriented static grating patches located along the orthogonal or collinear axis relative to the V1 column's preferred orientation, measured by MUA. Figure 5.2-B and 5.2-C show the two presented configurations.

We used either two or one patch to cover four positions around the RF. The patches were also presented at progressively different distances from the RF to ensure stimulation of both near and far surround. Position and orientation of the patches were randomized and presented for 500ms, interleaved with 750ms blank. The positions of the patches were tailored to the RF size of each penetration, specifically RF+(¼, ½ , 1 , 3/2 ,….) *RF size. In the two-patch condition, the two patches were flashed at the same time, at the same RF distance and along the same axes; these were presented in a separate block from the one-patch condition. Only surround stimuli that did not activate the RF (determined on the bases of CSD analysis) were selected for analysis. If there was any fast activation of L4C in the CSD profile, the condition was excluded.

We made a total of five penetrations, three of which were confined to the same

orientation column, while two of them, although vertical (as determined by the RF alignment across layers) were not confined to an orientation column. For the two penetrations in which there were orientation differences along the column between contacts, two sets of orientation stimuli were presented, each optimized to the orientation preferred by neurons in the supra and infragranular layers, respectively. The analysis was performed for each contact separately, so that the collinear versus noncollinear stimuli were specific to the orientation preference recorded at each contact. The orientation was not optimized for layer 4C and this layer was excluded from the analysis.

5.2.2 Power Analysis

The alpha (8-12Hz), beta (13-30Hz), low gamma (30-58Hz), and high gamma (62-95Hz) frequency bands were obtained from the low pass filtered LFP (1-100 Hz), which was down sampled at 2KHz. We computed the power of each frequency band based on a multi-taper method available in the Chronux toolbox (Bokil et al., 2010). Different frequency powers were extracted using three tapers with half bandwidth of 4Hz in each 200ms. We computed the power in three time periods relative to stimulus onset: blank (-200-0 ms), ERP (0-200 ms), and sustained (200-400 ms). The power increase was computed as the power difference between the ERP or sustained period and that during the blank. These comparisons were applied using the logarithmic scale of each time period as in the equation below (Berens et al., 2008a).

$$Power\ increase = \log(P_{stim}) - \log(P_{blank}) \qquad (5.1)$$

in which, P_{stim} is the absolute power of each band during stimulus presentation, consisting of either ERP (0-200 ms) or sustained (200-400 ms), while P_{blank} is the

absolute power during the 200ms before stimulus onset.

In this chapter, p values are computed applying the Wilcoxan Rank Sum test and are reported with the margins of 0.05, 0.001, and 0.0001.

5.3 Results

Figure 5.3 shows the increase in power in different frequency bands during the first 200ms after stimulus onset, a time window which is related to event related potentials. Both populations of cells in infra (IG)- and supra-granular (SG) layers show greater power increases in the high-gamma frequency band, in response to grating patches presented outside the RF in the collinear configuration compared to patches presented in the noncollinear configuration (Figure 5.3-A). This effect was significantly different for both populations (SG: n=32, p<0.001; IG: n=26, p<0.05). We did not observe significant differences between SG and IG layers in either collinear or noncollinear configurations (p>0.05). As shown in Figure 5.3.B-F, we divided the data into three distances from the RF center: near surround (<1.225°), near/far border (1.225°≤ distance <1.975°), and far surround (1.975°≤ distance <4°). Since the exact distances varied from penetration to penetration (as they depended on the size of RF), we computed the mean distance pooled across all penetrations based on the aforementioned grouping. Panels B and C in Figure 5.3 present similar data, in different formats, for high gamma rhythms, showing that the collinear and noncollinear conditions were significantly different from each other in SG layers (blue vs. red) for the near surround (Dist <1.225°, n=12 in SG, n=8 in IG), and in both SG and IG layers for the far surround (1.975 °≤ Dist < 4°; n=8 in SG; n=9 in IG). However, there were no statistically significant differences between the

collinear and noncollinear conditions in the near/far border, perhaps due to the small number of data available at these distances.

Other frequency bands also showed larger power increases in IG and SG layers for the collinear versus noncollinear condition, in both near and far surround ($p<0.05$) (Figure 5.3.D-F). However, the alpha band did not show significant differences in IG layers in the near surround. We also performed statistical analysis to determine differences at each distance between collinear and noncollinear conditions in both SG and IG layers at all frequency bands, as well as to compare the power increase of SG vs. IG in collinear and noncollinear configurations. Significant results are marked with asterisks in Figure 5.3.C-F.

Since most former studies have shown an increase in gamma activity during the sustained part of the response to stimulus presentation, we also performed an analysis of power changes in different frequency bands during the time window of 200-400ms after stimulus presentation, compared with the power during the blank. Figure 5.4 shows the results of this analysis in the same format as Figure 5.3, but during the sustained (200-400ms) response period. All frequency bands, including high and low gamma, beta and alpha showed significantly greater increases in power in the collinear versus noncollinear conditions in the SG layers ($p<0.05$), in response to near surround stimulation. The IG layers also showed significant differences in high gamma, low gamma and beta, but not in alpha ($p<0.05$). Another interesting statistical comparison is seen in panels E and F of Figure 5.4, where the power in the alpha and beta frequency bands in the SG layers is lower than the power of the baseline activity in the noncollinear condition at near surround.

Comparing the power increases across layers and conditions, we observe that the sustained high gamma rhythm no longer showed any significant difference between the collinear and noncollinear configurations in far surround (compare Figure 5.4-C with Figure 5.3-C). Low gamma is the only frequency band that showed differences between the collinear and noncollinear conditions in both IG and SG layers in response to both near and far surround stimulation (Figure 5.4-D). Comparison of Figure 5.4 with Figure 5.3 suggests that in the first 200 ms after stimulus onset high gamma, low gamma and beta encode collinearity in SG and IG layers, but in the subsequent 200 ms low gamma represents this property of the connectivity in both near and far surround. Despite the fact that high gamma loses selectivity to this effect in the far surround, beta and alpha are qualitatively selective to the collinearity but do not result in significance differences. According to power law, lower frequencies have higher powers, so we also looked into the broad power (1-95Hz) and found a similar behavior to that of the alpha band in the four plots, because of its higher absolute power compared to other frequencies.

5.4 Discussion

The preliminary results in this chapter indicate that brain oscillation can be employed to study neuronal population activity to characterize circuits that might serve perceptual tasks. Here, the power in different frequency bands, including alpha (8-12Hz), beta (13-30Hz), low gamma (30-58Hz), and high gamma (62-95Hz), was computed and compared with baseline activity in the absence of visual stimulation. We have studied the power increase in response to stimulation of the surround with grating patches presented in the collinear and noncollinear configuration relative to the recorded cell's orientation

preference. Although there are various reports on the separation of gamma band into low and high ranges, the largest change in the LFP during visual stimulation has been reported to be in the 30-80Hz range (Berens et al., 2008a; Gieselmann and Thiele, 2008). In addition, the observed increase in gamma band power during suppressed MUA was in the region of 25-100 Hz. Consistent with Xing et al. (2012) who reported increased gamma power in anesthetized monkeys in the range of 20-60Hz, we divided this frequency band into low (30-58Hz) and high (62-95Hz) gamma.

Our data show that the power in both gamma bands (30-95 Hz, low and high) was increased in the near surround, and larger in the collinear compared to the noncollinear configuration for both supra- and infragranular populations. Two studies (Berens et al., 2008a; Gieselmann and Thiele, 2008) investigated the suppression and feature selectivity of the gamma band during the sustained part of the response to stimulus presentation (200-500 ms), and most studies reported a transient gamma increase as being due to event related potentials caused by stimulus onset. Here, in the near surround, both transient and sustained gamma bands seem to preferentially encode collinearity over noncollinearity. However, in the far surround, during the sustained response period, high gamma was no longer sensitive to the collinear configuration, while low gamma was. This selectivity of high and low gamma suggests distinct underlying circuits for collinear patches in the two surround regions. But, the difference between high and low gamma in the transient and sustained periods, implies that the connections underlying far surround do not preserve the selectivity in the later stages of the oscillations.

Despite the fact that Gieselemann et al.(2008) showed that surround-only stimuli probed by annular gratings did not evoke any gamma power increase (see Figure 5.1-B),

here we have observed large increases in the gamma band power compared to baseline. However, weaker stimuli, such as far or noncollinear conditions, have negative values of relative power, indicating that the baseline power was greater than the power during the stimulus presentation, and similar to what was observed previously. For instance, transient low gamma, beta and alpha bands have negative values of relative power in the far surround and in noncollinear configurations (Figure 5.3.D-F). But, still the collinear configuration evokes power increases above baseline. In sum, comparing our result with the literature suggests that the collinear stimulation condition might be representative of the collinear organization of patchy horizontal (Bosking et al., 1997) and feedback projections (Angelucci et al., 2002) that are recruited by near and far surround stimuli.

Comparing the sustained and transient plots, one observes that the magnitude of power increase is lower during the sustained period, suggesting the power is stronger during the stimulus driven period in the anesthetized preparations. Investigating the sustained versus transient frequency powers in the far surround, both alpha and beta bands show similar behaviors as high gamma, being significant in the transient period, but not during the sustained period. However, in the far surround, similar to low gamma, alpha and beta show a preference for collinearity, while sustained high gamma does not. Using voltage sensitive dye imaging, Gilad et al. (2012) showed that the alpha coherence was higher within each area (V1-V1 and V2-V2) and between cortical areas (V1-V2) in the collinear conditions compared with the orthogonal configuration. They reported this effect while the stimulus-evoked response in the center alone condition was subtracted from the collinear configuration in which they also had RF activation with low contrast Gabor patches. They did not find any statistical difference in the gamma band compared

with the fixation only condition which could be due to slow time resolution of dye imaging technique.

Studying laminar differences in oscillatory behavior, stimulating the columnar RF with a four-degree (in radius) drifting grating patch, another study (Xing et al., 2012) found that the gamma band (25-60Hz) was more prominent in superficial layers and L4B during the sustained period, while an increase in gamma power was present in all layers during the transient period, but having stronger values in L2, L5, and L6. Over the population, we have not observed differences in encoding collinearity between layers, while in some rare conditions there were differences across layers. For example, in the transient low gamma, the collinear patches positioned in the near surround, resulted in larger power increase in SG layers than IG, while it evoked higher beta power in IG layers, compared to SG. In the study by Xing et al.(2012), the authors recorded from multiple cortical columns using tetrodes, while stimulating with large gratings that activated the RFs of all columns. In this study, the surround effects were not isolated. In our study, we recorded from a cortical column using linear arrays in response to near and far surround stimulation. In some penetrations that were not confined to a single orientation column (50μm), which is smaller than a receptive field column (~1-2mm), we selectively stimulated the SG and IG layers with different orientations optimized to these layers' orientation preferences. The recorded LFP of the SG and IG were extracted at different time points during the experiments in the anesthetized preparation, and this made it difficult to compare absolute power increases across layers. However, the preference for collinearity was compared within each set of stimuli in which collinear and noncollinear patches were randomly interleaved.

In our study we observed that most frequency bands are selective for collinear patches compared to noncollinear patches, although low gamma was selective to this stimulus parameter during both the transient and sustained response to the stimulus in both the near and far surround. This suggests that the circuits for near and far surround modulation, such as horizontal and feedback connections, are integrating the inputs in recurrent local networks generating activity in the gamma band. An alternative interpretation is that the long-range anisotropic horizontal connections contacting basket cells are the main substrate of gamma power increases. Feedback from V2 is also shown to terminate in a patchy and orientation-selective fashion (Federer et al., 2015), and could target inhibitory cells in V1. However, a different study showed that feedback is divergent and not orientation specific (Stettler et al., 2002). Therefore, feedback contacting anisotropic excitatory pyramids in V1 that are inhibited by interneurons would be an indirect alternative circuit for frequency oscillations in response to far surround collinear patches. Thus, stimulation of collinear patches might engage the orientation specific horizontal or feedback connections that are aligned in an anisotropic pattern in visual space encoding collinear stimuli.

Sampling from an orientation column and studying the time course of each frequency band will shed light on the underlying mechanisms of collinear patches that might be involved in contour completion. One could also measure the functional connectivity across layers in response to collinear patches.

5.5 References

Anderson JC, Martin KAC (2009) The synaptic connections between cortical areas V1 and V2 in macaque monkey. J Neurosci 29:11283-11293.

Angelucci A, Bressloff PC (2006) The contribution of feedforward, lateral and feedback connections to the classical receptive field center and extra-classical receptive field surround of primate V1 neurons. Prog Brain Res 154:93-121.

Angelucci A, Levitt JB, Walton E, Hupé JM, Bullier J, Lund JS (2002) Circuits for local and global signal integration in primary visual cortex. J Neurosci 22:8633-8646.

Bartos M, Vida I, Jonas P (2007) Synaptic mechanisms of synchronized gamma oscillations in inhibitory interneuron networks. Nat Rev Neurosci 8:45-56.

Berens P, Keliris GA, Ecker AS, Logothetis NK, Tolias AS (2008a) Comparing the feature selectivity of the gamma-band of the local field potential and the underlying spiking activity in primate visual cortex. Front Syst Neurosci 2:2.

Berens P, Keliris GA, Ecker AS, Logothetis NK, Tolias AS (2008b) Feature selectivity of the gamma-band of the local field potential in primate primary visual cortex. Front Neurosci 2:199-207.

Bokil H, Andrews P, Kulkarni JE, Mehta S, Mitra PP (2010) Chronux: a platform for analyzing neural signals. J Neurosci Methods 192:146-151.

Bosking WH, Zhang Y, Schofield B, Fitzpatrick D (1997) Orientation selectivity and the arrangement of horizontal connections in tree shrew striate cortex. J Neurosci 17:2112-2127.

Cardin JA, Carlén M, Meletis K, Knoblich U, Zhang F, Deisseroth K, Tsai L-H, Moore CI (2009) Driving fast-spiking cells induces gamma rhythm and controls sensory responses. Nature 459:663-667.

Cavanaugh JR, Bair W, Movshon JA (2002) Nature and interaction of signals from the receptive field center and surround in macaque V1 neurons. J Neurophysiol 88:2530-2546.

Federer F, Merlin S, Angelucci A (2015) Anatomical and functional specificity of V2-toV1 feedback circuits in the primate visual cortex. Soc Neurosci Abstr Online.

Fitzpatrick D (2000) Seeing beyond the receptive field in primary visual cortex. Curr Opin Neurobiol 10:438-443.

Fries P, Nikolić D, Singer W (2007) The gamma cycle. Trends Neurosci 30:309-316.

Fries P, Schröder J-H, Roelfsema PR, Singer W, Engel AK (2002) Oscillatory neuronal synchronization in primary visual cortex as a correlate of stimulus selection. J Neurosci 22:3739-3754.

Galarreta M, Hestrin S (1999) A network of fast-spiking cells in the neocortex connected

by electrical synapses. Nature 402:72-75.

Gieselmann MA, Thiele A (2008) Comparison of spatial integration and surround suppression characteristics in spiking activity and the local field potential in macaque V1. Eur J Neurosci 28:447-459.

Gilad A, Meirovithz E, Leshem A, Arieli A, Slovin H (2012) Collinear stimuli induce local and cross-areal coherence in the visual cortex of behaving monkeys. PloS one 7:e49391.

Gilbert CD, Wiesel TN (1989) Columnar specificity of intrinsic horizontal and corticocortical connections in cat visual cortex. J Neurosci 9:2432-2442.

Gregoriou GG, Gotts SJ, Zhou H, Desimone R (2009) High-frequency, long-range coupling between prefrontal and visual cortex during attention. Science 324:1207-1210.

Henrie JA, Shapley R (2005) LFP power spectra in V1 cortex: the graded effect of stimulus contrast. J Neurophysiol 94:479-490.

Hess R, Field D (1999) Integration of contours: new insights. Trends Cogn Sci 3:480-486.

Jensen O, Kaiser J, Lachaux J-P (2007) Human gamma-frequency oscillations associated with attention and memory. Trends Neurosci 30:317-324.

Jia X, Smith MA, Kohn A (2011) Stimulus selectivity and spatial coherence of gamma components of the local field potential. J Neurosci 31:9390-9403.

Kapadia MK, Ito M, Gilbert CD, Westheimer G (1995) Improvement in visual sensitivity by changes in local context: parallel studies in human observers and in V1 of alert monkeys. Neuron 15:843-856.

Lashgari R, Li X, Chen Y, Kremkow J, Bereshpolova Y, Swadlow HA, Alonso J-M (2012) Response properties of local field potentials and neighboring single neurons in awake primary visual cortex. J Neurosci 32:11396-11413.

Malach R, Amir Y, Harel M, Grinvald A (1993) Relationship between intrinsic connections and functional architecture revealed by optical imaging and in vivo targeted biocytin injections in primate striate cortex. Proc Natl Acad Sci USA 90:10469-10473.

Markram H, Toledo-Rodriguez M, Wang Y, Gupta A, Silberberg G, Wu C (2004) Interneurons of the neocortical inhibitory system. Nat Rev Neurosci 5:793-807.

Maunsell JH, Van Essen DC (1983) The connections of the middle temporal visual area

(MT) and their relationship to a cortical hierarchy in the macaque monkey. J Neurosci 3:2563-2586.

Polat U, Mizobe K, Pettet MW, Kasamatsu T, Norcia AM (1998) Collinear stimuli regulate visual responses depending on cell's contrast threshold. Nature 391:580-584.

Sceniak MP, Ringach DL, Hawken MJ, Shapley R (1999) Contrast's effect on spatial summation by macaque V1 neurons. Nat Neurosci 2:733--739.

Schmidt KE, Goebel R, Löwell S, Singer W (1997) The perceptual grouping criterion of colinearity is reflected by anisotropies of connections in the primary visual cortex. Eur J Neurosci 9:1083-1089.

Shmuel A, Korman M, Sterkin A, Harel M, Ullman S, Malach R, Grinvald A (2005) Retinotopic axis specificity and selective clustering of feedback projections from V2 to V1 in the owl monkey. J Neurosci 25:2117-2131.

Singer W, Gray CM (1995) Visual feature integration and the temporal correlation hypothesis. Ann Rev Neurosci 18:555-586.

Stettler DD, Das A, Bennett J, Gilbert CD (2002) Lateral connectivity and contextual interactions in macaque primary visual cortex. Neuron 36:739-750.

Traub RD, Whittington MA, Stanford IM, Jefferys JG (1996) A mechanism for generation of long-range synchronous fast oscillations in the cortex. Nature 383:621-624.

Wang X-J, Buzsáki G (1996) Gamma oscillation by synaptic inhibition in a hippocampal interneuronal network model. J Neurosci 16:6402-6413.

Xing D, Yeh C-I, Burns S, Shapley RM (2012) Laminar analysis of visually evoked activity in the primary visual cortex. Proc Natl Acad Sci 109:13871-13876.

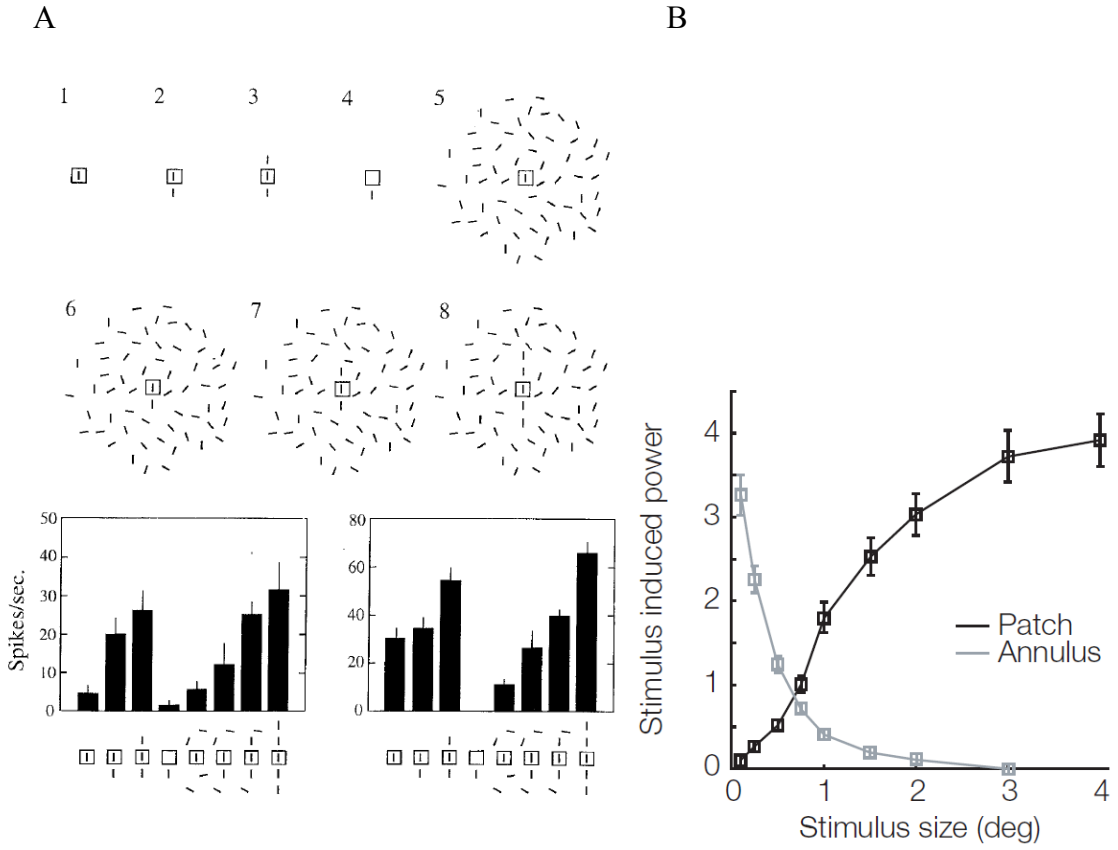

Figure 5.1: collinear facillitation and gamma increase by surround stimuli. A) From Kapadia et al. (1995) 1-8 shows the stimuli that were used in the task. The bottom two panels are the firing rate of two example cells for different stimulus configurations. B) From Gieselmann and Theile,(2008) , the black curve shows an increase in gamma band with larger gratings centered on the RF; the gray curve shows that stimulation of the surround region by annular gratings did not enhance gamma oscillations.

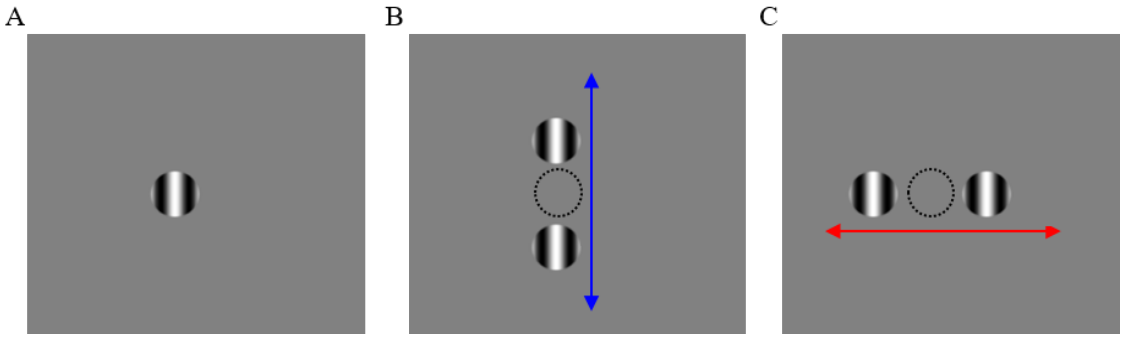

Figure 5.2: Visual stimuli. A) Shows the grating patch fitted to the columnar RF presented at the optimal orientation for most contacts. B) Shows the collinear surround patches positioned along the collinear axis relative to RF orientation. C) Depicts surround patches along the non-collinear axis.

Figure 5.3: Transient power increase (0-200ms after stimulus onset). A) Scatter plot of the high gamma power increase for supra-(blue circles) and infragranular layers (red circles). B) Shows the average of high gamma for near: dist<=0.85 from RF center, near/far border :1.225<=dist<1.975 and far surround: 1.975<=dist<4. Blue and red are supra collinear and non-collinear conditions, black and magenta are infra collinear and noncollinear conditions. C-F) Shows the same information as in B) but in barchart format with statistical results between possible pair for C) high gamma, D) low gamma , E) beta and, F) alpha bands.

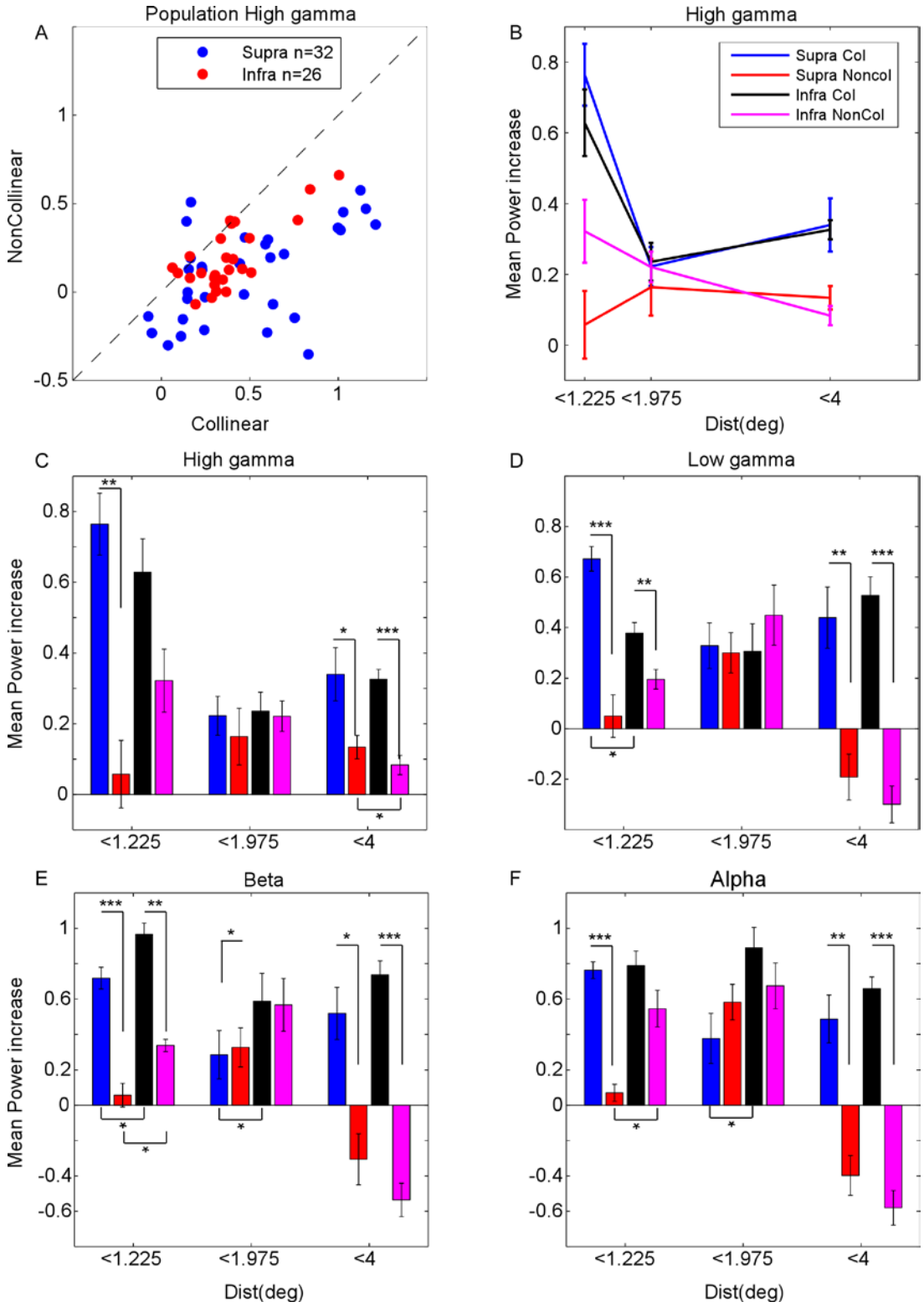
A
Population High gamma
Supra n=32
Infra n=26
NonCollinear
Collinear
B
High gamma
Supra Col
Supra Noncol
Infra Col
Infra NonCol
Mean Power increase
<1.225 <1.975
<4
Dist(deg)
C
High gamma
Mean Power increase
<1.225
<1.975
<4
D
Low gamma
E
Beta
Mean Power increase
Dist(deg)
F
Alpha
Dist(deg)

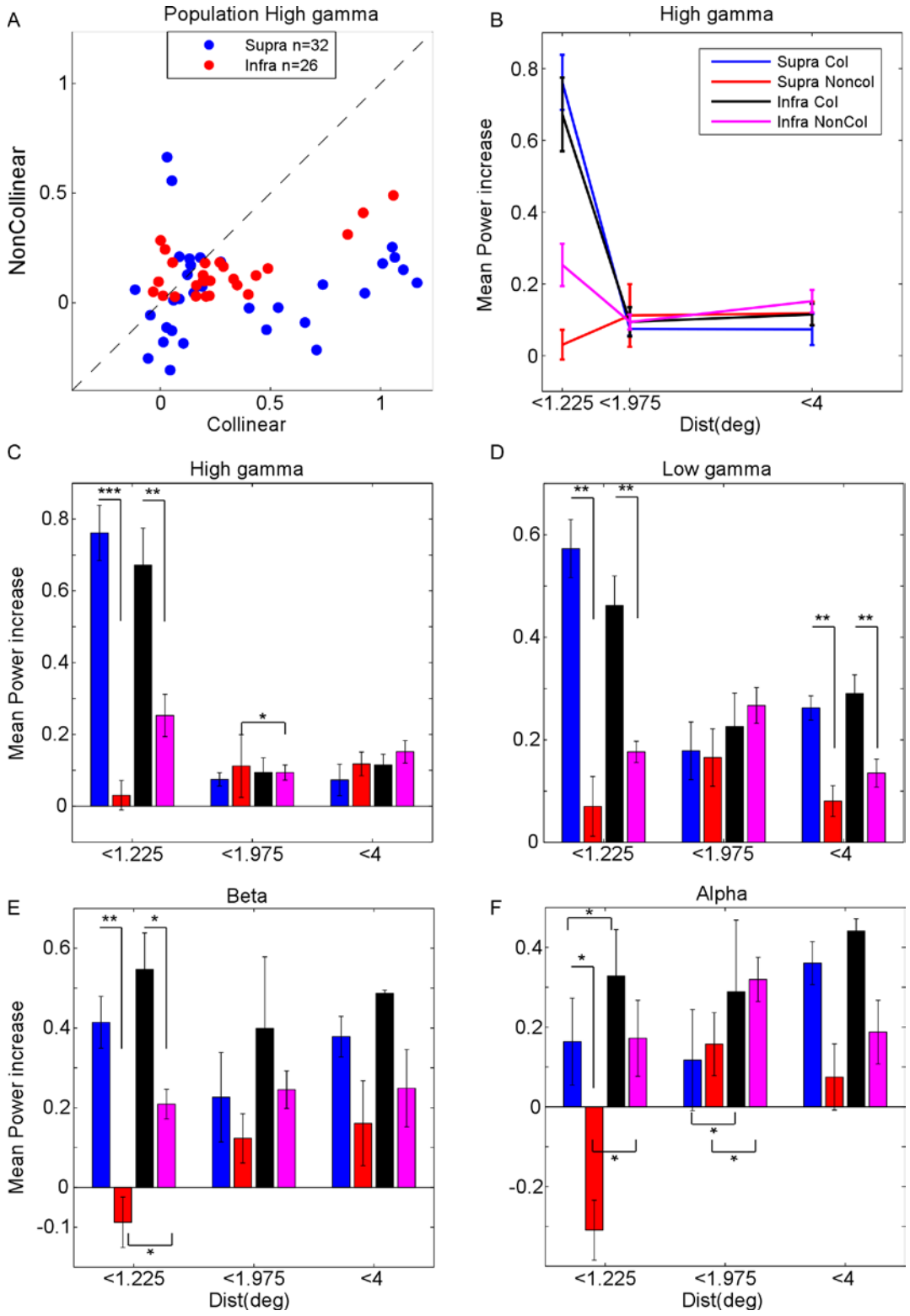

Figure 5.4: Sustained power increases (200-400 ms), figure legends as in 5.3.

CHAPTER 6

CONCLUSION

6.1 Summary

The presented results in this dissertation shed light on the underlying mechanisms of surround modulation in the primate's primary visual cortex, specifically, how different layers of V1 contribute to the processing of surround stimuli. It has been previously suggested that the RF surround consists of two regions called "near" and "far" surround, which are generated by different anatomical circuits (Angelucci et al., 2002; Bair et al., 2003; Angelucci and Bressloff, 2006). The modulatory influences arising from the near surround are mainly generated by thalamocortical feedforward and intra-V1 horizontal connections, while far surround modulation is generated by top-down feedback connections from extrastriate cortex. This hypothesis is based on both the anatomical extent of monosynaptic horizontal connections (Angelucci et al., 2002) and their slow conduction velocity (Grinvald et al., 1994; Girard et al., 2001) compared to faster inter-areal connections from extrastriate areas to V1 (Girard et al., 2001). These findings, support the idea that top-down feedback projections carry global information from the larger RFs of higher visual centers back to the smaller RFs in V1.

The main difference between the underlying circuits of the two surround regions is

the involvement of feedback as the main circuit for the far surround. Former physiological studies by our laboratory and others showed that the near and far surround have different properties; for example, the suppression is stronger in the near surround compared to the far surround, and the orientation tuning is different in these two surround regions (Cavanaugh et al., 2002; Shushruth et al., 2009; Hashemi-Nezhad and Lyon, 2012). Specifically, in a recent publication, we found that the modulation arising from the near surround is more sharply tuned for orientation than that arising from the far surround. This effect was also mirrored in human observers, meaning that a stimulus in the near surround suppressed the perceived contrast of a center grating more strongly than a stimulus in the far surround, when the RF and surround were iso-oriented. But, similar to neuronal firing rates, cross oriented gratings resulted in larger suppression in the far surround compared to near, leading to broader orientation tuning of far surround modulation (Chapter 2, Figure 2.7-A and B). This result implies that sharply orientation tuned near surround suppression might serve to detect small orientation differences in nearby edges, that could be beneficial for detection of object boundaries (Nothdurft et al., 2000). In contrast, broader orientation tuned far surround suppression could be useful to detect large orientation differences in distant edges, which could lead to direct saccades or attention to more salient objects in the visual periphery (Petrov and McKee, 2006).

To elaborate on this, since we were interested to study the contribution of V1 layers to surround modulation, in Chapter 2 we asked how the orientation tuning of near and far surround modulation varies across layers. Using histological reconstructions of electrode penetrations, and recording from all V1 layers using single electrodes, we found that near surround modulation is more sharply orientation tuned in L3B, L4B, and L4Cα than in

deeper layers, while far surround modulation is more orientation selective in L4B. These laminar differences in orientation tuning support the idea that near and far surround have different underlying circuits. In particular, the sharper tuning of near surround modulation in superficial layers is consistent with the existence in these layers of horizontal connections linking neurons with similar orientation preference (Malach et al., 1993). Also, long-range patchy connections in L4B and upper L4Cα (Lund et al., 2003) may contribute to the sharp tuning of near surround in these layers; instead, long-range connections in L6 which are divergent and nonspecific (Li et al., 2003) could be the substrate for the weaker tuning of near surround modulation in this layer. Moreover, the broader tuning of far surround modulation suggests that feedback connections, the main circuit underlying the far surround, are less orientation tuned than horizontal connections, or they are pooling signals from sharply orientation selective cells resulting in broader tuning. However, sharper tuning of far surround modulation in L4B suggests that feedback terminations to this layer are orientation selective.

Elaborating on the role of V1 layers in the processing of SM, and due to the fact that feedforward, horizontal, and feedback connections terminate in different V1 layers (Rockland and Pandya, 1979; Ungerleider and Desimone, 1986), in Chapter 3, we investigated the temporal dynamics of presynaptic inputs' activity across V1 layers in a cortical column evoked by stimulation of the near and far surround. We predicted that feedback recipient layers might show the earliest activity in response to far surround stimulation, and layers with prominent horizontal connections might show the earliest activity in response to near surround stimulation. To test these predictions, we used multicontact laminar probes that enabled us to record both MUA and LFP signals from

all layers at the same time. Applying current source density analysis on LFP data, we could measure the timing of the earliest inputs to the cortical column in response to RF, near and far surround stimulation. We found that, following stimulation of the RF, the first current sink was observed in the granular input layers, followed by activity in the supra and infragranular layers, which were activated by recurrent laminar networks. To prevent postsynaptic spiking activity caused by excitation of thalamic afferents and subsequently of the interlaminar network (granular first followed by extra-granular layers), near and far surround stimuli were presented in the absence of RF stimulation. Our results confirmed our hypothesis that in response to far surround stimulation the fastest inputs occurred in L1/2A and low IG (possibly L5B and 6), which are feedback recipient layers, while near surround stimulation evoked the fastest input activity in horizontal-specific layers, such as L2/3 and the top IG, as well as feedback recipient layers L1/2A and low IG. These findings provide more support for the hypothesized model proposed by Angelucci and colleagues (2002; 2006) that feedback not only contributes to higher cognitive tasks, but also provides global information (here via far SM) from higher visual centers back to V1 RFs to disambiguate local information. These results also emphasizes on the role of feedback as dominant as horizontal connections in the initiation of near surround modulation, because L1/2A and low IG were activated as fast as horizontal connection layers, such as top IG. This fast temporal dynamics of feedback inputs in response to near surround stimulation, was not originally expected by the model. In sum, the outcome of this aim, confirming the predictions of our previous model (Angelucci and Bressloff, 2006), demonstrates how distinct spatiotemporal profiles of inputs across V1 layers are associated with different circuits involved in

processing different surround components.

As explained in the second chapter, we found that near and far surround modulation have different functional properties, specifically orientation selectivity, across the layers of V1. Confirming the engagement of horizontal and feedback inputs across the layers of V1 in near and far surround suppression, in Chapter 4, we asked in which layer surround suppression and its orientation tuning are generated first. For example, in response to near surround stimulation, we learned in Chapter 3 that all layers except the granular ones receive the earliest inputs; we then asked in which layers these inputs first cause orientation untuned and tuned near surround suppression.

In other words, we aimed to measure the temporal behavior of postsynaptic spiking activity that is mirrored in the surround suppression. Measuring the latency of MUA activity at contacts located in each layer, we found that in response to RF and near surround stimulation, surround suppression first emerges in L4B/4Cα, while in response to RF and far surround stimulation, suppression occurred last in time in L4C. The untuned suppression in the near surround can be initiated by LGN afferents as well as horizontal connections in L4B/4Cα that receive the first inputs from the magnocellular pathway. However, the suppression from the far surround, which is weaker than from the near surround, was delayed in the middle of L4C, suggestive of a cortical origin. The large gap between the inner radius of the annular grating in the far surround and the edge of the RF makes it unlikely for the far surround stimuli to engage the spatially restricted LGN afferents. An interesting result was that stimulating the RF, near and far surround regions all at the same time by a large 20° grating disk, located the earliest suppression in the middle of L4C, as fast as L4B/4Cα, suggesting involvement of LGN and horizontal

connections in L4B/4Cα together.

By measuring the time difference of response to iso- and cross-oriented RF-surround stimulation, we found that tuned near surround suppression again emerged first in L4B/4Cα and top IG layers (L5). The tuning in the near surround can be computed by existing long-range connections that might be orientation specific in L4B/4Cα. Also, there are horizontal connections in L5 that are possibly involved. Earlier studies reported that surround suppression from LGN is not as orientation specific as surround suppression in the cortex is (Ozeki et al., 2004), so a role of thalamic afferents in the generation of orientation tuning is ruled out. Overall, these findings imply that untuned near surround suppression is generated by LGN afferents but the tuned element in near surround is conveyed by orientation tuned horizontal connections or possibly feedback inputs to L4B. However, far surround suppression, which is occurring out of the thalamic recipient layers, is initiated by feedback projections terminating in layers such as L1/2A and low IG, where suppression happens quickly. The distal dendrites of some IG and L4B cells terminating in L1 could be suppressed by feedback inputs to these layers. Also, the basal dendrites of top IG in low IG neurons might integrate feedback inputs to these layers due to far surround stimulation and generate suppression in top IG.

Other studies reported that the untuned suppression could be as fast as the RF response onset, suggesting a subcortical origin (Cavanaugh et al., 2002; Webb et al., 2005; Xing et al., 2005), but the tuned component of suppression occurs later in time, by about 17 ms delay, suggesting a cortical origin such as recurrent intra-V1 connections (Xing et al., 2005). Another recent study by Henry et al. (2013) found suppression to occur in the first 25ms after RF response onset, while the tuned component of

suppression emerged about 25ms later suggesting two different mechanisms. In Chapter 4, we found two different populations of cells, in one population, the orientation tuning of surround suppression occurred as fast as untuned suppression. However, for the second group, tuned suppression emerged later than untuned suppression. This outcome suggests that there might be two different mechanisms: one is generating both suppression and tuning that could have cortical origin, while the other one suggest that there are chains of synapses to generate tuning after suppression is emerged.

We were also interested to study the oscillations of LFP signal that are thought to reflect interactions of inhibitory and excitatory recurrent loops in the cortex (Fries et al., 2002; Berens et al., 2008). In addition, the power increase and coherency between different frequencies are thought to play an important role in encoding brain synchrony in various cortices involved in cognitive tasks, such as attention (Jensen et al., 2007), sensory stimulation (Fries et al., 2002) and feature binding tasks (Singer and Gray, 1995). In Chapter 5, we specifically measured the power increase of different frequency bands, while stimulating the near and far surround with grating patches that were located on either the collinear or orthogonal axis relative to the cell's orientation preference. We studied this stimulus configuration because it has been shown that stimulation of the surround along a collinear configuration enhanced the neuronal responses compared to orthogonal position when the RF was also stimulated (Kapadia et al., 1995; Polat et al., 1998). This was proposed to underlie contour completion.

We found that alpha, beta, and gamma bands showed power increases compared to the power during baseline activity during the transient part of the response (0-200ms) to the collinear condition compared with the orthogonal one, while the patches were

positioned in either the near or far surround. The main difference of our stimuli compared to those used in previous studies is that we did not stimulate the RF. So we could not measure the facilitatory or suppressive effects of collinear versus noncollinear stimuli on spiking activity. Our findings suggest that horizontal and feedback connections that serve as the main circuits for near and far surround, respectively, and contact both excitatory and inhibitory neurons are presumably generating recurrent neuronal oscillations. The preference of recurrent oscillations to collinear stimuli over noncollinear stimuli, denote that feedback and horizontal connections are organized in an anisotropic fashion in the visual field. This finding is consistent with some other reports that feedback from V2 to V1 is patchy, anisotropic in visual field, and orientation specific (Angelucci et al., 2002), resembling the functional organization of horizontal connections, which have also been shown to link neurons with similar orientation preference along a collinear axis (Malach et al., 1993; Bosking et al., 1997). However, these anatomical studies are not consistent with other reports of divergent (Maunsell and Van Essen, 1983; Ungerleider and Desimone, 1986) and orientation-unspecific feedback (Stettler et al., 2002).

We also found that during the sustained part of the response to visual stimuli (200-400ms) just the low gamma band (30-58Hz) showed significant differences in power between collinear and noncollinear conditions in the far surround. We also observed this selectivity for collinear patches in both supra- and infra-granular layers. In contrast to other reports (Gieselmann and Thiele, 2008) showing that annular gratings in the surround alone did not evoke gamma power increases, we found that collinear patches stimulating the surround alone could entrain brain oscillations stronger than noncollinear ones. This could be due to differences between annular and patch gratings, suggesting

that patch gratings are stimulating the patchy underlying circuit in a selective way, while the annular gratings are stimulating the whole surround region. In sum, the increase in the power of low gamma band during the sustained part of the response to stimulus presentation, which is comparable to other reports, suggests that the recurrent inhibitory and excitatory loops, generating gamma oscillations, are aligned in collinear fashion in the visual field.

6.2 Future Directions

In this dissertation, we investigated the role of different layers in the processing of surround modulation, which is a fundamental property of V1 neuronal responses. It is shown here that feedback, feedforward, and intrinsic V1 connections that have distinct patterns of projections across layers result in functional differences across layers.

In order to study the causal role of each connection type one could manipulate each circuit in the corresponding layer using "optogenetics" in a precisely timely manner. This methodological approach allows to silence or activate specific cell types expressing specific ion channels that are sensitive to light wavelengths (Boyden et al., 2005). The channels are expressed in the brain of the animal model either by transgenic mutations (such as in mice) or viral vectors (such as in primates). Despite the limitations of this approach, for example, low level of channel expressions in primates, optogenetic tools provide the opportunity to manipulate the desired brain circuits and cell types to study their functional roles. In particular, related to the present study, one can inactivate feedback terminals of V2 in L1/2A of V1 that express the inhibitory opsin (e.g., Archerhodopsin) and inactivate them by a laser light (green) while stimulating the

cortical column using far surround gratings. In this case, measuring the amount of suppression in each layer, such as L5 that have distal dendrites in L1/2A and comparing it to the control condition (no light) would allow to determine how much of the suppression in L5 is generated by feedback from V2.

Also, studying the physiological measures of V1 layers in response to simple grating patches or annuli does not necessarily imply that processing of natural images across layers would be similar. For instance, it has been shown that there is enhanced responses to feature contrasts under natural stimulations of RF (Felsen et al., 2005). Also, surround stimulation in natural images increases the efficiency of the transformed information (Vinje and Gallant, 2002). Thus, studying the laminar responses to stimulation of different image properties such as contrast, orientation contents and different regions of the image would be beneficial to tease out which image properties are encoded by each cortical layer.

In addition, studying the temporal profile of each frequency band would provide a robust measure of the involved circuitry in processing of collinear patches. In particular, by measuring the time frequency of the gamma band one could distinguish in which time point and in which layer the gamma increase is happening. Also, applying the granger causality analysis to the time frequency data would be beneficial to probe the functional connectivity between layers in response to visual stimuli.

The present dissertation provides a thorough understanding of how V1 layers are involved in processing of simple sensory stimuli. Benefiting from the presented methods and results, role of laminar networks in computation of sensory stimuli could be investigated in other cortices that have similar laminar structures.

6.3 References

Angelucci A, Bressloff PC (2006) The contribution of feedforward, lateral and feedback connections to the classical receptive field center and extra-classical receptive field surround of primate V1 neurons. Prog Brain Res 154:93-121.

Angelucci A, Levitt JB, Walton E, Hupé JM, Bullier J, Lund JS (2002) Circuits for local and global signal integration in primary visual cortex. J Neurosci 22:8633-8646.

Bair W, Cavanaugh JR, Movshon JA (2003) Time course and time–distance relationships for surround suppression in macaque V1 neurons. J Neurosci 23:7690-7701.

Berens P, Keliris GA, Ecker AS, Logothetis NK, Tolias AS (2008) Comparing the feature selectivity of the gamma-band of the local field potential and the underlying spiking activity in primate visual cortex. Front Syst Neurosci 2:2.

Bosking WH, Zhang Y, Schofield B, Fitzpatrick D (1997) Orientation selectivity and the arrangement of horizontal connections in tree shrew striate cortex. J Neurosci 17:2112-2127.

Boyden ES, Zhang F, Bamberg E, Nagel G, Deisseroth K (2005) Millisecond-timescale, genetically targeted optical control of neural activity. Nat Neurosci 8:1263-1268.

Cavanaugh JR, Bair W, Movshon JA (2002) Nature and interaction of signals from the receptive field center and surround in macaque V1 neurons. J Neurophysiol 88:2530-2546.

Felsen G, Touryan J, Han F, Dan Y (2005) Cortical sensitivity to visual features in natural scenes. PLoS Biol 3:e342.

Fries P, Schröder J-H, Roelfsema PR, Singer W, Engel AK (2002) Oscillatory neuronal synchronization in primary visual cortex as a correlate of stimulus selection. J Neurosci 22:3739-3754.

Gieselmann MA, Thiele A (2008) Comparison of spatial integration and surround suppression characteristics in spiking activity and the local field potential in macaque V1. Eur J Neurosci 28:447-459.

Girard P, Hupé JM, Bullier J (2001) Feedforward and feedback connections between areas V1 and V2 of the monkey have similar rapid conduction velocities. J Neurophysiol 85:1328-1331.

Grinvald A, Lieke EE, Frostig RD, Hildesheim R (1994) Cortical point-spread function and long-range lateral interactions revealed by real-time optical imaging of macaque monkey primary visual cortex. J Neurosci 14:2545-2568.

Hashemi-Nezhad M, Lyon DC (2012) Orientation tuning of the suppressive extraclassical surround depends on intrinsic organization of V1. Cereb Cortex 22:308-326.

Henry CA, Joshi S, Xing D, Shapley RM, Hawken MJ (2013) Functional characterization of the extraclassical receptive field in macaque V1: contrast, orientation, and temporal dynamics. J Neurosci 33:6230-6242.

Jensen O, Kaiser J, Lachaux J-P (2007) Human gamma-frequency oscillations associated with attention and memory. Trends Neurosci 30:317-324.

Kapadia MK, Ito M, Gilbert CD, Westheimer G (1995) Improvement in visual sensitivity by changes in local context: parallel studies in human observers and in V1 of alert monkeys. Neuron 15:843-856.

Li H, Fukuda M, Tanifuji M, Rockland KS (2003) Intrinsic collaterals of layer 6 Meynert cells and functional columns in primate V1. Neurosci 120:1061-1069.

Lund JS, Angelucci A, Bressloff PC (2003) Anatomical substrates for functional columns in macaque monkey primary visual cortex. Cereb Cortex 13:15-24.

Malach R, Amir Y, Harel M, Grinvald A (1993) Relationship between intrinsic connections and functional architecture revealed by optical imaging and in vivo targeted biocytin injections in primate striate cortex. Proc Natl Acad Sci USA 90:10469-10473.

Maunsell JH, Van Essen DC (1983) The connections of the middle temporal visual area (MT) and their relationship to a cortical hierarchy in the macaque monkey. J Neurosci 3:2563-2586.

Nothdurft HC, Gallant JL, Van Essen DC (2000) Response profiles to texture border patterns in area V1. Vis Neurosci 17:421-436.

Ozeki H, Sadakane O, Akasaki T, Naito T, Shimegi S, Sato H (2004) Relationship between excitation and inhibition underlying size tuning and contextual response modulation in the cat primary visual cortex. J Neurosci 24:1428-1438.

Petrov Y, McKee SP (2006) The effect of spatial configuration on surround suppression of contrast sensitivity. J Vis 6:224-238.

Polat U, Mizobe K, Pettet MW, Kasamatsu T, Norcia AM (1998) Collinear stimuli regulate visual responses depending on cell's contrast threshold. Nature 391:580-584.

Rockland KS, Pandya DN (1979) Laminar origins and terminations of cortical connections of the occipital lobe in the rhesus monkey. Brain Res 179:3-20.

Shushruth S, Ichida JM, Levitt JB, Angelucci A (2009) Comparison of spatial summation properties of neurons in macaque V1 and V2. J Neurophysiol 102:2069-2083.

Singer W, Gray CM (1995) Visual feature integration and the temporal correlation hypothesis. Ann Rev Neurosci 18:555-586.

Stettler DD, Das A, Bennett J, Gilbert CD (2002) Lateral connectivity and contextual interactions in macaque primary visual cortex. Neuron 36:739-750.

Ungerleider LG, Desimone R (1986) Cortical connections of visual area MT in the macaque. J Comp Neurol 248:190-222.

Vinje WE, Gallant JL (2002) Natural stimulation of the nonclassical receptive field increase information transmission efficiency in V1. J Neurosci 22:2904-2915.

Webb BS, Dhruv NT, Solomon SG, Taliby C, Lennie P (2005) Early and late mechanisms of surround suppression in striate cortex of macaque. J Neurosci 25:11666-11675.

Xing D, Shapley RM, Hawken MJ, Ringach DL (2005) Effect of stimulus size on the dynamics of orientation selectivity in Macaque V1. J Neurophysiol 94:799-812.